Laser-cooled Atomic Ensembles in Hollow Optical Fibers

by

Sai Sreesh Venuturumilli

A thesis
presented to the University Of Waterloo
in fulfillment of the
thesis requirement for the degree of
Master of Science
in
Physics

Waterloo, Ontario, Canada, 2021

Author's Declaration

I hereby declare that I am the sole author of this thesis. This is a true copy of the thesis, including any required final revisions, as accepted by my examiners.

I understand that my thesis may be made electronically available to the public.

Abstract

This thesis explores hollow-core fibres as a platform for quantum optics experiments with laser-cooled atomic ensembles. The non-diffracting, tightly-confined guided modes of these fibers grant us a $\sim \mu$m-wide one-dimensional space to study atom-light interactions.

In order to describe on-going experiments, simulations are carried out to understand atomic motion into the hollow fibers. Following which, a preliminary case study of a quantum optics experiment to convert wavelengths of single photons with Cs atomic ensembles inside the hollow fiber is presented. Lastly, basic optical properties of photonic crystal membranes are briefly explored. These can form novel cavities when appended to hollow fibers.

Acknowledgements

Table of Contents

List of Tables

List of Figures

Chapter 1

Introduction

"In the first place it is fair to state that we are not experimenting with single particles, any more than we can raise Ichthyosauria in the zoo."

E. Schrodinger, 1952 [1]

So long, Dr. Schrodinger! We are currently riding a wave of technological change in our society. Within half a century, tools such as nanofabrication, lasers and computing have enabled the observation and investigation of curious ideas such as superposition, coherence, indistinguishability and entanglement of atoms and light. Philosophical aspects relating subjects, objects and measurements aside [2], we find ourselves amidst a fertile ground to fashion sustainable tools with the simplest and most ubiquitous units of our reality: photons and atoms – especially as they promise efficiency, scalability, precision and novel algorithmic capabilities. As suggested, there is a richness in the description of the dynamics of basic systems such as a single two-level atom coupled to a one-dimensional photonic channel.[19] Increasing the number of particles multifoldedly adds to the nuance required to talk about the landscapes they live in.

1.1 Quantum Optics and Photonic Quantum Information Processing

An electromagnetic mode is a pattern of vibration of electric ($\vec{E}$) and magnetic ($\vec{B}$) vectorial fields which can extend indefinitely like $3D$ plane-waves; or be confined like the resonant modes of a membrane. Boundary conditions, often specified in terms of material configurations of dielectrics or metals, determine these patterns of oscillations. The quickness of change is given by its frequency: that is, how long it takes for a pattern to repeat itself in time. The space-time relationship of these oscillations is provided using vector algebra and differential equations via Maxwell's equations. This allows one to cross the bridge from the geometry of material source-charges and currents to visualize these modes of movement. In addition, there is a measure of the '*loudness*' of these modes: referred to as energy. A key insight which birthed the development of 'quantum'[264] theories, is that energies of *each mode* come in discrete units. Meaning that, a given pattern of oscillation can only house integer 'amounts' of energy: termed a photon, much like how a TV remote can only up the volume in unit chunks. These integer steps are proportional to its frequency: $E = h\nu$.

Incorporating quantised fields with classical electromagnetism requires a know-how of operator algebra, [41] which adds statistical detail required to describe light – such as its spatial and temporal correlations, along with phase-space distributions.[40] Energies of atoms: electromagnetic and motional, also come in quantised, discrete units. 'Quantum Optics' is about understanding the energetic transactions between atoms and light at the smallest level. Wherein, one is lead to questions such as how atoms singly-and-collectively bathe in the radiation field. While experiments provide us with a window to inquire into these facets of nature, ideas inspired from such a description turn out to be technologically relevant.

Consider information processing, for instance. States of physical systems represent information. In the 'classical' realm, one can grant systems with definite states. Each arrangement of beads in an abacus corresponds to a numeric state; intelligent operations on which can help us perform relatively complex calculations. States and computations can also be represented via continuous variables.[275] Algorithmic complexity and the issue of infinite precision aside, both routes: discrete and continuous variable logical processing are suggested to be

Turing complete [275] – originally elaborated via two-state bits. However, our notion of definiteness gives way to a newer unit of logic – a qubit: $c_0|0\rangle + c_1|1\rangle$. Unknown until measured, the switch *is* both on: $|1\rangle$ *and* off: $|0\rangle$, and there *is and isn't* a photon in the box? Such a superposition can be extended to n-state systems (qudits), where $n \to \infty$ (qumodes).[26] By marrying qubits, qudits and qumodes in different ways, one can conduct algorithms – such as searching a database or factorizing prime numbers; and also study how the computation scales with memory and temporal resources.[36] Atoms and photons, depending on which of their degrees of freedom we're looking at, can represent both discrete and continuous variable quantum information, and thus, aid in such an exploration.

Further, the reality of such states in nature also presents us interesting questions from a communication point of view. How do we share such seemingly paradoxical information? It doesn't appear to be possible to truly convey these coherences via fixed-state information? On-going experimental researches in quantum networking [62, 32], distributing entanglement [60] and teleportation of quantum states [66] contribute towards a de-mystification of the ways in which seemingly distant objects share an 'underlying' connection. Also, the suggested dissipationless nature of quantum processes can prove to be fruitful for a range of engineering purposes [17] such as light sources [31] and sensors.

Here, on-going experimental investigations of the NPQO laboratory to integrate atoms with light in hollow optical fibers are elaborated upon. Before which, it might be helpful to briefly parse through some recent emerging detail concerning light and matter.

Populating Fields of Light – One Photon at a Time
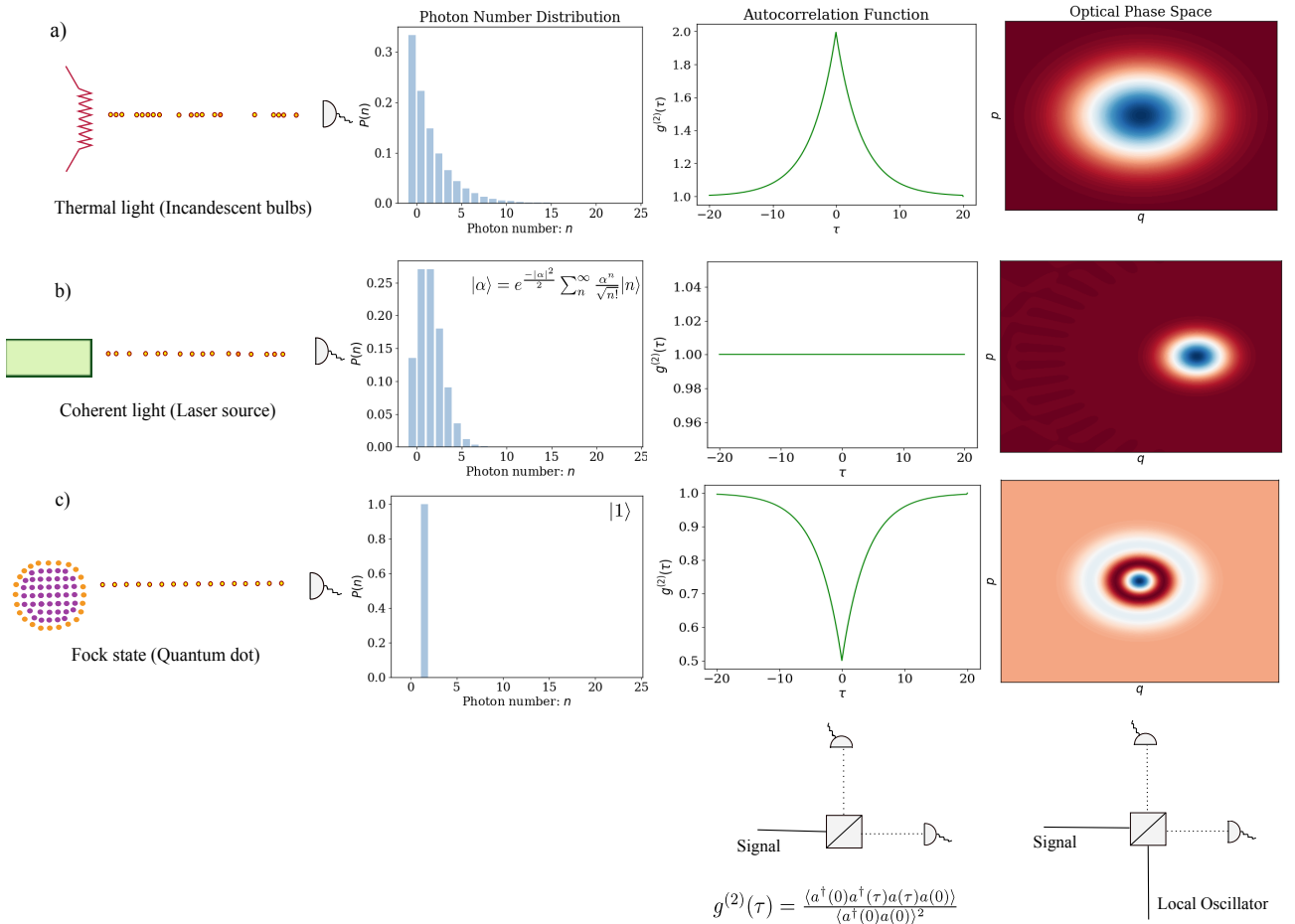
Figure 1.1: Examples of different sources of radiation: a) A resistive filament emits thermal radiation. Such a source gives out blackbody photon-number statistics, bunched photons along with a Gaussian phase-space (here, specified by the Wigner function) distribution. b) Lasers provide coherent radiation which translates to a Poissonian photon-number distribution. While also gaussian in the phase-space, these correspond to minimum uncertainty states – resembling classical particles. c) Emitters such as quantum dots can birth single-photon Fock states, which are characterized by a non-Gaussian optical phase space and a sub-Poissonian auto-correlation function. Plots are readily obtained using template codes provided in Ref.[217].

Experiments show that even after stripping away all energy from the electromagnetic field, we aren't left with space devoid of activity.[47] This unusual broth of flux is oft talked about using 'virtual' particles.[59] As suggested,[47] while not directly measurable, they leave signatures of their presence by morphing energy levels of atoms, affecting electron transport and making geckos walk on walls.[254] From this vacuum, 'real' photons can be birthed by emission corresponding to energetic transitions in matter. Traditional sources of illumination: incandescent lights, vapor lamps, LEDs, lasers and the more recent quantum dot displays deal light in the currency of electronic energies.[Fig.1.1] Even though photons are indistinguishable [6], material processes within these sources dictate the quality of radiation they emit. The incoherently bumping electrons in a tungsten filament gives us thermal light, while the phase-maintaining stimulated emission in lasers lends us coherent light. At a finer level, sourced from their discrete energy level-structure, individual quantum emitters like atoms, color centers and quantum dots can provide us with single photons. Properties such as photon-number distributions, temporal correlations and their amplitude-phase relationships can allow for their categorization, and can be studied using photon-number detectors, Hanburry-Brown Twiss interferometers and homodyne measurements, respectively.[40]

Light's wave-like properties can be seen via interference and spectroscopy experiments. The vectorial nature of its oscillation can be gathered from polarization measurements. These correspond to its phase, frequency (wavelength) and angular momentum. At a given location, plane-waves of electric fields can have the form $\vec{E} = C\cos\{(\vec{k}\cdot\vec{r}_0 - \omega t) + \phi\}\hat{n}$. However, photo-detection experiments only give us integer counts. One way to package these features together is via incorporating a numeric aspect to its amplitude: $\vec{E} \to \hat{E}$. Each photonic mode, contextual to the system, can be thought of by analogy to a quantum harmonic oscillator.[3] To grant the energy steps to be $\hbar\omega$, position and momentum operators can be defined as: $\hat{H}_{\vec{k}} = \hat{p}_{\vec{k}}^2 + \omega_{\vec{k}}^2\hat{q}_{\vec{k}}^2$. Eigen-states corresponding to the energy $n\hbar\omega$ can be written as $|n\rangle$ – known as a Fock state. Then, a general state of light for each mode can be written as:[40]

$$|\Psi\rangle = c_0|0\rangle + c_1|1\rangle + c_2|2\rangle + c_3|3\rangle + ... + c_n|n\rangle + ...$$

To navigate this space, creation and annihilation operators are helpful: $\hat{H}_{\vec{k}} = \hbar\omega_{\vec{k}}\hat{a}^\dagger\hat{a}$; and relate with absorption and emission of photons.[Fig. 1.10] Also, similar to a quantum harmonic oscillator, $\hat{p}$ and $\hat{q}$ can be expressed as:

$$\hat{q} = \sqrt{\frac{\hbar}{2\omega}}(\hat{a} + \hat{a}^\dagger) \quad \hat{p} = -i\sqrt{\frac{\hbar\omega}{2}}(\hat{a} - \hat{a}^\dagger) \qquad \hat{a}|n\rangle = \sqrt{n}|n-1\rangle \quad \hat{a}^\dagger|n\rangle = \sqrt{n+1}|n+1\rangle$$

A plane-wave real-valued field ($\phi \to 0$) can be written as an operator in terms of $\hat{a}^\dagger, \hat{a}$:

$$\vec{E}(\vec{r}, t) = [C_0\exp i(\vec{k}\cdot\vec{r} - \omega t) + C_0^*\exp i(\vec{k}\cdot\vec{r} + \omega t)]\hat{n} \to \hat{E}(\vec{r}, t) = \left[\bar{C}_0\exp i(\vec{k}\cdot\vec{r} - \omega t)\hat{a} + \bar{C}_0^*\exp i(\vec{k}\cdot\vec{r} + \omega t)\hat{a}^\dagger\right]\hat{n}$$

Akin to how position and momentum provides the state of a classical particle, $\hat{p}$ and $\hat{q}$ represent the phase-space of light. These relate with the amplitude and phase of the field. The commuting relation: $[\hat{q}, \hat{p}] = i\hbar[\hat{a}, \hat{a}^\dagger] = i\hbar$, points towards an uncertainty in knowing both aspects of the field at the same time – we can either measure its amplitude or its phase with precision.[40] This uncertainty ties to vacuum fluctuations and the concept of 'squeezing'. In this optical phase-space, Wigner functions classify states of light into two broad camps: Gaussian and non-Gaussian. While traditional sources house Gaussian features, non-classical states can have non-trivial features such as a negative quasi-probability distributions, examples of which are Fock states. Turns out, that these novel forms of quantum light find themselves as useful resources for all-optical universal quantum computing.[29]

Generally, a multi-mode, multi-photon [16, 13] state (which can be entangled [155]) can be quite complicated to digest. Indeed, highly coupled many-body states of light can showcase a solid-like crystallization and fluid-like hydrodynamic behaviour.[27, 75] Photons in a medium can also attract, repel, and whilst donning an effective mass, form 'molecules'![29]

One Atom ... Many Atoms – Immersed in the Same Electromagnetic Field

A material-interfacing ought to aid in a study and application of the diverse and relatively unexplored forms of light.[74] Atomic ensembles, for instance, can engender interactions between photons. With their nonlinear response [198, 266], one can envision a variety of quantum optics protocols – allowing one to change, store and source light. Photon-photon coupling in three-level ladder [Ξ] and $\Diamond$ energy level schemes can be used for cross-phase modulation [78] and frequency conversion, [222, 226, 232] respectively. Another example of the technological relevance of collective states of atomic ensembles is the storage of photonic quantum information as quantum memories.[93, 95, 96, 97, 65, 102, 79] A brief depiction is shown in [Fig. 1.2] where a photon can

be translated into collective atomic resonances. Using Λ-type three-levels in atoms, a few protocols have been realized to transfer a photonic quantum state onto atomic ensembles. While one arm of the transition is used as a control, the other arm translates the quantum state of light onto the atomic ensemble. These include the DLCZ (Duan–Lukin–Cirac–Zoller) protocol and far-off resonant Raman scheme.[63, 64] Polariton-based protocols (quasi-particles corresponding to the coupled excitation of matter and light) have also been proposed to implement quantum memories.[93] In addition, atoms can also act as single photon sources [31], entangled photon sources and photon subtractors. For instance, a double-Λ [202, 105] [Fig. 1.3] level scheme has been suggested for photon-pair generation, and, a ladder [Ξ] scheme might be suitable for heralded single photon subtraction.
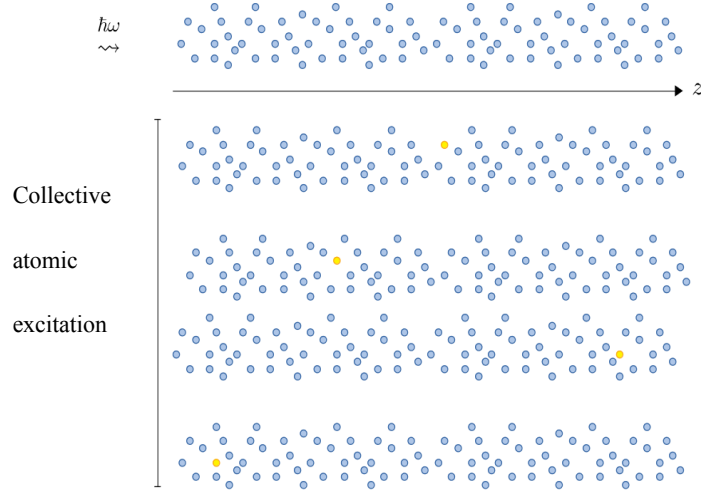
Figure 1.2: A single quantum of excitation can be shared among many atoms. Dynamics of collective states can only be followed along as a whole, as contrasted to evolving the state of each atom individually.

Conversely, a reliable interface also ought to help us study fundamental properties of a collection of atoms and its interaction with light – such as their shared resonances and radiative properties.[103, 104, 105] Spaces of collective states allude to themes of wholeness [30] and the Ship of Theseus' paradox that 'the sum is more than its parts'. Interestingly, in analogy to light, ensembles of two-level atoms can also be talked about using harmonic oscillator algebra. Represented by 'collective operators': $\hat{X}$ and $\hat{P}$, the ensemble shares a one-to-one mapping with $|\Psi\rangle$.[88, 61] Also analogously, there exist non-classical, non-Gaussian and entangled states of ensembles which seem to find themselves as useful tools for information processing.[67] In addition, squeezing and matter-wave interferometry allows collective quantum states to be very sensitive – possibly proving amenable to applications such as gravitational wave metrology.[91]
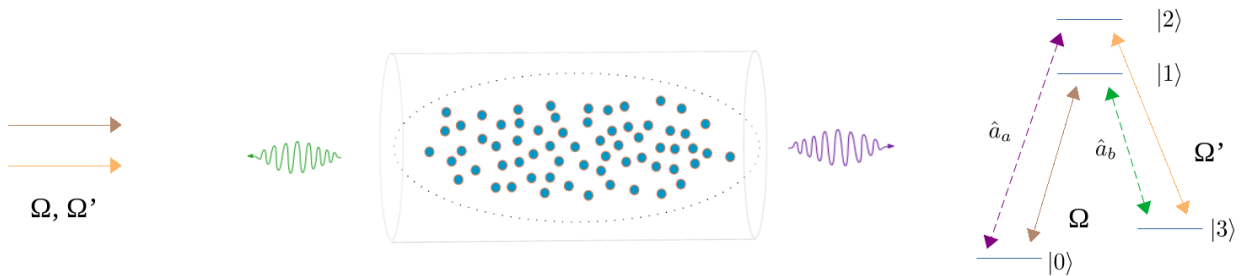
Figure 1.3: As suggested in Ref.[105], when laser lights (represented by brown and orange arrows) are appropriately applied on a double-Λ energy level scheme of an atomic ensemble, entangled photon pairs (represented by purple and green arrows) can be generated from vacuum!

1.2   Overview of Thesis Content

→ In Chapter 2, the effect of light energy on atomic motion is briefly reviewed. Within certain approximations, atomic movement might be specified as point-particles moving in a potential landscape. By conveying the ODE

of particle dynamics on parallel processors, one can follow millions of atoms in 3D potentials.

→ In Chapter 3, the experimental set-up of loading gravity-assisted atoms into hollow fibers [Fig. 1.4 a)] is numerically re-created. These simulations are used to explore different initial conditions of the experiment. The number of atoms making their way into the hollow fiber depends on the magneto-optically trapped cloud's size, positioning and temperature along with laser power and detuning. Loading estimates using a red-detuned dipole beam and a blue-detuned hollow-beam tunnel which provide analytical potentials are presented. This computation allows us keep a log of their time of entry into the fiber, trajectories within the hollow space along with features of the loaded atomic ensemble. Also, comparisons with reported experimental and numerical results are presented.

→ In Chapter 4, adapting an existing model, a preliminary analysis of single photon wavelength conversion using atomic ensembles in hollow optical fibers is presented. A packing of atoms inside the hollow fibers can create a 1D nonlinear medium. This nonlinearity, attributed to the electronic coherences of the atoms, can birth a photon of newer frequency given an input photon. The ◊-energy level scheme in Cs atoms can connect the input and signal fields, which can be treated via coupled-wave equations. The main interest is to see how efficiently and noiselessly can conversion take place, and how this translates into the requirements of applied field parameters and the optical depth of the atomic medium.

→ In Chapter 5, electromagnetic properties of 2D photonic crystal membranes are briefly discussed with the intention of understanding atomic motion [Fig. 1.4 b)] in such an optical environment. First, the allowed modes and transmission spectra for plane-wave fields are presented. And, larger region simulations grants us scattered radiation when Gaussian fields are incident.
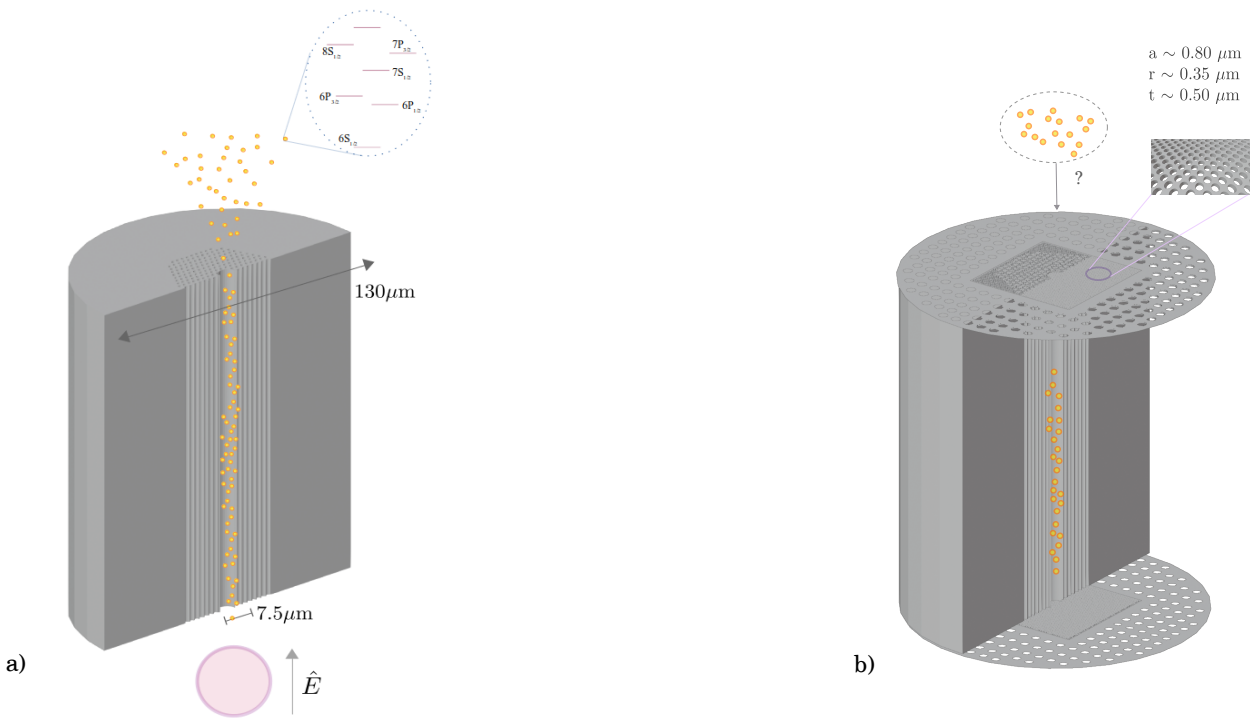
Figure 1.4: a) Schematic of herding and interacting with atoms inside a hollow ∼7 μm waveguide. b) Schematic of a hollow fiber capped with 2D photonic crystal membranes.

→ Statement of Contribution:

With the aim of studying motion of many atoms in optical environments, I've tried to write preliminary parallel programs; using which loading into hollow-core fibers is estimated in a couple basic scenarios.

I've tried to contribute to the analysis of using atomic ensembles in hollow fibers for wavelength conversion; and study introductory electromagnetic properties of photonic crystal membranes. These involve adapting existing literature and methods to the setups of experimental interest.

1.3 Strong Light-Matter Interactions

Our main concern is to interface atomic ensembles and light without wasting or losing photons. That is, each given photon ought to be involved with the arranged atomic transitions. This is parametrized by the optical depth (OD), which is a measure of the opacity of the medium. For a single atom, one might picture it as the overlap between the optical mode area and the scattering cross-section [Fig. 1.5] of an atom. The optical mode area can be reduced using a lens. As an example, if we focus a laser beam resonant to a spot size of $d = \sim 100$ μm, we find that $P_{interaction} \sim 0.01$ % (for a wavelength $\lambda \sim 1$ μm).

$$\sigma_{cross} \approx \frac{3\lambda^2}{4\pi} \longrightarrow P_{interaction} = \frac{\sigma_{cross}}{A} \sim \frac{\lambda^2}{d^2}$$
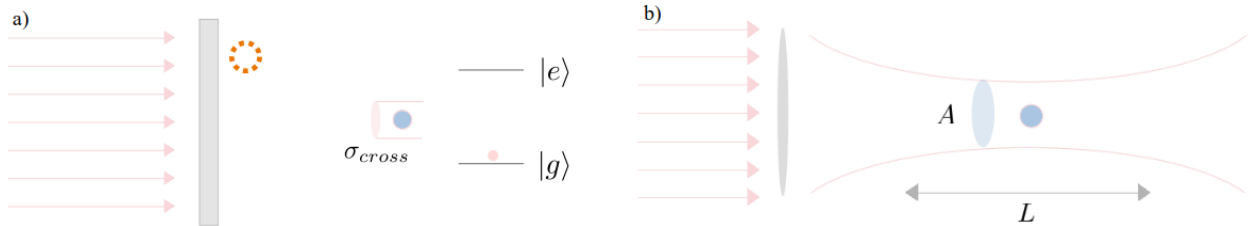
Figure 1.5: a) Photon plane-waves can give a 'click' on a detector, which is uniform across its area. It is suggested that atoms only respond to light incident upon its cross-section area $\sim \sigma_{cross}$.[33] b) One way to transfer this energy from light onto the atom is to focus it using a lens.

To increase $P_{interaction}$, one can add more atoms and thereby, increase the likelihood of absorbing a single photon. Transmission through a sample as suggested by Beer-Lambert's law scales with the number of particles as: $\exp(-k\text{OD})$, where $\text{OD} = NP_{interaction}$ (with k being a constant). Although, the Rayleigh length (L), associated with a traditional focusing, limits the number of atoms we can gather and talk to strongly.[265] If hypothetically, this length can be extended, a photon can see a long train of atoms to talk to.[Fig. 1.6]
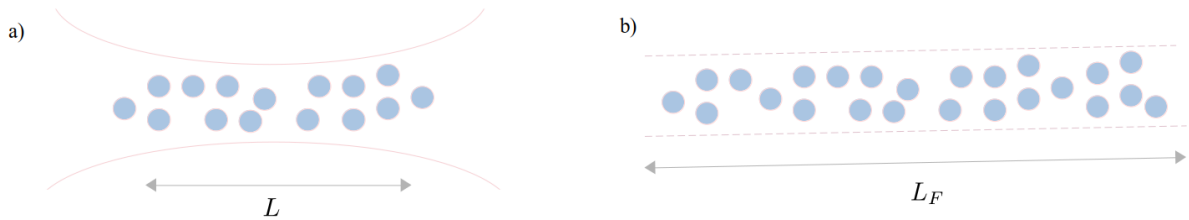
Figure 1.6: a) Interaction probability when many atoms are placed at a focusing spot of a laser beam. Naively, interaction of a photon with many-atoms scales increases with the number of atoms. Diffraction-limited focusing in free-space limits the number of atoms one can significantly interact with. b) In a non-diffracting mode, light can see an extended collection of atoms ($L_F > L$). Thereby making photon-level light interact with the medium.

1.4 Atomic Ensembles Inside Hollow-Core Fibers

[Fig. 1.6 b)] can be realized with the use of hollow optical fibers.[68] Traditional optical fibers allow for a low-loss transport of light due to total internal reflection between the core and cladding: $n_{core} > n_{cladding}$. Hollow fibers can also guide light, albeit by different guiding mechanisms as their core has a refractive index of 1.

[Fig. 1.8] illustrates the allowed modes when a hollow region is surrounded by a lattice of holes etched in silica. Such a reflection mechanism is attributed to the photonic band-gap (PBG) effect – (The same band-gap idea as in the case of solid-state materials [Sec. 5.1]). In addition to PBG guidance, hollow fibers: such as anti-resonant, Kagome and inhibited coupling (IC) fibers [70] allow for channelling light through their core.

To interact with the energies of Cs atoms in the wavelength ranges of $\sim$800 - 900 nm [77] and/or $\sim$1300 - 1400 nm, [70] the following two types of fibers are considered – $\sim$7 μm (core diameter) PBG fibers to interact with the former range and $\sim$30 μm IC hollow fibers to interact with both the optical and telecom wavelength ranges.

These are shown in [Fig. 1.7]. Contrasted to the involved design of the PBG fiber, the inhibited coupling fiber houses a simpler design.
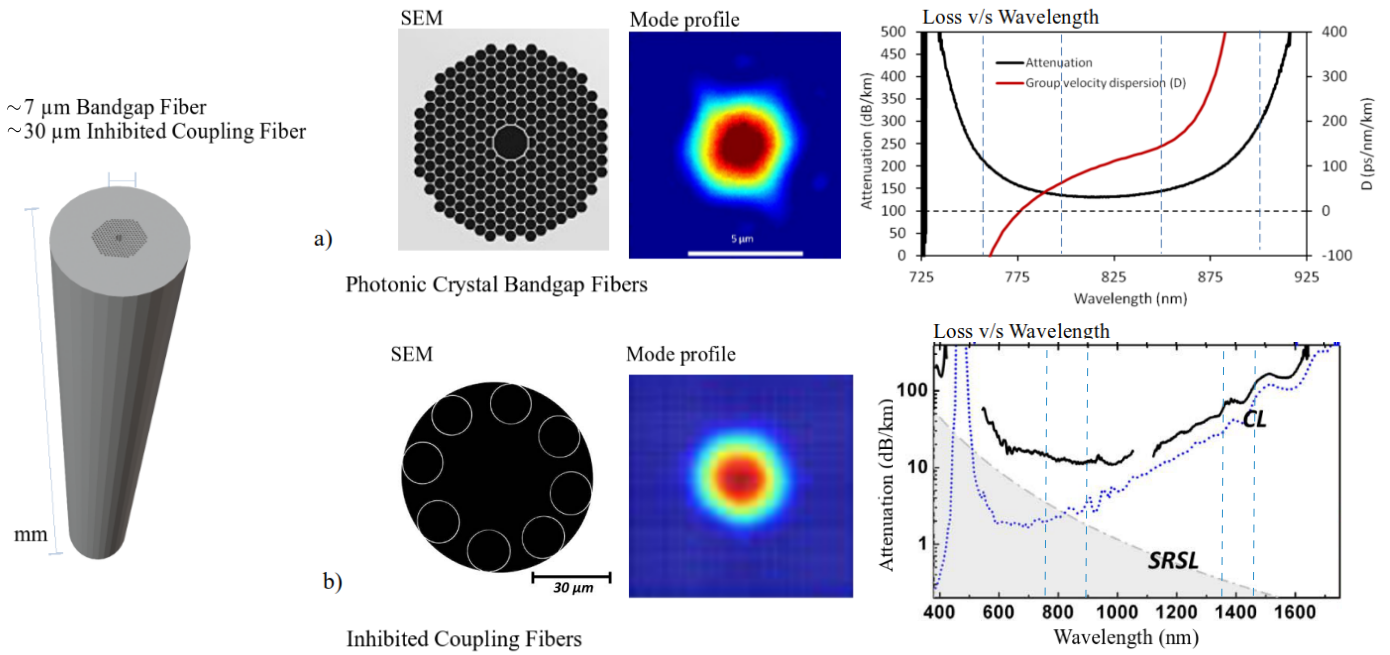
Figure 1.7: The two-types of hollow optical fibers being considered. A scanning electron microscope image of the fiber face with its mode profile, and guiding wavelengths (the dashed vertical lines correspond to Cs wavelengths of interest [Fig. 4.3]) for a) a $\sim 7\mu m$ diameter photonic crystal band-gap fiber (Adapted with permission from NKT Photonics Inc: [77]) and b) a $\sim 30\mu m$ diameter inhibited coupling hollow fiber. (Adapted with permission from [70] ([Fig. 5 b), d)] and inset of [Fig. 6 a)]) © The Optical Society.) For a) the mode profile refers to its near-field intensity [77] and b) shows a reconstructed mode based on S^2 imaging of a $\sim 30\mu m$ fiber.[70] In b), The dotted blue and black lines in the attenuation curve correspond to calculated and measured attenuation values, respectively.
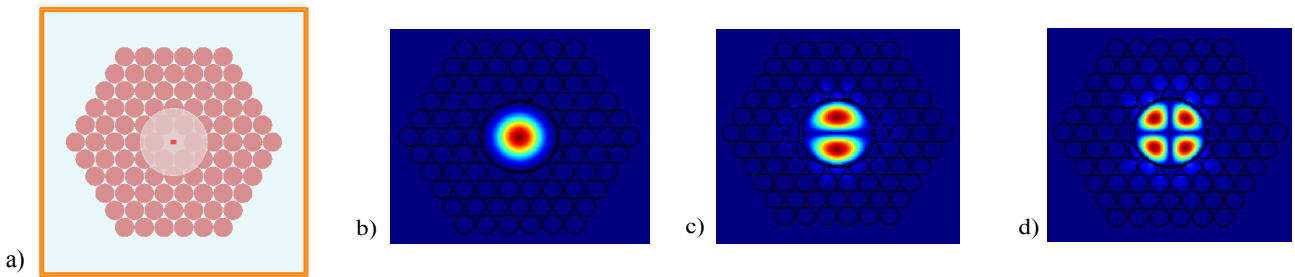
Figure 1.8: a) Simulation region, as defined in the Lumerical MODE solutions software package [262], in order to (roughly) replicate the geometry of a ~ 7 μm hollow fiber shown in [Fig. 1.7 a)]. b), c) and d) show the fundamental and higher-order modes – which share features with the LP_{00}, LP_{01} and LP_{11} modes of cylindrically-symmetric step-index fibers.

Atomic ensembles inside the fiber can be used to study many of the above mentioned protocols and aspects of light-matter interaction – and allow for a miniaturization of quantum optics setups.[145] Also of interest, is the low-energy footprint of such a device.[86] Due to their confined modes, hollow-cores require lower light powers compared to the same situation in free-space.[Fig. 1.9]

Already, such fibers loaded with laser-cooled atoms have been in used in the exploration of a variety of quantum phenomena, such as nonclassical properties of matter [81, 80, 82, 83, 84, 87], photon-level optical nonlinearities [85], and photon storage.[79] Interestingly, Ref.[82] comments about the creation of quantised motional states within the fibers and Ref.[87] mentions alludes to the possibility of creating Bose-Einstein condensates in the fibers. And, proposals have been put forth for using hollow optical fibers to create strong non-linear mediums

allowing for an observation of phase-transitions of light within them.[75, 76] Also of interest, is to arrange atoms within this space. As suggested in Ref[87], creating one-dimensional lattices, or even three dimensional configurations of atoms within their hollow space adds to the kinds of many-body atom-light dynamics that can be studied.
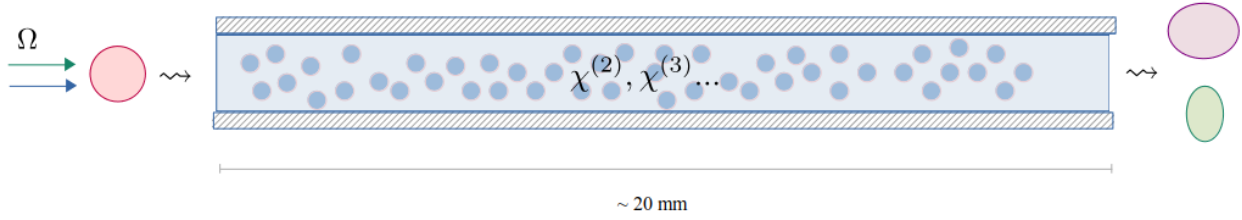
Figure 1.9: Classical light fields (Ω), represented by coloured arrows, can prepare atoms into different electronic coherences, granting the ensemble nonlinear optical properties. This can effect light transport at the photon level – as mentioned to in [Fig. 1.6]. Hollow-core fibers, due to their small mode areas also reduce the power requirement of the applied classical fields.

1.5 Coupling Atoms to Nanophotonic Structures

These micro-structured fibers can be contextualized in the emerging paradigms of engineering atom-light interactions: namely, cavity QED (quantum electrodynamics) and waveguide QED.[20, 21, 22] [Fig. 1.11] By trapping light between mirrors and creating nm-scale streams for light to flow in, a stronger interaction with atomic energies can be achieved. Their spatial confinement of the modes are mentioned via modal volume and effective area, which determine the strength of atom-light coupling.
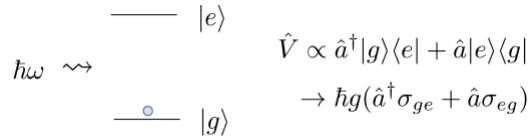
Figure 1.10: An incoming photon can interact with the atom via absorption and emission, which is usually thought of using the dipole approximation and a rotating wave approximation.[127, 37] At the quantum level, field and atomic operators mingle, parameterized by g, the coupling constant.
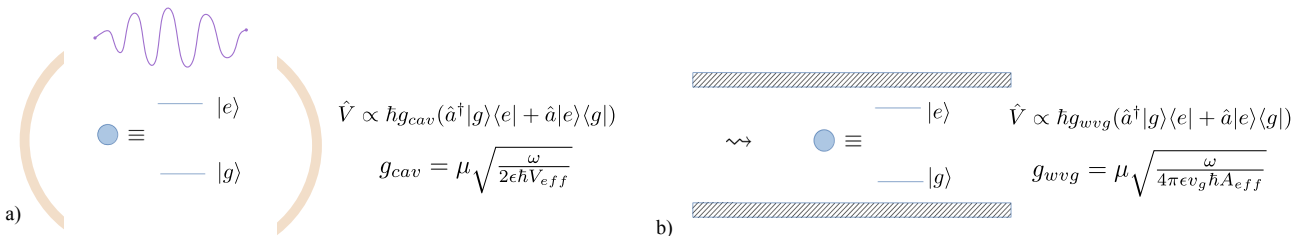
Figure 1.11: a) By tuning mirror reflectivity and cavity size, and by b) creating small channels of light, we can realize different kinds of atom-light interactions. The former allows quantised confined modes and the latter, narrow travelling fields. A definition for A_{eff} is provided in Pg. 29.

In the case of waveguides, incorporating a preferential coupling (g_{wvg}) to their modes shows a 'competition' between the free-space emission and emission confined by the structure. Parameters such as β, D allow us to roughly categorize systems based on their single-photon interaction probability P and its chirality. β is a the fraction energy from an excited atom is transferred to a waveguide: $\frac{\Gamma_{wvg}}{\Gamma_{total}}$, where Γ is the spontaneous emission rate; and D refers to the directional nature of photon emission from the emitters. Hollow-optical fibers, while

reducing mode-areas, don't appear to morph spontaneous emission rates as much as nano-scale waveguides. Sitting in an intermediary space from free-space to nanophotonics, their hollow spaces can accommodate more atoms. The table below shows examples of systems where quantum emitters such as quantum dots or atoms can be coupled to waveguides: such as optical fibers, nanobeams and photonic crystal waveguides (PCW), along with rough parameters associated with them.

D in %	β in %	A_{eff} (μm^2)	System	Geometry specifications (nm), N_{atom}
–	~0.1[267]	~20	Hollow Fibers with Cs	~ 7000 diameter, $N_{atom} \sim 10^4$
~92(8)	~20 [23],b)	~2	Nanofiber with Cs [23],a)	500 diameter, $N_{atom} \sim 200$
~99(1)	70		Nanobeam with QD [25]	280 width, 140 height
–	98	–	GaAs PCW with InAs QD [24]	–
~90(10)	98	–	GPW PC with In(Ga)As QD [25]	70 radius, ~250 gap, 160 thickness
–	~25	~0.2[268]	APCW PCW with Cs [90, 151]	200 gap, 350 feature size, $N_{atom} \sim 1$

It might also be possible to further increase photon ensemble interactions by creating a cavity around hollow fibers – as shown in [Fig. 1.4 b)]. Refs: [72, 71] explore the place of such a system given figures of merit relevant for cavity QED systems such as: single-atom cooperativity, finesse and loss-rates.

More generally, venturing into the nanoscale [143, 144, 148, 149] allows for novel interfacing of atoms to materials. Their electromagnetic field mode-structure or photonic bath can be tuned – in both the near and far-fields. Contrasted to single atoms placed in free-space, cavity and waveguide modes, an atom here can see quite a different field-space.[249, 250, 251] For instance, these can provide for an enhancement, suppression and a change in spontaneous emission rates [248, 253], long-ranged interactions [249], and have been used to tune the directionality [11, 14, 15] of emission (noted in some of the systems above). Additionally, understanding this design-space provides for symmetry-protected interactions which can be robust to fabrication errors.

Chapter 2

Modelling Atomic Dynamics

Atoms, being the tiny units of natural magic they are, need to be delicately herded into places where we can interact with them. After quietening the buzz of a room-temperature cloud of atoms in vacuum, one may guide them to their destined locations. Such cooling and placement has been made possible by designing fields of light. Functionalities have matured to such an extent that it is now possible to form ultracold (nK) condensates [107], to make creative videos with single atoms [108], and to form custom 1D [109], 2D [110] and 3D [111] lattices separated by $\sim \mu$m [112] with about a hundred atoms singly occupying each site. A finer interaction with individual atoms is being made possible by placing them in and around μ-nanophotonic structures.[143, 144, 145, 146]

Chapter Overview: Here, we are interested in quantifying the movement of ^{133}Cs atoms [Fig.2.1] so that one may assess loading scenarios into a hollow fiber via simulations. Firstly, basic expressions for optical dipole forces are briefly contextualized and reviewed. Next, conditions which allow us to treat atoms as moving point-particles are mentioned. Stepping aside the matter-wave nuance of atoms, numerical integration of atomic trajectories in analytical potentials is briefly discussed. As experiments start out with $\sim 10^8$ atoms, a preliminary attempt to parallelize the simulation is presented.

2.1 Describing Motion of Atoms in Light

Light's energy can make matter move – wherein amplitude, phase and polarization of lights can be tuned to provide linear and angular momentum [113] to particles – even at the level of single quanta of motional energies. While motion of charged particles in electromagnetic fields appear to be more readily digestible, experiments (since the 1970s) on neutral atoms have demonstrated the deflection of alkali atomic beams by near-resonant light along with a damping of their motion to form atomic molasses – forming the ground upon which a variety of laser cooling and trapping protocols have been developed.[131, 121]

As a brief overview-prelude, it might be instructive to revisit the issue of the motion of (non-relativistic) 'wave-particles'. Given a frame of reference, on the one hand, we have intuitive and precise trajectories along which particles move at varying rates in time, and on the other, we have a seemingly non-trivial language of quantized matter waves in a non-commutative space to paint their dynamics. Formalisms such as Newton's and Hamilton's ordinary differential equations, Hamilton-Jacobi's partial differential equations [114] and Lagrange's variational calculus (principle of least action) [129] seem to provide equivalent, yet ontologically different perspectives to talk about the former. As a bridge to the latter, relations in analytical mechanics are seen to be analogous to the movement of light rays in geometric optics (Fermat's principle of least time) and Huygen's wavefronts.[129, 126] This connection informed the ideas of de Broglie and eventually Schrodinger [128, 130] to endow matter with wave-like properties of interference [133, 134] and diffraction.[140, 141, 142] In addition, the path-integral formalism's generalization of the Lagrangian and de Broglie-Bohm theory's quantum potential provide further viewpoints to talk about motional quantum dynamics.

Here, we follow the Hamiltonian formulation to infer forces on atoms. Hamiltonian, a function corresponding to the total energy and time-evolution of a system, is introduced as an operator, $\hat{H}$, in quantum theory's governing differential equation.[115, 273] An example of its solutions being the discrete atomic spectra of Hydrogen-like atoms [Fig:2.1 b)]. Often implied in such an approach is a separate treatment of electronic and nuclear degrees of freedom.[116] Due to the mass of nuclei, atoms are followed along by their centre of mass – while wave-like resonances are used to describe electronic energies. Although, nuclear kinetic energy can be incorporated via

the momentum operator: $\hat{p}_n = -i\hbar\nabla_n$. With the kinetic energy terms, $\hat{H}$ – for a Hydrogen-like atom – in the presence of an external electromagnetic field can look like:

$$\hat{H} = \frac{\hat{p}_n^2}{2m_n} + V_n(\vec{r}_n) + \underbrace{\frac{\hat{p}_e^2}{2m_e} + V_e(\vec{r}_e)}_{\hat{H}_{atom}} + \hat{H}_{field} + \hat{H}_{atom-field} \approx \frac{\hat{p}_n^2}{2m_n} + \cancel{V_n(\vec{r}_n)}^{0} + \hat{H}_{atom} + \hat{H}_{field} + \hat{H}_{atom-field}$$

That is, the total energy of an atom-plus-field system includes the motional and potential energy of the electron-nuclear system, along with the energy in the field and the atom-light interaction energy. On the atom side of things – introducing position and momentum operators: $\{\hat{p}_n, \hat{r}_n\}$, provides for a qualitatively different phase space for particles [117]. And, considering the electromagnetic field ought to properly invoke the role of quantized radiaition fields, including the quantum vacuum, and its interaction with the atom. Following such dynamics appears to be quite nuanced.[118]

Although, when two energy levels of atoms and simple classical light fields are considered, some canonical ideas concerning the equations of motion for atoms and their physical interpretation have emerged. These, as re-presented below, can be gathered from review literature and texts such as Refs.[123, 120, 121, 124, 122, 4]. Particularly, (to some extent) in terms of light absorption, emission (spontaneous and stimulated) and the Doppler effect – one might interpret how dissipative, conservative, viscous and momentum diffusion forces upon atoms can come to be. Multi-level atoms and additional degrees of freedom such as polarization of light add to the kinds of optical forces.

In order to derive these, we restrict ourselves to describe the energetic movement between fields and atoms in two steps. First, $\hat{H}_{interaction} = \hat{H}_{atom-field}$ can be used to evaluate the electron's interaction with the electromagnetic field. In the absence of an external potential directly affecting the nucleus, $V_n(\vec{r}_n) \to 0$, $\hat{H} = \hat{H}_o + \hat{H}_{interaction}$, where $\hat{H}_o = \text{KE}_n + \hat{H}_{atom} + \hat{H}_{field}$. From this, (mean) forces on the atomic centre can be estimated via Ehrenfest's theorem. Alternatively, without going into the subtleties, some aspects of these forces can also be viewed by considering a neutral atom as a small classical dipole.[125, 4, 120, 49]
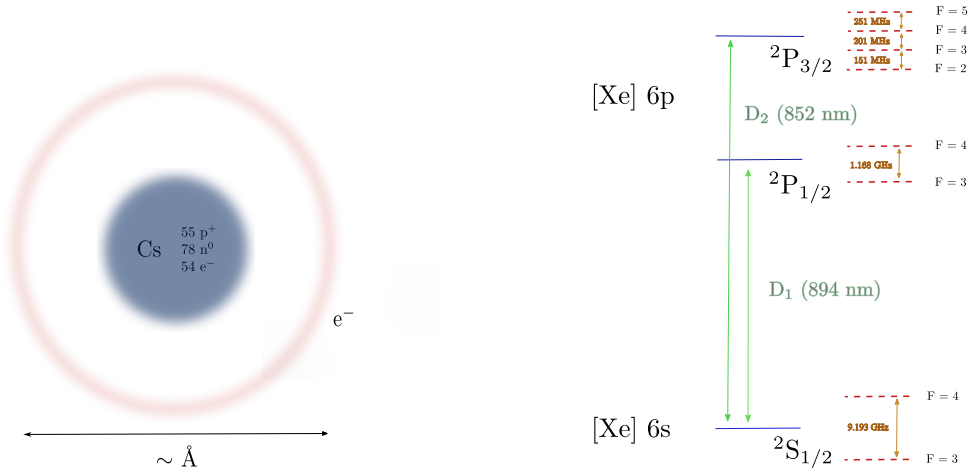
Figure 2.1: a) Cs nucleus contains 55 protons and 78 neutrons, amounting to a rest mass of $\sim 2.206 \times 10^{-25}$ kg. As an alkali metal in the sixth row, 54 of its electrons form a stable core [Xe] with a lone valence electron in the $6s$ orbital providing for its electronic properties. The sixth shell of single electron wavefunction can be associated with an Å level length scale, which is of the same order of magnitude as van der Waals and atomic radii of Cs. b) A spin-orbit fine structure split of the [Xe] 6p orbitals as D_1 and D_2 lines in Cs. Electron and nuclear spins interact to provide a hyperfine structure.

2.2 Potential Landscapes with Dipole Optical Forces

Atom as a two-level system interacting with classical fields

A classical electromagnetic field interacts with the charges of an atom. Two of the atom's energy levels resonant at an angular frequency ω_{eg}, are represented by: $|g\rangle$ and $|e\rangle$ [Fig:2.2] (of interest here, are the states linked by D_1 and D_2 lines in the Cs atomic structure [Fig:2.1]). This interaction is usually pictured via a dipolar coupling between the incident field's energy and the valence electron-nuclear charge system.[4, 122] That is,

$\hat{H}_{interaction} = -\hat{d} \cdot \vec{E}$, where $\hat{d} = q_e\hat{r}$ is the dipole moment operator. A linearly polarized (along some direction $\hat{n}$) electric field at the position of the atom is expressed as: $\vec{E} = \vec{E}_+ + \vec{E}_- = \frac{E_0}{2}(e^{i(\omega't+\phi)} + e^{-i(\omega't+\phi)})\hat{n}$. And, a rotating wave approximation [4, 119] allows us to write: $-\hat{d} \cdot \vec{E} = -\frac{\hbar|\Omega|}{2}(\kappa|g\rangle\langle e| + \kappa^*|e\rangle\langle g|)$ [269], where $|\Omega| = \frac{\mu_{eg}E_0}{\hbar}$ is the (real part of) Rabi frequency, $\mu_{eg} = |\langle e|\hat{d}|g\rangle|$ is (amplitude of) the transition dipole matrix element and κ accounts for the complex exponential terms of the field and the dipole matrix element (ϕ_d): $e^{i(\omega't+\phi+\phi_d)}$. For this approximation, the applied fields are assumed to be close to resonance. ϕ_d is assumed to be set [4] such that the matrix representing atomic and interaction energies can be written as:

$$\hat{H}_{atom} = \hbar \begin{pmatrix} 0 & 0 \\ 0 & \omega_{eg} \end{pmatrix} \qquad\qquad \hat{H}_{interaction} = \hbar \begin{pmatrix} 0 & \frac{|\Omega|}{2}\kappa \\ \frac{|\Omega|}{2}\kappa^* & 0 \end{pmatrix}$$

$$E(r_{atom}, t, \phi) = E_0 cos(\omega't + \phi)$$
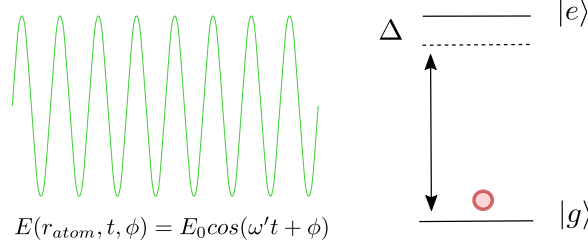
Figure 2.2: At the location of the atom, a monochromatic field interacts with the electronic states of the alkali atom. ω is the angular frequency of the transition, and the incident field is detuned by $\Delta = \omega_{eg}$ - ω'.

For the Hamiltonian, $\hat{H}' = \hat{H}_{atom} + \hat{H}_{interaction}$, time evolution of the wavefunction $|\psi(t)\rangle$ is given by Schrodinger's equation, which can also be written in terms of the density matrix, $\rho(t) = |\psi(t)\rangle\langle\psi(t)|$, as:

$$\frac{d|\psi(t)\rangle}{dt} = -\frac{i}{\hbar}\hat{H}'|\psi(t)\rangle \longrightarrow d_t\rho = -\frac{i}{\hbar}[\hat{H}', \rho]$$

As mentioned in Ref.[4], effects of the environment are phenomenologically included. Decay and dephasing terms correspond to the loss of superposition and decoherence of the superposition in the electronic wavefunction: $|\psi\rangle = c_g|g\rangle + c_e|e\rangle$, respectively. $\hat{D}$ is considered via: $\gamma_\perp$(dephasing rate) $= \Gamma/2 + \gamma_c$, where Γ is the spontaneous emission rate and $\gamma_c \to 0$ relates with dephasing due to collisions. Contribution from the Langevin noise terms ($\hat{\mathcal{F}}$) are not considered. They however, play a role in 'momentum diffusion terms'.[122] With this, one obtains the following temporal dynamics of the electronic wavefunction:

$$\dot{\rho} = -\frac{i}{\hbar}[\hat{H}', \rho] - \hat{D} + \hat{\mathcal{F}}$$

Shifting to a rotating frame ($\rho \to \widetilde{\rho}$, $|\psi\rangle\langle\psi| \to \hat{R}|\psi\rangle\langle\psi|\hat{R}^\dagger = \hat{R}\rho\hat{R}^\dagger$, where $\hat{R} = \begin{pmatrix} 1 & 0 \\ 0 & e^{i\omega't} \end{pmatrix}$) makes $\hat{H}_{interaction}$ time-independent: $\widetilde{\hat{H}}_{interaction} = \hbar \begin{pmatrix} 0 & \frac{|\Omega|}{2}e^{i\phi} \\ \frac{|\Omega|}{2}e^{-i\phi} & \Delta \end{pmatrix}$. The atomic state evolution equations, also referred to as the optical Bloch equations (which also apply for electron spins in magnetic fields), now take the form: ($\Omega \to |\Omega|\,e^{i\phi}$)

$$\dot{\widetilde{\rho}}_{gg} = \frac{i}{2}(\widetilde{\rho}_{ge}\Omega^* - \widetilde{\rho}_{eg}\Omega) + \Gamma\widetilde{\rho}_{ee} \qquad\qquad \dot{\widetilde{\rho}}_{ge} = (i\Delta - \gamma_\perp)\widetilde{\rho}_{ge} + i\frac{\Omega}{2}(\widetilde{\rho}_{gg} - \widetilde{\rho}_{ee})$$

$$\dot{\widetilde{\rho}}_{eg} = (-i\Delta - \gamma_\perp)\widetilde{\rho}_{eg} - i\frac{\Omega^*}{2}(\widetilde{\rho}_{gg} - \widetilde{\rho}_{ee}) \qquad\qquad \dot{\widetilde{\rho}}_{ee} = \frac{i}{2}(\widetilde{\rho}_{eg}\Omega - \widetilde{\rho}_{ge}\Omega^*) - \Gamma\widetilde{\rho}_{ee}$$

$\widetilde{\rho}_{ee}$, $\widetilde{\rho}_{gg}$ provide us the population of the levels ($\widetilde{\rho}_{ee} + \widetilde{\rho}_{gg} = 1$) and $\widetilde{\rho}_{eg}$ tells us about their coherence (superposition) between the levels. The latter term, as briefly mentioned in Pg.16, relates with the optical response of a two-level atom. These equations can be integrated numerically.[217] As an example, [Fig.2.3] shows the temporal dynamics of the population terms with and without Γ ($= 2\pi \times 5.23$ MHz) when incident light with $\Omega = 5.23$ MHz is on-resonant to a Cs atom's D_2 line.

In the steady-state condition, time evolution of density-matrix terms can be set to zero, i.e. $d_t\widetilde{\rho} \to 0$, and the atomic state can be inferred as: (assuming $\phi \to 0$) [124, 123]

$$\widetilde{\rho}_{eg} = \frac{i\Omega(4\Delta^2 + \Gamma^2)}{(\Gamma + i\Delta)(4\Delta^2 + \Gamma^2 + 2\Omega^2)} \qquad\qquad \widetilde{\rho}_{ee} = \frac{\Omega^2\Gamma}{(4\Delta^2 + \Gamma^2 + 2\Omega^2)}$$
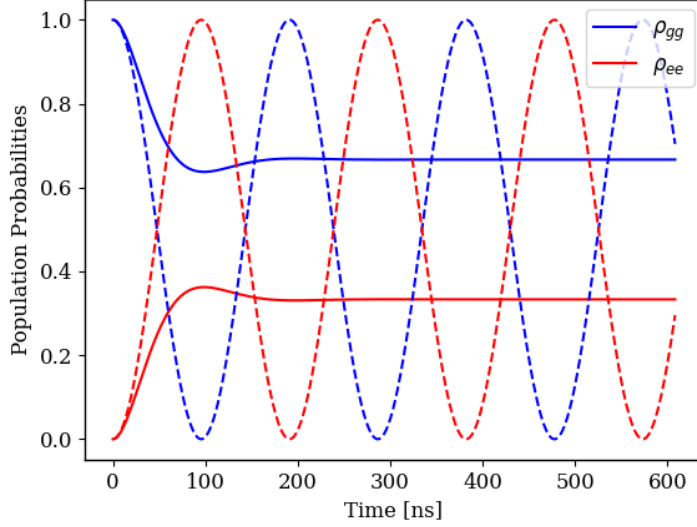
Figure 2.3: Time evolution of the population terms ρ_{ee} and ρ_{gg} with and without (dashed) the inclusion of spontaneous emission Γ. Atoms are initially (at $t = 0$) in ground state $\rho_{gg} \to 1$. Rabi oscillations (dashed) can be interpreted in terms of absorption and stimulated emission. When Γ is taken into account via the Master equation, these oscillations are damped into a steady-state solution.

Given the time-evolved state of the electronic wavefunction, the effect on nuclear motion can brought into the discussion by considering the Hamiltonian: $\hat{H} = \mathrm{KE}_n + \hat{H}'$. For a steady-state wavefunction, Heisenberg's equations of motion for nuclear momentum operators can be evaluated via:

$$\frac{d\hat{p}_n}{dt} = \frac{i}{\hbar}[\hat{H}, \hat{p}_n]$$

This step, brings in the spatial dependence of the field parameters – phase ($\phi(\vec{r})$) and intensity ($\Omega(\vec{r})$) – as the nuclear momentum operator is the gradient of atomic position: $-i\hbar\nabla_n$.

$$\frac{d\hat{p}_n}{dt} = \frac{i}{2}[\Omega(\vec{r})(e^{i\phi(\vec{r})}|e\rangle\langle g| + e^{-i\phi(\vec{r})}|g\rangle\langle e|), \hat{p}_n] \qquad \nabla_n\left[\Omega(\vec{r})e^{i\phi(\vec{r})}\right] = \nabla_n\Omega(\vec{r})e^{i\phi(\vec{r})} + \Omega(\vec{r})e^{i\phi(\vec{r})}\nabla\phi(\vec{r})$$

Then, Ehrenfest's theorem provides us the mean force an atom would experience at each point by taking the expectation of $\frac{d\hat{p}_n}{dt}$. This is sometimes termed the 'quantum' version of Newton's equations of motion: [121]

$$\langle\frac{d\hat{p}_n}{dt}\rangle = \langle\vec{F}\rangle = q_e\langle\nabla(\hat{d}\cdot\vec{E})\rangle \longleftrightarrow \vec{F} = \hbar(\nabla\Omega\rho_{ge} + \nabla\Omega^*\rho_{eg})$$

Here, when considering the incident field to be a plane-wave (assuming $\Omega \to \Omega(\vec{r})e^{i\phi(\vec{r})} \to \Omega e^{-i\vec{k}\cdot\vec{r}}$) the force term, $\vec{F}_{scattering}$ is written as: [120, 124]

$$\vec{F}_{scattering} = \frac{\hbar\vec{k}\Omega^2}{2}\left[\frac{\Gamma}{4\Delta^2 + \Gamma^2 + 2\Omega^2}\right] \qquad \Gamma_{scattering} \sim \frac{3\pi c^2}{2\hbar\omega_{eg}^3}\left(\frac{\Gamma^2}{\Delta^2}\right)I(\vec{r})$$

Shown in [Fig.2.4], when atoms absorb and emit light, one might interpret two momentum transfers taking place. Absorption 'events' provide a momentum transfer of $-\hbar\vec{k}$. Corresponding to which, a (averaged) dissipative force is given by $\vec{F}_{scattering}$. Also, spontaneous emission recoil is suggested to provide a 'momentum kick'.[192] This contributes to a diffusion of atom's momenta. Although, moving away from plane-waves appears to be a bit subtle. Firstly, additional terms to account for spatially varying phase-terms are needed $\phi(\vec{r})$.[137, 138] And as suggested in Ref.[122], momentum diffusion can have 'anomalous' features when an atom, for instance, is placed near a node of a standing-wave field.

On the other hand, while plane-waves don't lend a dispersive force, $\vec{F}_{dispersive}$, a combination of them can lead to a conservative potential which depends on the magnitude of the intensity gradient.[120, 124, 123]

$$\vec{F}_{dispersive} = -\hbar\nabla\Omega^2\left[\frac{\Omega\Delta}{4\Delta^2 + \Gamma^2 + 2\Omega^2}\right] \qquad U_{dipole} \sim -\frac{3\pi c^2}{2\hbar\omega_{eg}^3}\left(\frac{\Gamma}{\Delta}\right)I(\vec{r})$$
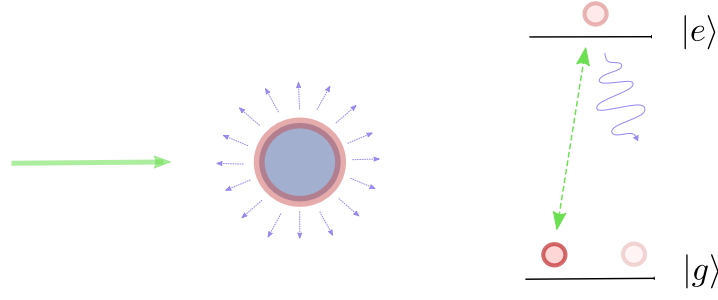
Figure 2.4: In addition to energizing electrons, atoms receive a mechanical push due to absorption. Emission of this energy provides a recoil. A Cs atom absorbing a photon at wavelength 852 nm receives a momentum kick of $\hbar k \approx 7.8 \times 10^{-28}$ kg m/s, which translates to a velocity change of ~ 0.003 m/s. And an acceleration (if interpreted as $\Gamma \Delta v$) $\sim 10^4$ m/s^2.

In addition, depending on the sign of Δ, $\vec{F}_{dispersive}$ can create attractive or repulsive forces. [Fig.2.5] shows how one can form potential wells or hills using intensity gradients. This force can be interpreted as a re-distribution of stimulated emission.[122]
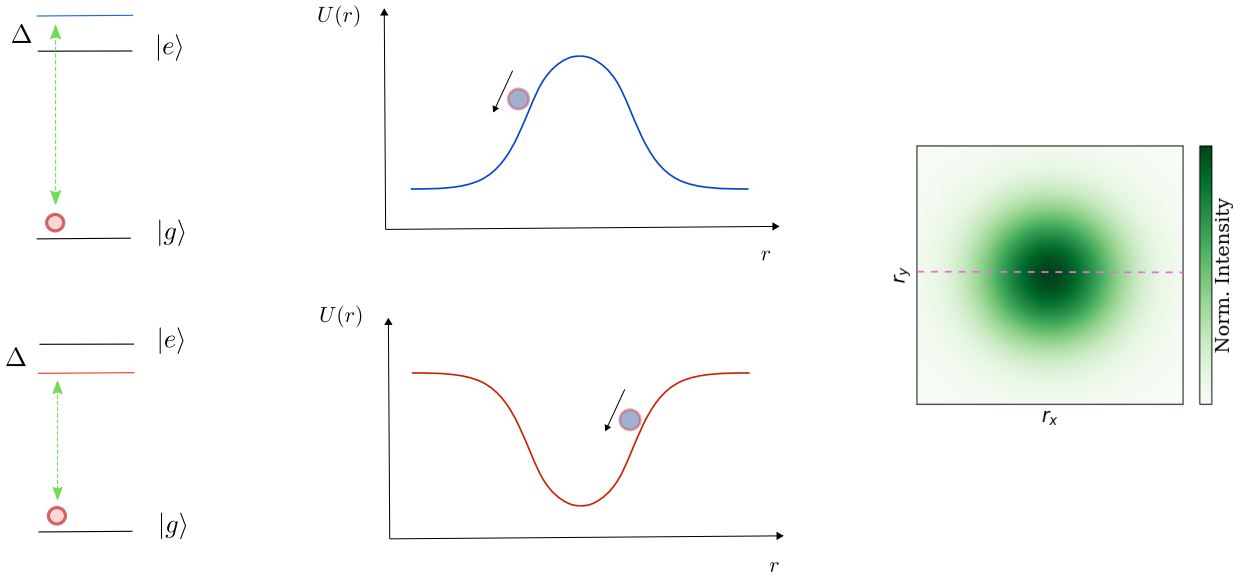
Figure 2.5: Blue-detuned (top) and red-detuned (bottom) light can be used to create intensity-dependent repulsive and attractive forces, respectively. Such a potential, for instance, can be realized along the dotted in a Gaussian field profile.

When light is detuned sufficiently off-resonance, the absorption-emission cycles can be neglected and thus, the intensity gradients mainly contribute towards the force. Although, in this case, the counter-rotating terms which were ignored in the rotating-wave approximation also ought to be considered. Ref.[136] considers this in detail, while here, as suggested in Ref.[120], the following intensity-dependent conservative potential is assumed:

$$U_{dipole}(\vec{r}) = \frac{-3\pi c^2}{2\omega_{eg}^3}\left[\frac{\Gamma}{\omega_{eg} - \omega'} + \frac{\Gamma}{\omega_{eg} + \omega'}\right]I(\vec{r})$$

This potential expression can be generalized to consider the case of multiple atomic energies. For three-level ^{133}Cs (and also, ^{85}Rb, ^{87}Rb atoms), D$_1$ and D$_2$ lines [Fig. 2.1] provide for the following form of the potential:

$$U_{dipole}(\vec{r}) = \frac{-3\pi c^2}{2}\left[\frac{\Gamma_{D_1}}{3\omega_{D_1}^3}\left(\frac{1}{\omega_{D_1} - \omega'} + \frac{1}{\omega_{D_1} + \omega'}\right) + \frac{2\Gamma_{D_2}}{3\omega_{D_2}^3}\left(\frac{1}{\omega_{D_2} - \omega'} + \frac{1}{\omega_{D_2} + \omega'}\right)\right]I(\vec{r})$$

Dressed state perspective

Qualitatively, U_{dipole} can be seen via energy eigenvalues of the combined atom-light system.[Fig. 2.6] While not discussed, this ac Stark shift dressing (when sufficiently off-resonant and of low intensity) [211] can either split

their energy-gap or leave it unaffected. The former kind of dressing is realized when state-insensitive 'magic' wavelengths are used.[176]
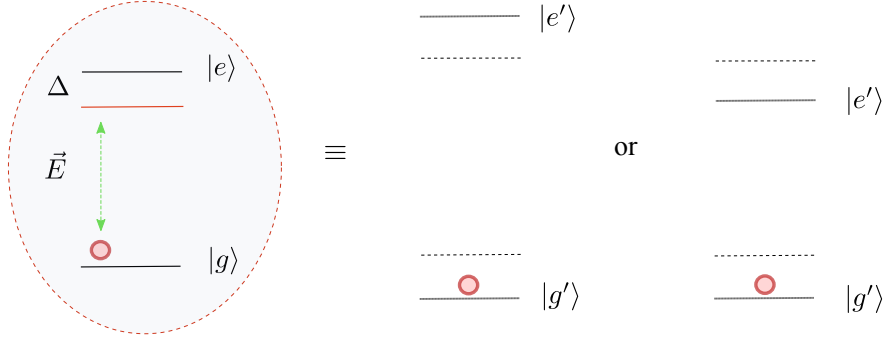
Figure 2.6: Possible dressings of a two-level atom by an off-resonant classical field. Energies of a bare atom are $|g\rangle, |e\rangle$, and energies of the atom-light (dressed atom) are: $|g'\rangle, |e'\rangle$

Atom as a small spring-mass dipole

The derivation noted above might appear somewhat queer as, while spatial dependence of the force comes about due to a quantum mechanical definition of momentum, atoms are eventually treated as particles. Another aspect that doesn't appear readily clear in a dynamical sense is that of spontaneous emission.[270] A more classical picture on the situation is provided via a charged spring-mass model [Fig.2.7]. That is, the electron-nuclear charge system can be viewed as a small dipole.[33, 120] Here, this separation is assumed to be much smaller than the wavelength of radiation – $|\Delta r| \ll \lambda$ – and atomic resonances (ω_{eg}) are thought of as a classical oscillator along with a damping (γ) term: [120]

$$\ddot{r} + \gamma \dot{r} + \omega^2 r = \frac{q_e E(t)}{m_e}$$
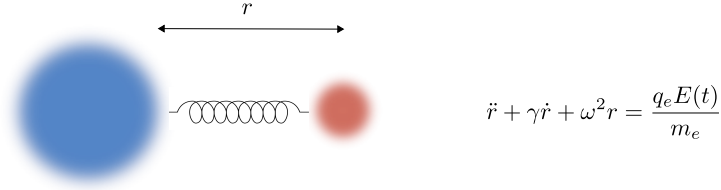
Figure 2.7: The linear part of atomic response can be modelled by a damped spring-mass system.

The incident electric field polarizes the atom: $\vec{d} = q_e \vec{r} = \vec{d}_+ + \vec{d}_-$; $\vec{d}_+ = \alpha \vec{E}_+$, where α (polarizability) can be found by transforming the oscillator equation [Fig. 2.7] into the frequency domain: [120]

$$\alpha_{imaginary} = \frac{q_e^2}{m_e} \left(\frac{\gamma \omega'}{(\omega^2 - \omega'^2)^2 + \omega'^2 \gamma^2} \right) \qquad \alpha_{real} = \frac{q_e^2}{m_e} \left(\frac{(\omega^2 - \omega'^2)}{(\omega^2 - \omega'^2)^2 + \omega'^2 \gamma^2} \right)$$

In this picture, gradient of the dipolar interaction potential leads to the dispersive force (which might gel with the re-distribution of stimulated emission interpretation of $\vec{F}_{dispersive}$ [122]). Upon time-averaging over the oscillations, dispersive force and the associated interaction potential are written as: [125, 120]

$$\vec{F}_{dispersive} = \frac{\alpha_{real}}{4} \nabla E_0^2 \qquad\qquad U_{dipole}(\vec{r}) = -\frac{1}{2} \langle \vec{d} \cdot \vec{E} \rangle_t = -\mathrm{Re}(\alpha) E_0^2$$

Also, as in the two-level model, scattering forces (the factor $\vec{k}$, for plane-waves can be replaced by $\nabla \phi$ for more general phase gradients [125]) on a dipole can be interpreted via an absorption-emission process ($\alpha_{imaginary}$), which is dissipative and corresponds to the mean scattering force. Based on which, a photon scattering rate might be supposed: [125, 120]

$$\vec{F}_{scattering} = \frac{\alpha_{imaginary}}{2} E_0^2 \vec{k} \qquad\qquad \Gamma_{scattering} = \frac{P_{abs}}{\hbar \omega} = \frac{1}{\hbar \epsilon_0 c} \mathrm{Im}(\alpha) I(\vec{r})$$

As elaborated in Ref.[120], these forces relate with in-phase and out-of-phase oscillations of the charges. Polarizability (α) can also be inferred via its density matrix terms: ρ_{eg}, wherein the real part corresponds to the dispersive effects and the imaginary part corresponds to scattering: $\alpha \leftrightarrow \rho_{eg}$. [Fig.2.8] compares these two

models of an atom. While the response of a damped harmonic oscillator is strictly linear, ρ_{eg} terms contain higher-order field dependent terms.
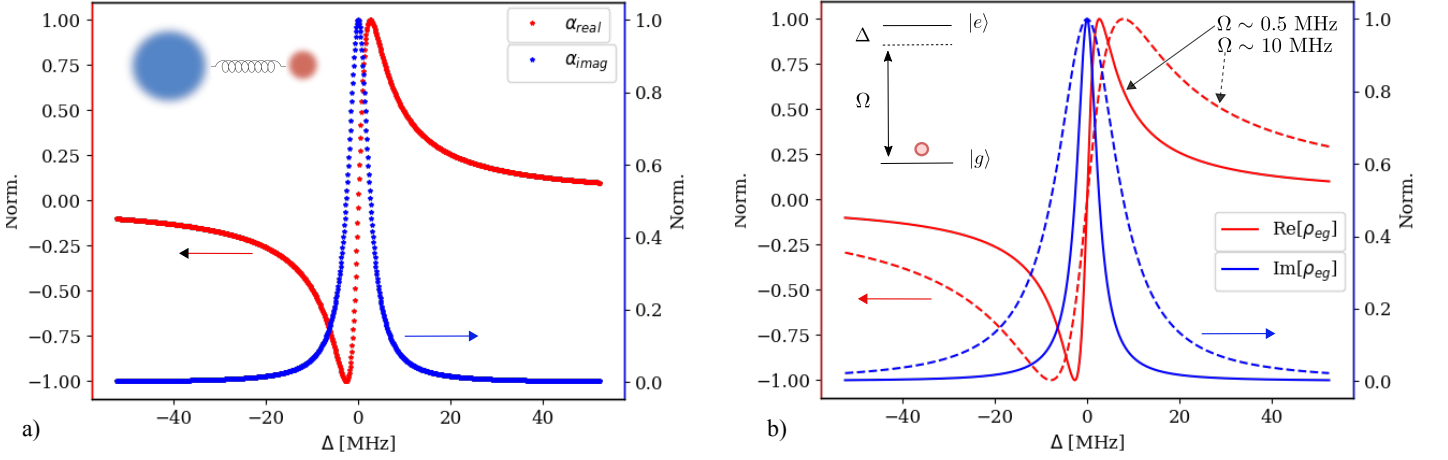
Figure 2.8: a) The real and imaginary part of polarization (normalized) response of a spring-mass dipole. b) In relation, real and imaginary part of the coherence terms in ρ_{eg} (obtained using [217]) of an atom point towards absorption and dispersion. A difference being, that while spring-mass dipole response is linear, a two-level atom shows an intensity-dependent line-width broadening.

Another difference between the models is the how scattering forces are considered. In the spring-mass case, only a dissipative force term is entertained and in the two-level model, $\Gamma_{scattering}$ calls for a diffusion of its momentum via spontaneous emission events. Although, tangentially, thinking of atoms as an oscillating dipole and also a two-level model might help clarifying ideas relating quantum antenna.[12, 13]

Velocity-dependent forces

The above discussion pertains to forces upon atoms at rest. Moving atoms don an additional velocity-dependent term. In some cases, this might be interpreted arising in relation to the Doppler effect – where the velocity of the atom towards or away from the field determines its detuning. Approximately, an atom can experience an extra viscous force – $\vec{F}_{viscous} = -\beta\vec{v}$ (details of which depend on, for instance, whether standing-wave or travelling-wave fields are considered [121]) – in addition to scattering and dispersive forces. Such a damping force is used to create atomic optical molasses.[139] Interestingly, this adds to the toolbox of tweaking atomic motion. That is, along with position-dependent forces, velocity-dependent forces can alter the phase-space distributions of atomic clouds.[121]

When can atoms be thought of as point particles?

Analogous to the ray-optics regime for light, matter-waves can be considered as point particles. Atomic wavepackets can have an initial position and momentum spread: Δr_{atom} and Δp_{atom}.[140, 141, 142, 123, 122] For the dipole-approximation to be valid, $\Delta r_{atom} \ll \Delta r_{I,var}$ and $\Delta r_{atom} \ll \lambda$.[Fig. 2.9] If large enough, atomic waves can diffract through intensity patterns in light.[134, 134]

Internally, atom consists of its electronic energies and how they're effected by light. An example of time-scales concerning internal degrees of freedom relate with spontaneous emission lifetimes, which plays a role in providing a recoil to its external degrees of freedom – its nuclear motion. The calculated potential assumes a point particle settling into the steady-state at each position, so if the processes concerning its electronic evolution are much quicker, one can 'adiabatically eliminate fast internal variables'. These time-scales are compared via: $\frac{\hbar k^2}{2m} \ll \Gamma$ – which is met for most atomic transitions.[122]

Also, as the atom's spatial extent limits its point-like consideration, especially if the fields vary over its de Broglie wavelength. Δr_{atom} which, if assumed to be $\sim\lambda_{dB}$, suggests a consideration of its velocity. For instance, velocities from (mm/s to m/s) can be associated with λ_{dB}:

$$\lambda_{dB} = \frac{h}{m_{\mathrm{Cs}}v} \longrightarrow 100nm \leftrightarrow 5nm$$

16
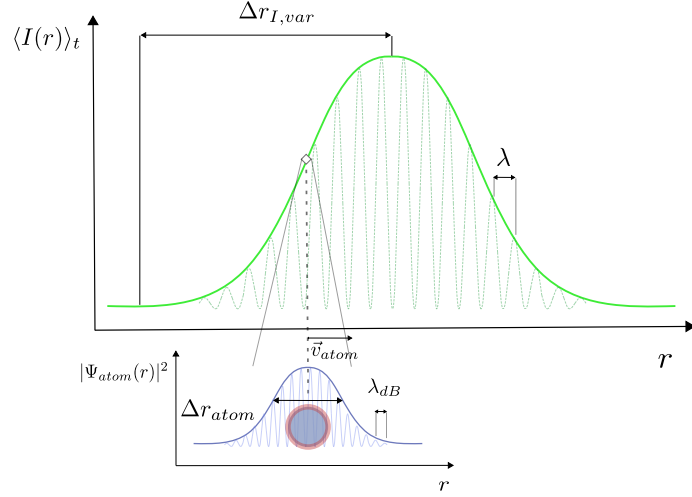
Figure 2.9: Some length scales relevant when considering atomic motion in optical fields. Time-averaged intensity of light, along with its spatially varying component. Typically, light fields can be focused until its $\Delta r_{I,var} \sim \lambda$. An atom is represented by its own (external degrees of freedom) wave-function.

The following discussion centres around far-off resonance traps [174], and is restricted to conservative potentials ($U_{opt} = U_{dipole}$) in relatively low field intensities, where $\vec{F}_{scattering}, \Gamma_{scattering}$ and $\vec{F}_{viscous}$ aren't taken into account. For the mentioned velocity range, atoms are assumed to be point-particles.

2.3 Numerical Integration of Atomic Motion

Given a (static) potential in 3D space, $U(x, y, z)$, we wish to follow point-particle movements. The rate of rate of change of position can be represented in terms of a difference equation. For instance, the central-difference form of a double derivative is written as:

$$\frac{d^2\vec{r}}{dt^2} \longrightarrow \frac{\Delta\left(\frac{\Delta\vec{r}}{\Delta t}\right)}{\Delta t} = \frac{\left(\frac{\vec{r}_{n+1} - \vec{r}_n}{\Delta t}\right) - \left(\frac{\vec{r}_n - \vec{r}_{n-1}}{\Delta t}\right)}{\Delta t}$$

Finite-differences translate the question of integration into a sequence of arithmetic operations, which can be written down as computer programs.[157, 158, 159, 160, 161] Time-stepping (Δt) position, velocity and acceleration ($\vec{r}_i, \vec{v}_i, \vec{a}_i$) of the ith particle allows us to keep track of the particles. For instance, [Fig. 2.10] shows a rather non-trivial movement of an atom for the mentioned conditions. Intensity-gradient forces in the vertical direction keep it from falling.

Also, introducing a finite-step is susceptible to errors. The order of error depends on the method of integration [162] used: such as Euler - $O(\Delta t)$, velocity-Verlet - $O(\Delta t^3)$, Leapfrog - $O(\Delta t^4)$. For example, in the Verlet algorithm, the updated position can be approximated via the following update: $\vec{r}(t + \Delta t) = 2\vec{r}(t) - \vec{r}(t - \Delta t) + \Delta t^2 \vec{a}(\vec{r}) + O(\Delta t^4)$. In general, the error depends not only on Δt, but also variations in the field.

In a conservative force-field: $\vec{F} = -\nabla U_{opt}(\vec{r})$, keeping a tab on the energy conservation: $|\Delta U_i| = |\Delta KE_i|$ (where U_i is the net potential of the particle) helps us keep a check on the integrator's stability. In a tangential mention, Leapfrog and Verlet methods are 'symplectic' and time-reversible which reflect the conservation principle of the Hamiltonian. Due to this, astronomical and molecular dynamics [169, 168] codes often use these methods to keep track of particles over long time-scales.

In addition, other non-symplectic higher-order methods of integrating such ODEs such as Runge-Kutta (RK) and predictor-corrector methods provide routes to treat dynamics where the forces can be velocity-dependent or non-conservative. And interestingly, properties of these algorithms can be related to transformations in analytical mechanics.[162]

To evolve atoms in 3D analytical potentials, Euler, velocity-Verlet and 4th order RK methods are attempted. Also, instead of a fixed time-step, adaptive time-steps – such as an RK-Cash-Karp (RKCK) algorithm – can be used. For comparison, [Fig. 2.11] shows the fractional changes in energy and time taken for the these methods of integration.
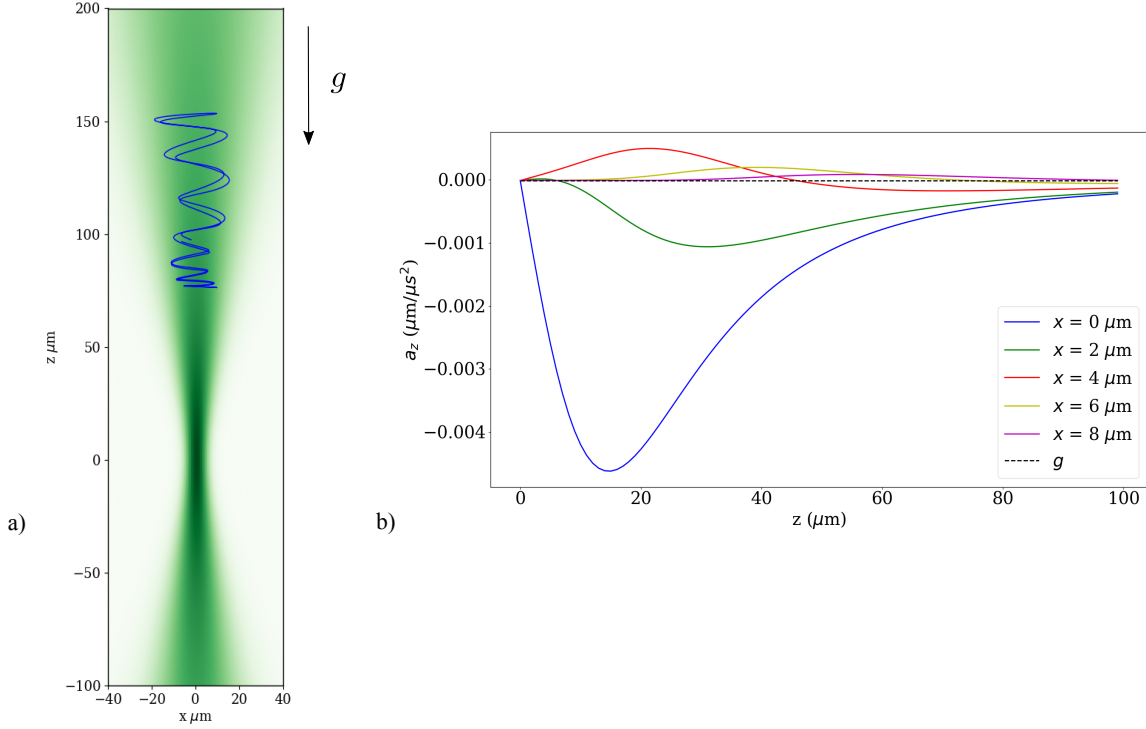
Figure 2.10: The conservative potential is formed by a laser beam at 935 nm, with a power of 40 mW at the beam waist of 2.75 μm. a) For the initial condition $(r_x, r_y, r_z) = $ (-6.4, -10.5, 96.6) μm and $(v_x, v_y, v_z) = $ (0.04, -0.02, -0.01) m/s, the trajectory can be confined upwards inspite of gravity. b) This can be understood in terms of the upwards gradient of the diverging field intensity. While along the axis, the atom sees a potential well until the center of the beam; off-axis values can give an upwards force to the atom.

Method	Error	Notes
Euler	$O(\Delta t)$	Non-symplectic
Velocity-Verlet	$O(\Delta t^3)$	Symplectic
Runge-Kutta	$O(\Delta t^4)$	Non-symplectic
Runge-Kutta Cash-Karp	$O(\Delta t^4)$	Non-symplectic, Adaptive Δt

Onwards, to form atomic trajectories, the following (modified) [163] velocity-Verlet method is used for the updates – $(\vec{r}, \vec{v}, \vec{a})$ can be changed to $(\vec{r}_{new}, \vec{v}_{new}, \vec{a}_{new}; \vec{v'}_{new}$ is termed a half-step and $\vec{a}_{new}$ uses a position dependent update via $\vec{F}(\vec{r})$).

$$\vec{v'}_{new} \leftarrow \vec{v} + \vec{a}\frac{\Delta t}{2} \qquad \vec{r}_{new} \leftarrow \vec{r} + \vec{v'}_{new}\Delta t \qquad \vec{a} \leftarrow \vec{a}_{new} \qquad \vec{v}_{new} \leftarrow \vec{v'}_{new} + \vec{a}_{new}\frac{\Delta t}{2}$$

Keeping Track of Millions of Atoms with Parallel Programs

Experiments typically start out with hundred million atoms (more about which is briefly discussed in Pg.22) spread across a few millimetres, and we want to follow their journey into μm spaces. Iterating 10^8 particles, where each particle takes $\sim T_{evolve}$ seconds [Fig.2.11], suggests a run-time of $\sim$ 2000 hr. One place of improvement is to realize the computation closer to the clock-rate of the processors. Supposing each of the 10^8 particles are updated within $\sim$10-100 clock cycles, translating to $\sim$1 s of computing time, then, time-evolving for about 10,000 time-steps ($\sim$10 ms) suggests a $\sim$2 - 200 hr run-time. Ideally, we'd like to explore different configurations of the experimental setup, allowing for quick diagnostics and exploration of the experimental parameter space. The efficiency of code depends on the manner in which it represents atomic dynamics. From a beginner's point of view, some matters of programming relevance include: data structures used for the particles [171], the 'low-leveledness' of the programming language and libraries invoked. Further, compiler/code optimizations and algorithmic nuances can allow for faster memory accesses and higher efficiencies. In addition to the program, software architectures and computational hardware are also relevant to the nature of the simulation. Such a particle system is well-suited to be mapped onto the parallel data flows encouraged by modern hardware's (such as a GPU) multi-threadedness, as shown in [Fig. 2.12].[164, 166, 167, 170]
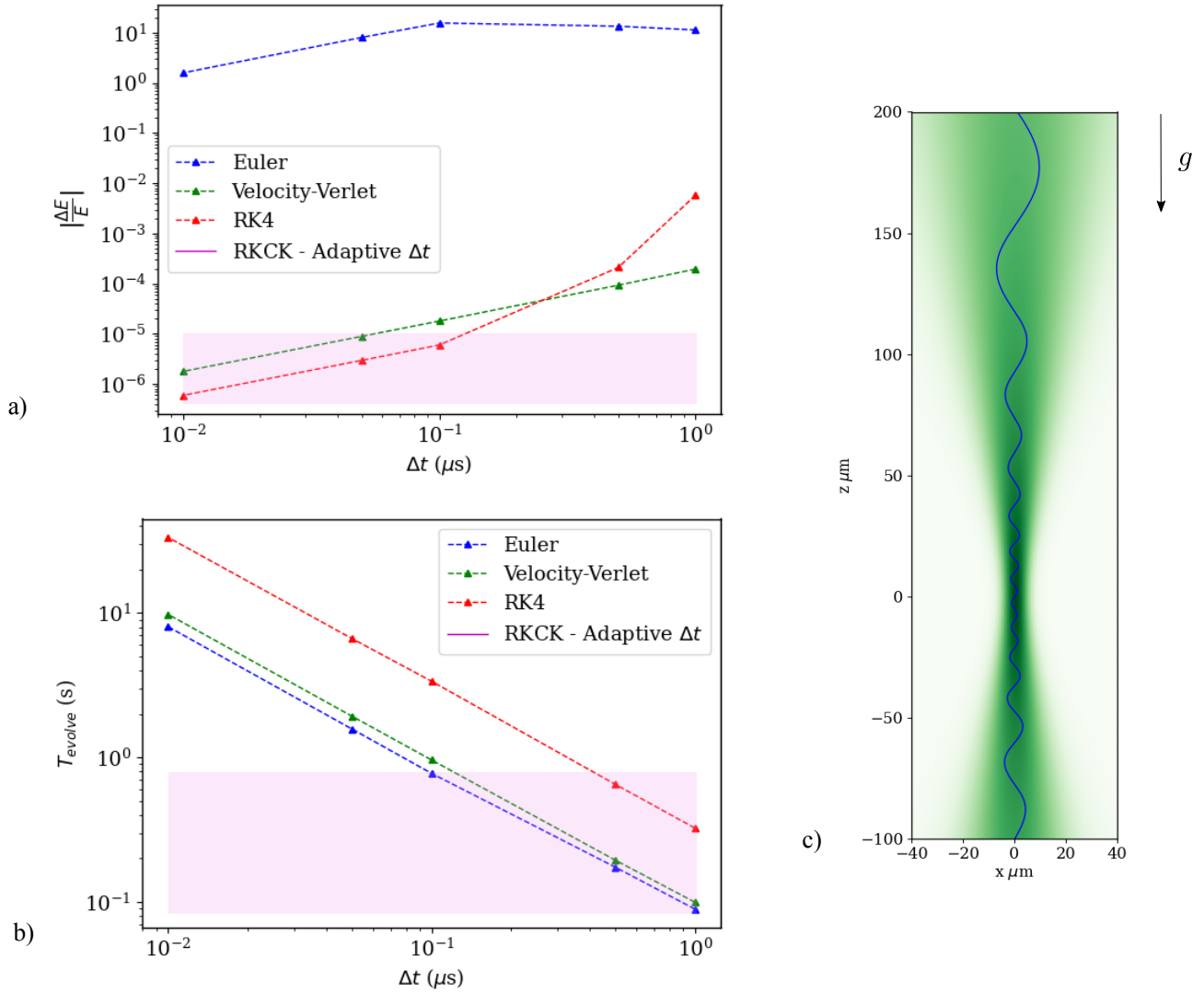
Figure 2.11: For the atomic trajectory shown in c), the attempted integration methods show different fractional changes in energy (which can serve as a proxy for the accuracy of the computation). The conditions of the light beam are the same as in [Fig. 2.10]. And, the initial conditions of the Cs atom are $(r_x, r_y, r_z) = (5.7, -9.6, 277)$ μm, $(v_x, v_y, v_z) = (-0.03, -0.01, -0.04)$ m/s. Written with Python's NumPy library, b) shows the time taken to run such a computation. The pink areas in a) and b) correspond to a rough range of runtime and 'errors' when an adpative time-stepping algorithm is implemented.

A GPU launches indexed microprocessors when its kernel is invoked. At the bottom of its memory hierarchy is a thread, which nibbles away small calculations – in this case: the update steps and function calls to get the forces. When potentials are analytical, the calculations are relatively self-contained within each thread. And when the potential is expressed via a data-grid or when there are particle-particle interactions, the threads have to call onto a shared memory. [Fig. 2.13] compares the time taken for parallel and serial programs to carry out thousand update steps on $1 - 10^8$ atoms.
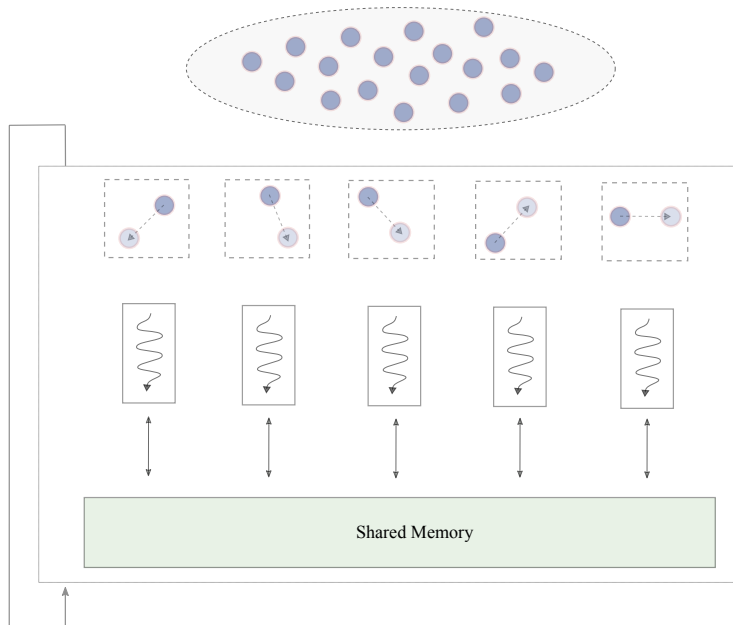
Figure 2.12: A high-level illustration of mapping each particle onto different processing streams in a parallel processor.

Many updates on such a simple program to add detail to atomic trajectories are possible. Firstly, the force fields experienced by the atoms can be generalized to incorporate momentum diffusion, damping and dissipative forces.[177, 188] In addition to single-particle dynamics, atom-atom interactions [172] can also be considered. A standard approach to keep track of cut-off range distances [173] for particles involves a grid-based algorithm. Such a step reduces the number of operations from $O(N^2)$ to $O(N)$. Further, conventional approaches on such processors also allows one to directly render/animate these dynamics, which can be of interest.[165, 166]
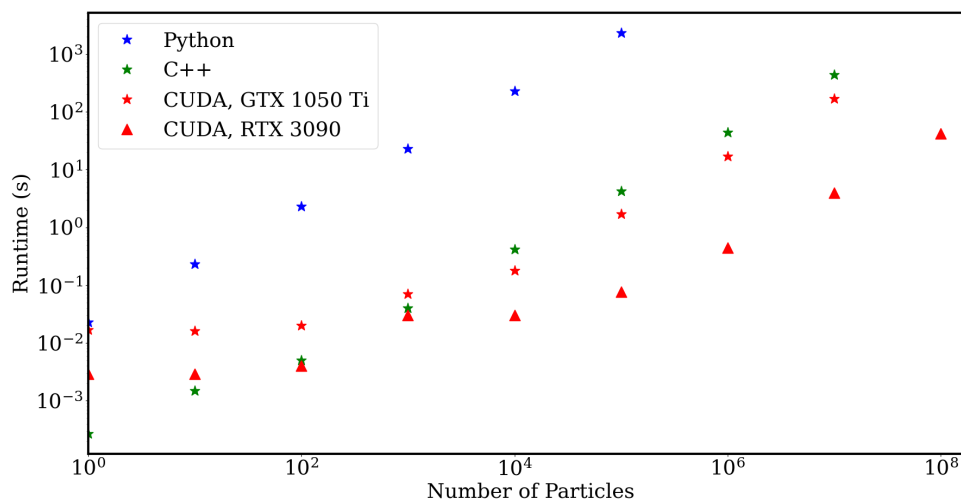
Figure 2.13: Runtime taken for a thousand velocity-Verlet time-steps on different number of particles. Python (Using NumPy), C++ (with an -O3 optimization flag), which are serial programs, were run on a i7-8750H CPU. Parallel programs were tested on commercially available graphics cards: GTX 1050 Ti and RTX 3090 (using: vast.ai). In Python, $(\vec{r}, \vec{v}, \vec{a})$ for the particles are represented using 1D arrays; and for C++ and CUDA programs, the particles are represented using an array of structures.

Chapter 3

Guiding Laser-cooled Atoms into Hollow-Core Optical Fibers

Optical forces such as $\vec{F}_{dispersive}$ can be used to trap atoms and $\vec{F}_{scattering}$ is often used to cool an atomic gas – although, the stochastic nature provides a recoil limit to the temperature (which is $\sim$100 μK for Cs atoms). Lower (referred to as sub-Doppler) temperatures upto 1 μK can be reached using polarized lights and magnetic fields – which involve the atomic hyperfine levels.[121, 184] Such initial conditions for atoms are often met in Magneto-Optical Traps (MOT) (an example of which is in [Fig. 3.1]). From this mm-scale MOT, the atoms have to be guided into μm-scale hollow-core fibers.

The efficacy of ensemble-light interactions inside hollow-core fibers often relate to the optical depth of the medium in which they take place, which is in turn proportional to the number of loaded atoms when the experiments take place inside the hollow region. Moving optical potentials [178, 179] have been proposed [180] (suggesting a loading efficiency [the fraction of atoms loaded per total number of atoms] of upto $\sim$40%) and used to guide atoms from free-space into a sideways-positioned fiber [80, 81, 82, 83, 84], wherein, a study reported 5% loading efficiency from a trap placed a few mm away.[193] Red-detuned diverging beams from vertically aligned fibers, with a MOT prepared a few mm above the tip, were used to attain efficiencies of the order 0.01% [189], 0.1% [190] and 1% [192, 87] – pointing towards quite some room for improvement. Some of the experimental results have also been followed along by simulations.[192, 185] However, some discrepancies in the number of loaded atoms are put forth in Ref.[87]. In addition, dark funnel [87] and hollow tunnel beams [190, 187, 188] were employed to increase atomic densities.

In the NPQO laboratory, Cs atoms released from a filament in a vacuum chamber are cooled and gathered using a MOT, wherein temperatures of $\sim 30\mu$K clouds [189] have been realized using $\sigma_+ - \sigma_-$ polarization gradient cooling. Once cooled, atoms are released from the MOT so that they might make it into a vertically oriented fiber, with the help of optical dipole trapping beams.

Chapter Overview: Using the introductory simulation recipe put forth in the preceding chapter, atomic trajectories into hollow-core fibers are estimated. Specifically, red-detuned Gaussian beams and blue-detuned hollow-beam tunnels form conservative analytical potentials through which atoms can travel. These results are compared with experimental and numerical reports. The loading efficiency's dependence on experimentally relevant parameters – trapping beam and MOT cloud parameters – is also explored. In addition, the ensemble inside the hollow fiber is visualized for one of the loading scenarios, wherein, details such as atom-atom spacing and velocity distributions are relevant whilst understanding atom-light interactions. However, the accuracy of the results have not been studied in detail.

3.1   Gravity-Assisted Dipole Red-detuned Gaussian Trap

The experimental set-up to be analysed is shown in [Fig. 3.1 b), c)]. Assuming the atom-cloud (with 10^8 atoms) has no transverse velocity, the number of atoms that can be gathered inside the hollow fiber is $\sim$900. This ought to reduce as temperature is increased.

A diverging Gaussian profile starting at the fiber-tip provides U_{dipole}. This can be employed to funnel more atoms into the fiber, corresponding to the schematic in [Fig. 3.1 a)]. Red-detuned from Cesium's 852nm and 894nm transitions, a 935 nm magic-wavelength [Fig. 2.6] laser forms a far-off resonance trap (FORT).[174] This
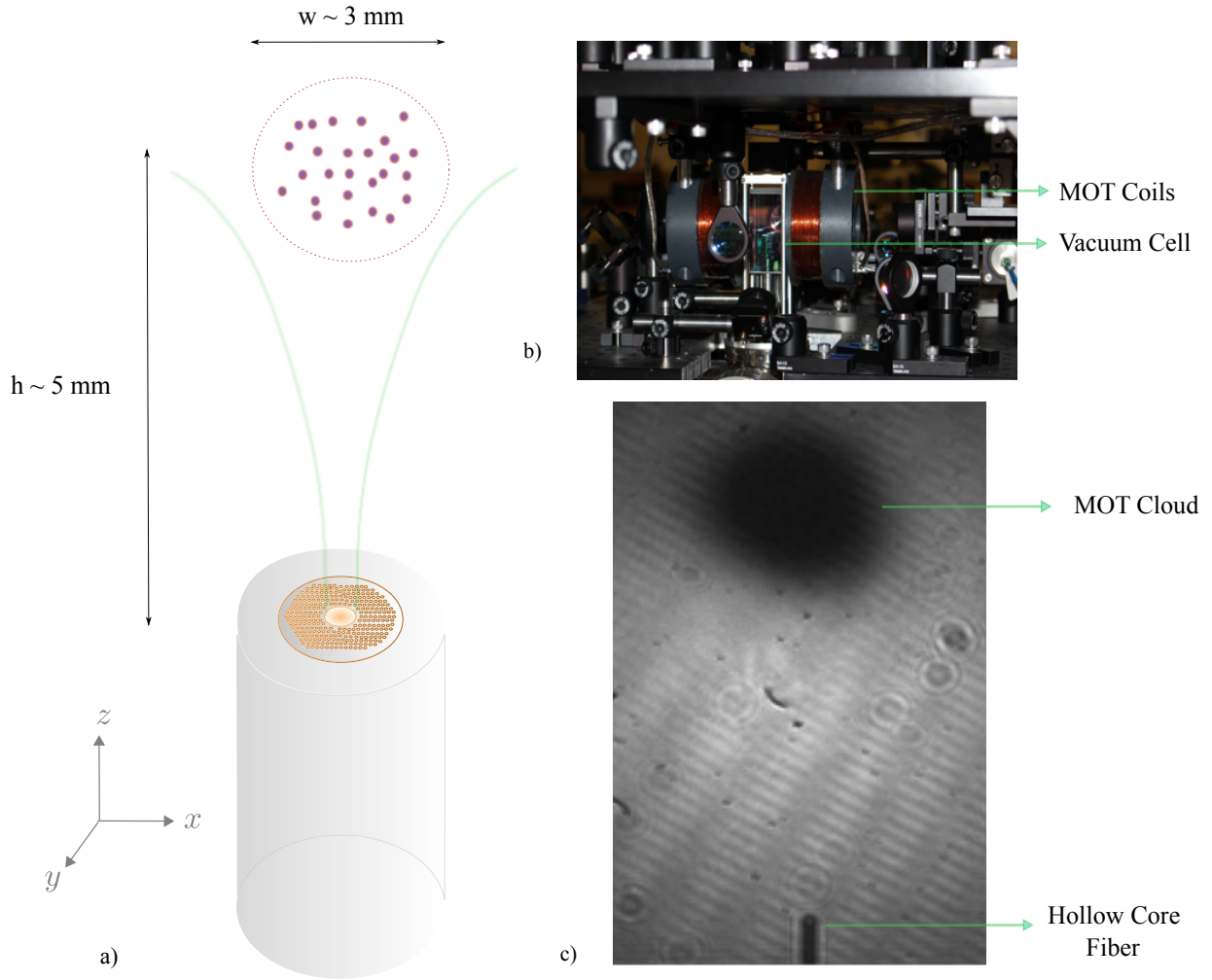
Figure 3.1: a) Schematic of the initial condition of a MOT cloud atom a hollow fiber. b) Picture of the experimental setup. The hollow-core fiber resides in the vacuum cell, and the Cu coils generate the magnetic fields to form the atomic cloud inside the cell. [Image source: [34]] c) Snapshot of a MOT cloud formed atop the hollow fiber. [Image source: [34]]

can be assumed to be conservative, and has the added benefit of avoiding intensity dependent effects due to the confined mode of the fiber. For Gaussian beams, it is suggested that phase-gradient and velocity-dependent forces appear to cancel out.[138]

Similar to the simulations performed in Refs.[186, 192], the experimental conditions as elaborated upon in Ref.[189] are numerically re-created. Loading dynamics have also been followed via a different approach in Ref.[185], which takes into account the cylindrical symmetry of the setup. All these simulation approaches appear to be conducive for translation onto parallel hardware.

Initially, as also suggested in Ref.[185], positions are sampled uniformly in a sphere of a given radius and location. Within which, velocities are sampled from a Maxwell-Boltzmann distribution – according to the temperature of the MOT cloud. [185] suggests that about 10^8 are samples are needed to limit the error in the loaded number of atoms to ~1%. Optical dipole forces and gravity provide for the accelerations that move the atoms. Snapshots of such an evolution are shown in [Fig. 3.2].

	Yoon et al. [Experiment] [189]	Yoon et al. [Simulation] [185]
Atomic species	Cs	Cs
HC-PCF and Mode Diameter	7.5 μm, 5.5 μm	7.5 μm, 5.5 μm
MOT Height, Diameter	5 mm, 3 mm	5 mm, 3 mm
MOT Cloud Temperature	32 μK	32 μK
Dipole Laser Wavelength	935 nm	935 nm
Dipole Laser Power	50 mW	40 mW
Reported Loading Efficiency	1.6×10^{-4}	1.1×10^{-4}
Simulated Loading Efficiency	1.8×10^{-4}	1.4×10^{-4}
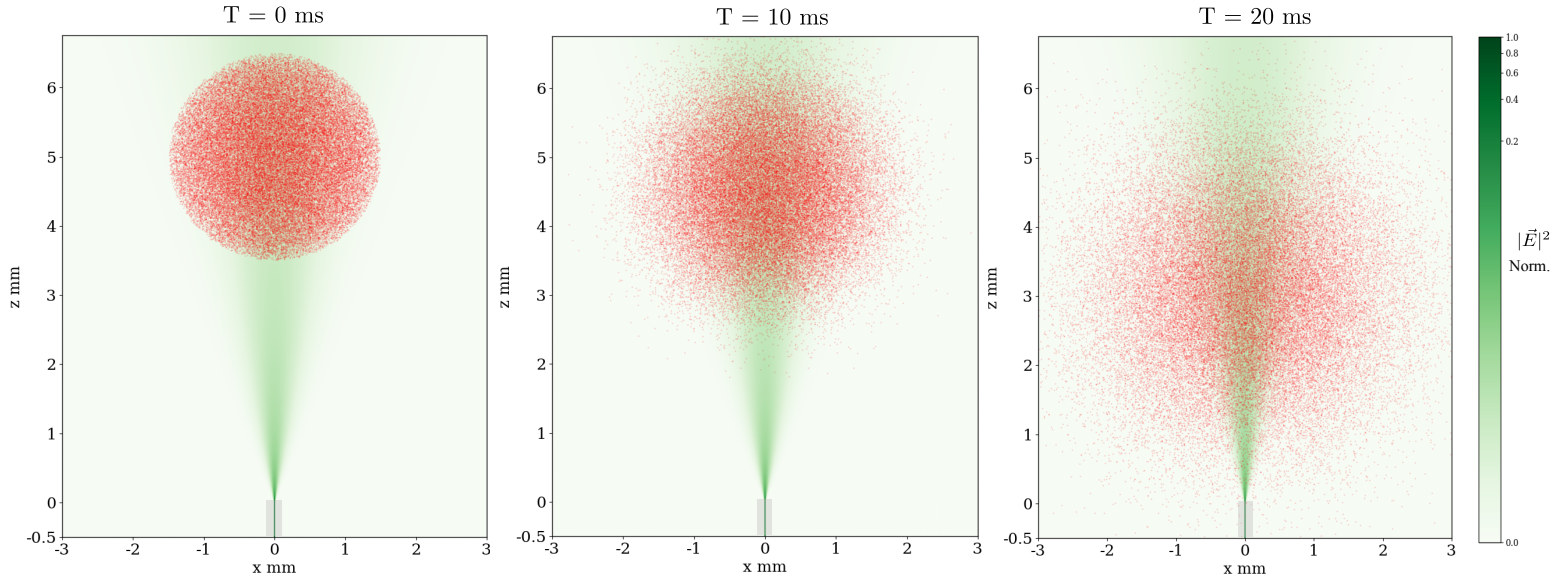
Figure 3.2: An illustration of simulating the dropping of ~50,000 Cs atoms from a MOT cloud (T = 32 μK) placed 5 mm atop the hollow fiber in the presence of a red-detuned Gaussian dipole trapping beam with power P = 40 mW. The fiber face is at z = 0 mm.

With an adaptive time-step and a check to drop atoms significantly out of reach, a run of 100 million atoms (for a time-step of 0.01 μs) in such a setup can take about an ~hour. The results of loading efficiency (the condition for loading is mentioned in: [Fig. 3.7]) are noted in the table above. Some of the atoms that can be loaded into the fiber can be seen in [Fig. 3.3 a), b), d)]. A noticeable effect of the potential can be seen within 500 μm of the fiber face. This can be understood in terms of the potential well that is formed along any given horizontal plane [Fig. 3.3 c)]. As the potential is conservative in nature, atoms moving into the trap from the side (with sideways velocities) can escape it. However, atoms moving into the trap from the top with a small enough velocity are trapped. These trapping velocity contours are sketched in [Fig. 3.4]. Broadly, the role of such a guiding mechanism is to big-mouth the hollow fiber in order to swallow a larger fraction of the falling atoms.

Comparison with Other Literature

As a brief check, the simulation is tested ($N_{atom} = 10^7$ and $\Delta t = 0.1$ μs) with reports also interested [190, 192, 186] in the gravity-assisted trapping of atoms into hollow optical fibers. †Although, loading dynamics in Ref.[186] and Ref.[192] also consider a stochastic momentum kick process, as required by the applied field strengths and detuning. The FORT approximation is limited as $\vec{F}_{scattering}$ is prominent when the dipole trapping wavelength is close to ~780, 794 nm transitions of Rb D lines, and also when laser intensities are high. *The MOT clouds in the reports start with a Gaussian density distribution, rather than the spherical distribution considered here.

	Bajcsy et al. [Exp.] [190]	Hilton et al. [Exp. & Sim.] [192]	Yang et al. [Sim.] [186]
Atomic species	^{87}Rb	^{85}Rb	^{85}Rb
Hollow-Core and Mode Diameter	7 μm, 4 μm	45 μm, 33 μm	64 μm, 44 μm
MOT Height, Diameter	6.3 mm, 0.68 mm	25 mm, 1* mm	5 mm, 2* mm
MOT Cloud Temperature	40 μK	5 μK	10 μK
Dipole Laser Wavelength	802 nm	797.25† nm	821† nm
Dipole Laser Power	25 mW	1† W	0.5† W
Reported Loading Efficiency	~5×10^{-4}	3.2 %	19×10^{-4}
Simulated Loading Efficiency	3.8×10^{-4}	19 %	80×10^{-4}

A part of the variation in the comparisons with Refs.[192, 186] might relate with the mentioned scattering loss mechanism. However, a dipole force based calculation (without $\Gamma_{scattering}$) in Ref.[185] suggests a ~4 % loading efficiency in their estimate of Ref.[192]'s results. It would be helpful to re-verify energy conservation with a larger number of atoms and a smaller time-step and also, check the simulation results after incorporating $\Gamma_{scattering}$. Also, in the simulations of experiments reported in Ref.[189] and Ref.[190], the core and mode diameters of the HC-800-02 fiber [Fig. 1.7] are taken as: (7.5 μm, 5.5 μm) and (7 μm, 4 μm), respectively.
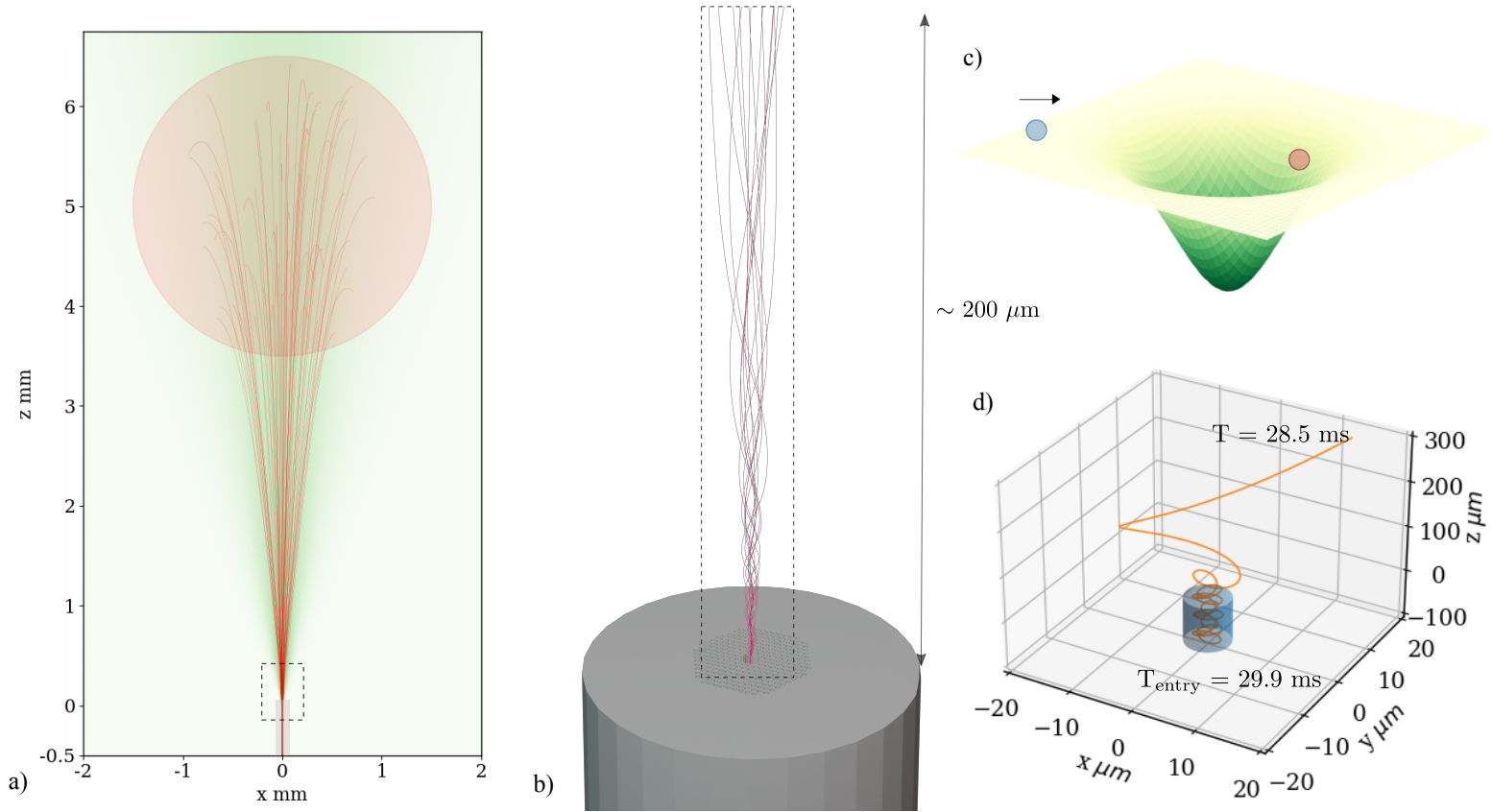
Figure 3.3: a) ∼70 trajectories of atoms (out of ∼0.5 million) that make their way into the hollow-core region. b) A close-up of 15 of the trajectories showing the effect of the dipole trapping beam. c) An xy intensity cross-section of the Gaussian profile forms a potential well. Atoms that make their way into the well from the top (with low transverse velocity) are trapped. d) A scaled version of one path of the atoms showcasing the role of the dipole trapping beam. For the pictures: $\Delta t = 0.1$ μs. For this time-step, (in this simulation setting) the maximum fractional change in energy is ∼0.05.

Effect of Laser Power and MOT Cloud Temperature
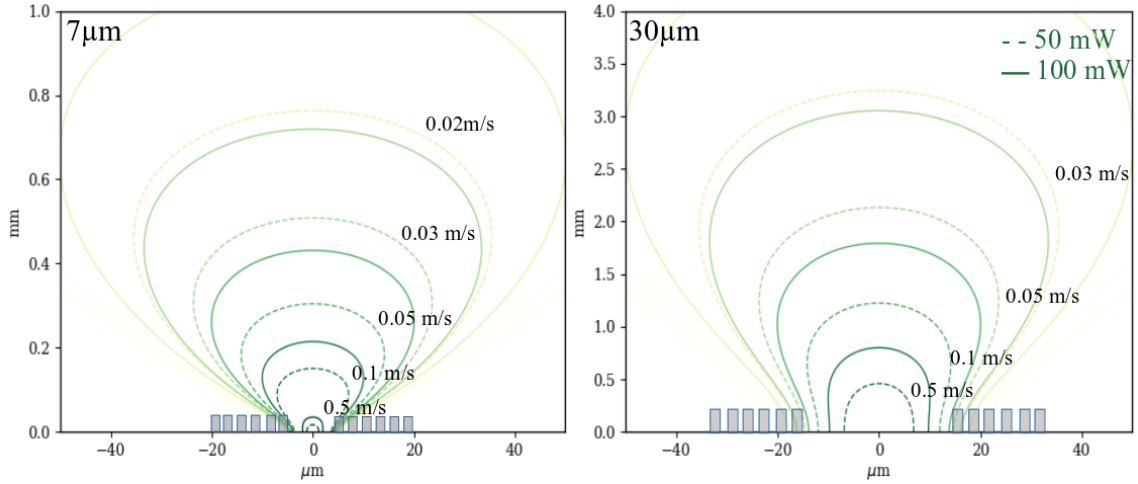
Figure 3.4: Contour potential surfaces in terms of the trapping velocities outside 7 and 30 μm fibers. For atoms moving with same velocities, higher powers can capture them from a larger volume.

For the discussed loading scenario [189], [Fig. 3.5] shows variations of the loading efficiencies for 7.5 μm and 30 μm fibers (which is assumed to have a Gaussian fundamental mode with a beam waist of 11.8 μm) [Fig. 1.7] when temperature of the MOT cloud and intensity of the dipole beam is varied. The lower limit of the MOT temperature is set to 1 μK, as it is experimentally viable.[184] And, the role of the dipolar trapping beam's intensity can can be gathered from [Fig. 3.4]. The linear increasing trend of the captured atoms is also suggested via simulations in Ref.[185], and which might relate with the heuristic argument of the overlap of the MOT cloud with the effective capture range for different laser powers.[192]
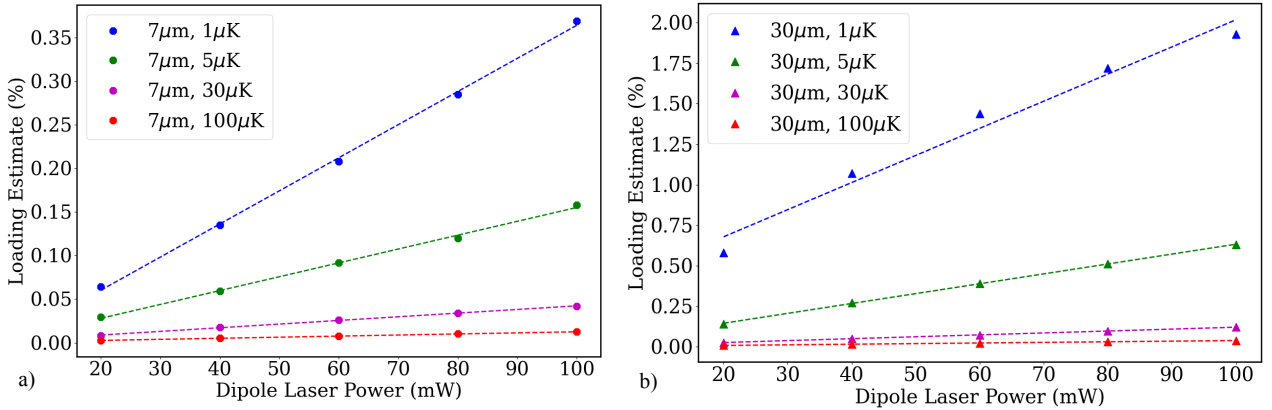
Figure 3.5: Approximate scans ($N_{atom} = 10^6$ and $\Delta t = 0.1$ μs) to check for the dependence of loading efficiencies on dipole laser power and the initial MOT cloud temperature for a a) 7.5 μm core fiber and b) 30 μm core fiber. Data are denoted by markers, while the dotted lines are a fitted linear line.

Sizing and Displacing the MOT Cloud

It might not always be possible to start with the MOT right above the fiber. To check whether this plays a significant role in loading atoms the MOT is displaced side-ways. [Fig. 3.6 b)] shows loading efficiency into 7.5 μm fibers considering upto 1 mm off-centred MOT clouds with a temperature 30 μK and trapping beams with $P = 50$ mW. And, for the same conditions of the MOT temperature and dipole trapping beam, [Fig. 3.6 a)] shows the dependence on the number of loaded atoms to the size of a centred MOT cloud. Intuitively, a centred MOT with small size should allow for a higher loading efficiency.
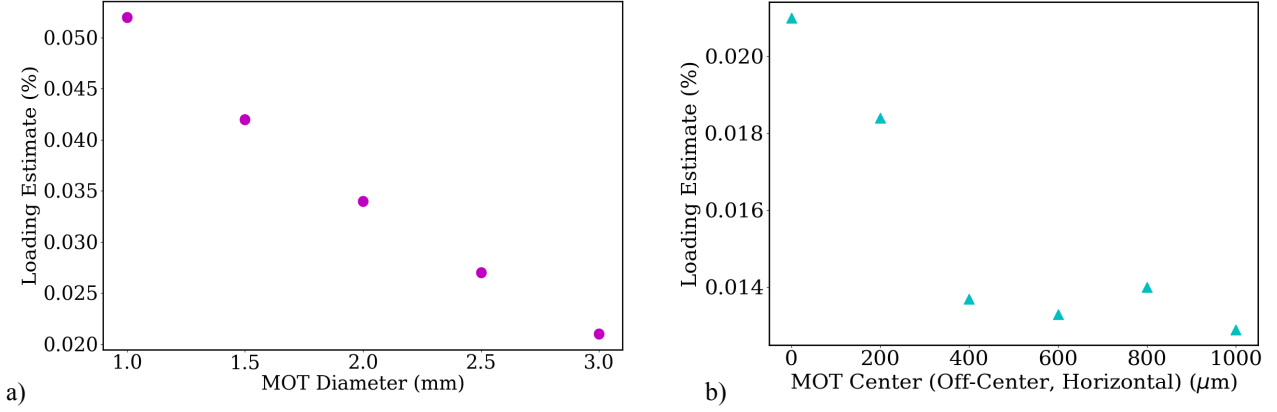
Figure 3.6: Approximate scans ($N_{atom} = 10^6$ and $\Delta t = 0.1$ μs) to test the effect of a) changing the radius of the MOT and b) misaligning it. The MOT is $z = 5$ mm above a 7.5 μm fiber and at a temperature of 30 μK with the dipole trapping beam power: P=50mW.

3.2 Inside the Hollow-Core

The atomic trajectories can be continued into the fiber. At fiber entry, some Cs atoms are lost due to collisions with the wall. These are reported when atoms come closer than 100 nm to the fiber surface, when van der Waals surface effects become predominant.[190] Typically, they appear to settle into their orbits once they make their way inside ~100 μm of the hollow fiber. After which, their entry is tagged. And, after travelling along the length of the fiber: $|z| > 20$ mm, atoms are assumed to exit the fiber. [Fig. 3.7] summarizes the entry and exit conditions for a short 400 μm fiber.
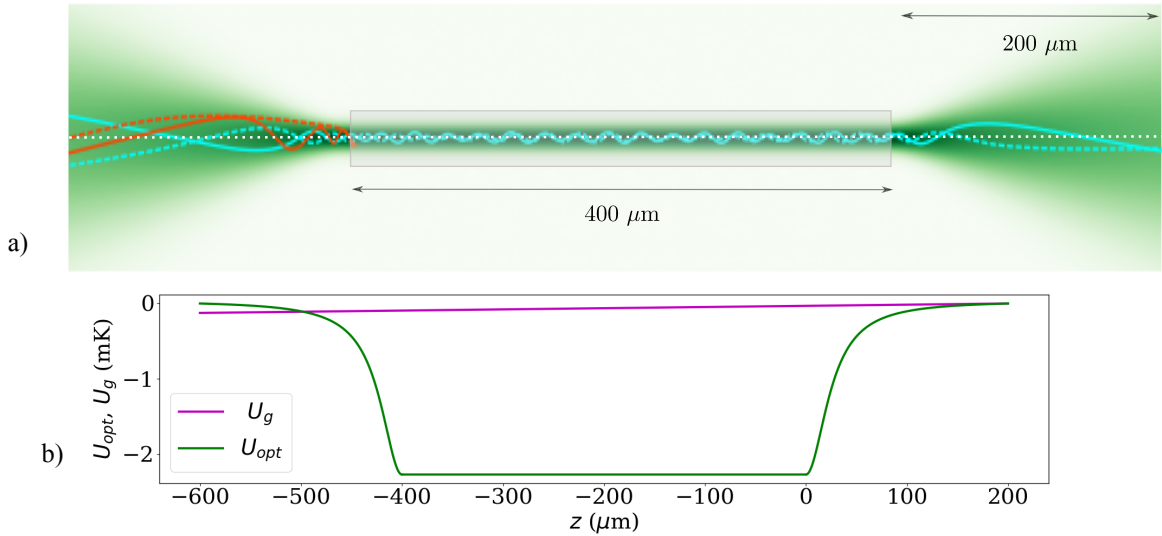
Figure 3.7: a) Field strength and fiber dimensions follow the 40 mW configuration of Ref.[189]. Red trajectories show atoms 'colliding' with the wall as they come within $r_{hcpcf} - r_{vdW} = 100$ nm of the fiber surface. Blue trajectories show atoms entering and exiting the fiber. b) Potential drops due to the intensity gradient along its axis [dashed white line in a)] alongside the gravitational potential are shown. When the fiber length is ~ 20 mm, then the gravitational potential difference is larger than ΔU_{opt}, suggesting that all entering atoms do exit the fiber.

Experimentally, atom numbers inside the fiber have been kept track of as suggested in Ref.[189]. These results (for this case, reported laser powers is 40 mW – which is measured after the light exits the fiber) are compared with simulations in [Fig. 3.8] for dipole trapping powers of 40 mW and 50 mW. An explanation for the early rising time, perhaps, might relate to the manner in which the experiment is carried out. Atom numbers are estimated by their absorption curves – whose intensities are gathered from the top. As shown in [Fig. 3.3 b)], the atoms which haven't yet entered the fiber might appear in the absorption peak. Also, Ref.[186] reports a
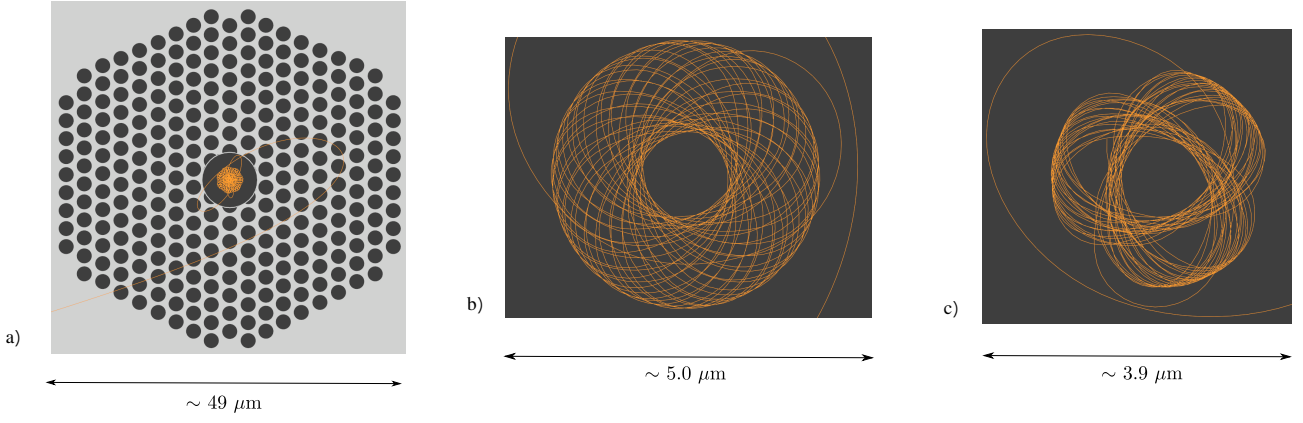
Figure 3.9: A top-down view of the atoms entering and settling into their 'unstable' [188] orbits inside the 7.5 μm hollow-core region of the fiber. For these trajectory calculations, $\Delta t = 0.1$ μs.

loss mechanism when higher-order modes of the hollow-core [Fig. 1.8] are considered, which might explain the observed trend.
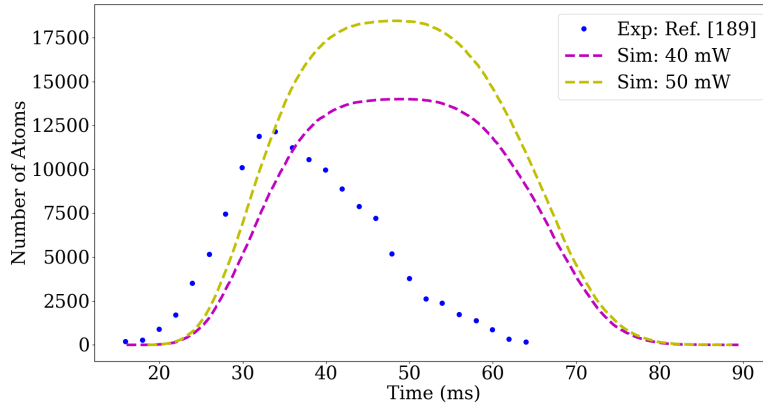
Figure 3.8: Number of atoms in the fiber versus time. The blue dots correspond to the experimental results reported in Ref.[189]. The yellow and magenta dashed lines correspond to simulations performed with $P = 40$ and 50 mW dipole trapping powers.

When $P = 40$ mW, [Fig. 3.9] shows how atoms enter and move inside the hollow fiber in the $x - y$ direction. Analysis of such trajectories has been more deeply commented about in Ref.[188]. For the same experimental conditions, [Fig. 3.10] shows how the ensemble looks like inside the hollow region of the fiber, along with a more to-scale version of the rather 1-dimensional hollow-core space!

As the ensemble moves through, its atom-atom distances, position and velocity distributions can be logged. [Fig. 3.11] With the minimum atom-atom separation in such a configuration being ~ 60 nm [Fig. 3.11 c)], atom-atom interaction potentials needn't be considered in this scenario. Ref.[189] also attempts a transverse temperature measurement by tracking the time taken by atoms before colliding with the fiber-wall once the guiding dipole trapping beam is shut-off. The reported measurement points towards a ~ 2.3 mK transverse temperature, which is close to the accelerating ΔU_{opt} mentioned in [Fig. 3.7]. And, the simulated temperature inferred from the ensemble's average transverse K.E, is ~ 0.4 mK. This merits a cross-checking of the simulation, but such a temperature might also be plausible – as all of the energy increase from ΔU_{opt} needn't exclusively speed up transverse velocities.

Properties of the Atomic Ensemble Inside the Hollow Fiber

While atom-light interactions in the hollow-core region merits a more thorough discussion, a few broad comments can be made. The transverse μm-size confinement of the hollow fibers can lead to two effects on atomic energies [Fig. 3.12 a), b)]. Firstly, the atoms placed far from the center interact weakly with input photons due to a large

27
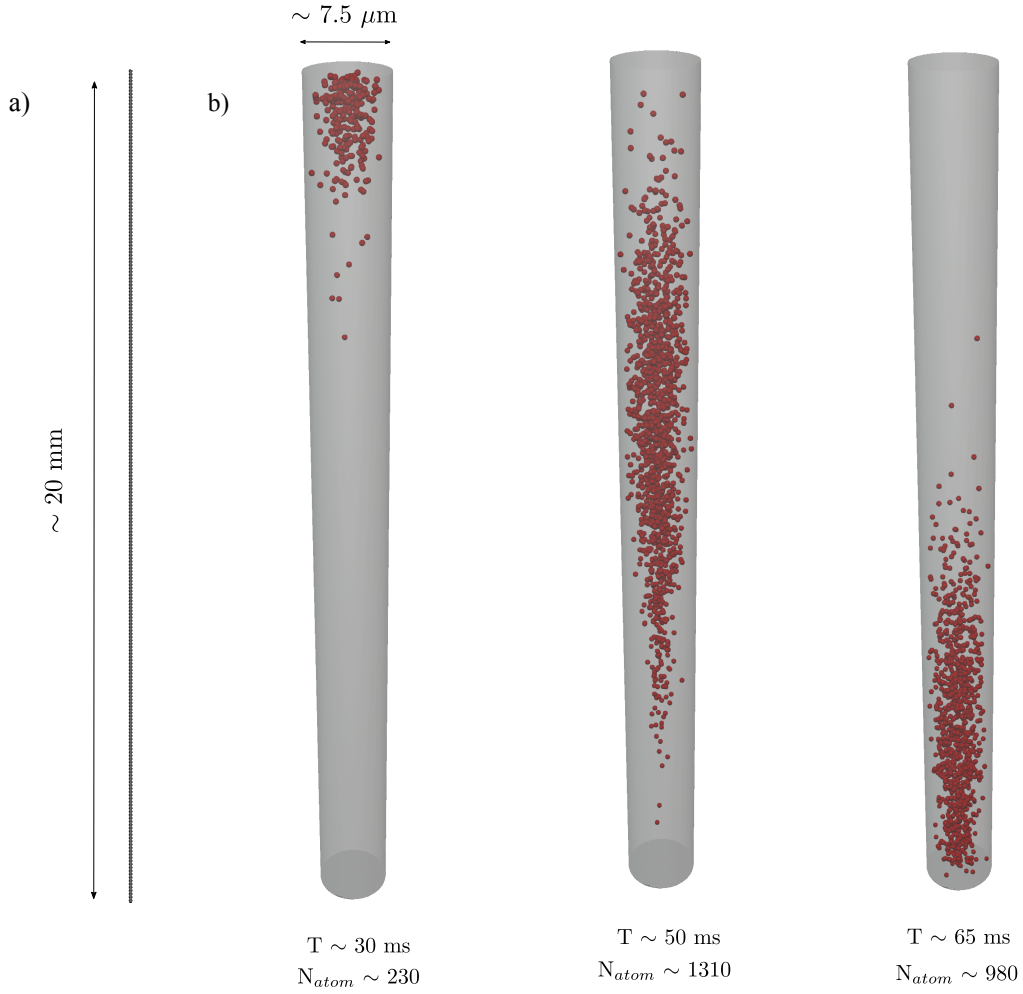
Figure 3.10: a) A more to-scale version of the 20 mm, 7.5 μm hollow-core region of the fiber. b) Snapshots of the atomic ensemble as it enters and exits the fiber when 10 million atoms are released from the MOT cloud.
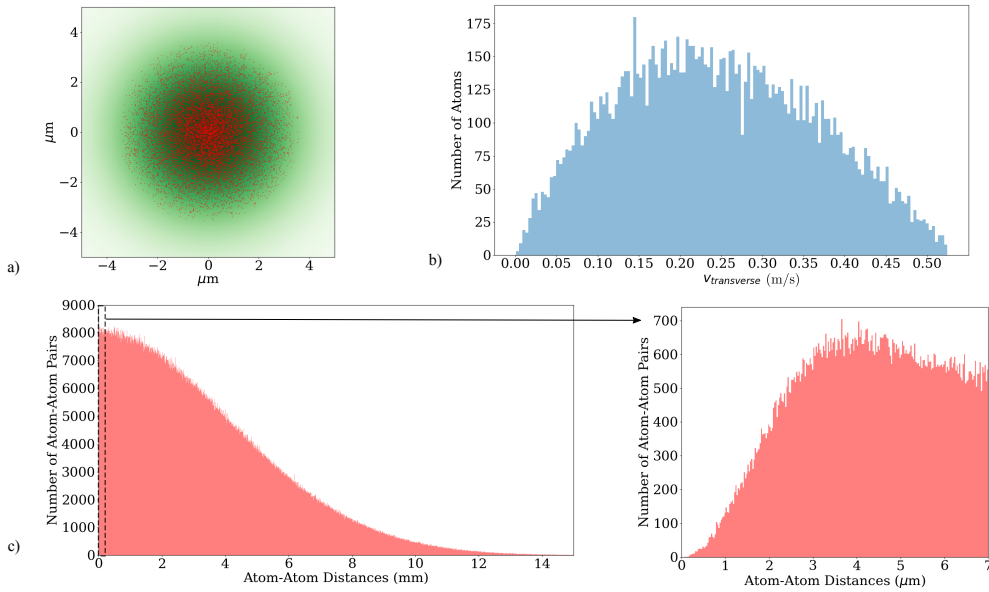
Figure 3.11: Starting with 100 million atoms, $\sim$ 13,600 atoms are loaded. At T = 50ms (Corresponding to the situation depicted in [Fig. 3.10 b)]): a) xy position distribution of the loaded atoms. b) Transverse velocity distribution: $v_{transverse} = \sqrt{v_x^2 + v_y^2}$. Using the average K.E, an estimate of the transverse temperature is $\sim$0.4 mK. c) Distribution of atom-atom distances. Zooming into the $\sim\mu$m space tells us about small atom-atom distances. In this case, $d_{min} \sim 63$ nm. [Note: The bin sizes for the two histograms are different.]

effective mode area (A_{eff}) – which plays a role in the coupling constant g_{wvg} [Fig. 1.10, Fig.1.11]. Secondly, the strength of the coupling scales inversely with the radius of the hollow region.[Fig. 3.12 b), c)] The following definitions are sourced from Ref.[55].

$$A_{eff} = \frac{\int\int \epsilon(\mathbf{r})|\vec{E}(\mathbf{r})|^2 dxdy}{[\epsilon(\mathbf{r}_a)|\vec{E}(\mathbf{r}_a)|^2]} \qquad g_{wvg} = \mu\sqrt{\frac{\omega}{4\pi\epsilon c\hbar A_{eff}}}$$
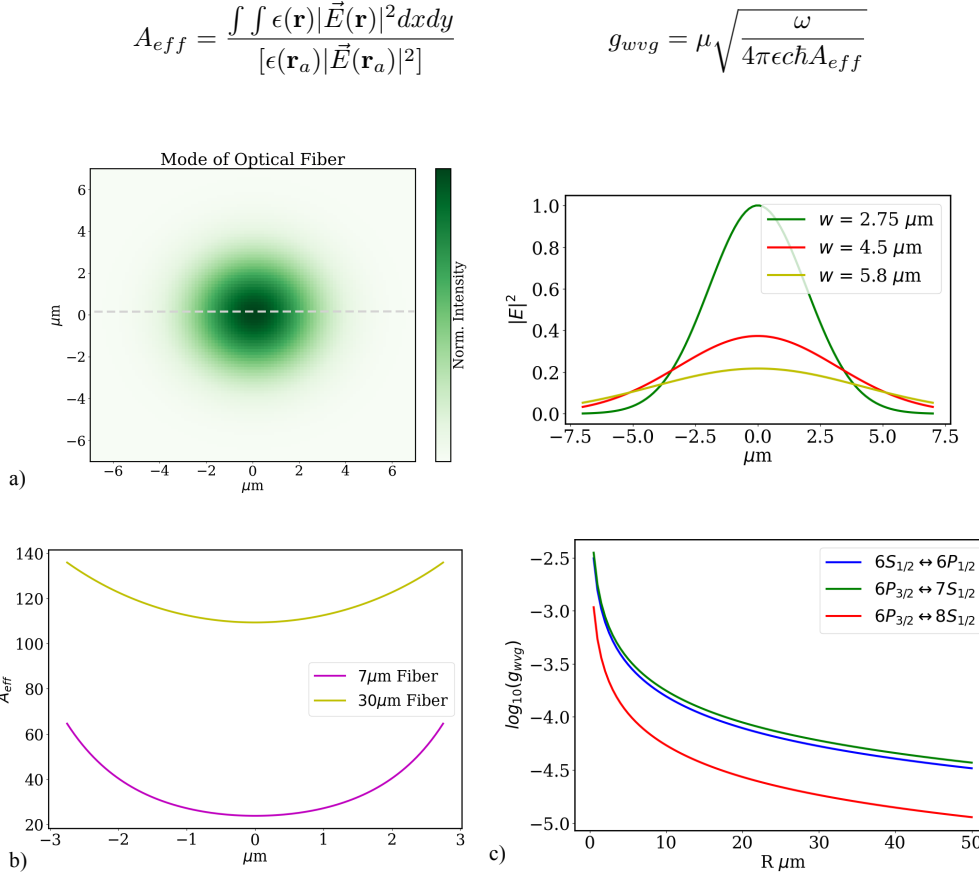
Figure 3.12: a) Normalized intensity of a Gaussian mode (considering a 2D integral: $\int |E|^2 dxdy$) with varying mode diameters. Placing an atom at high-intensity regions enhances its coupling with the waveguide mode, as parameterized by g_{wvg}. b) Estimates of A_{eff} ($\epsilon(\mathbf{r})$ is taken as 1 inside the hollow-core) for atoms placed at different locations in 7 and 30 μm hollow-cores. c) Coupling constant, g_{wvg}, for placing atoms at the center of fibers with varying mode diameters.

Such a coupling makes the optical depth (OD) depend on how the atoms are spread across the mode. [Fig. 3.13] follows two definitions of optical depths.

$$\text{OD}_1 = \rho\sigma_{cross}L[230] \sim \frac{3N_{atom}\lambda^2}{4\pi A_{eff}} \qquad \text{OD}_2[190, 192] = \chi N_{atom}\frac{2c_{\text{CG}}^2\sigma_{cross}}{\pi w_0^2}; \chi = \frac{2(w_0/2)^2}{w_{r,0}^2 + (w_0/2)^2}$$

In OD_1, mode area A is taken as A_{eff} – to account for the spatial variation of an atom's coupling to the field. OD_2 considers a Gaussian spread of atoms as in [Fig. 3.11 a)]. Where w_0 is the beam waist, $w_{r,0}$ is the waist of the atomic distribution, $\lambda = 852$ nm and c_{CG} is the Clebsch-Gordon coefficient $\sim$0.3 for one of the Cs D$_2$ transitions (852 nm).[194] In addition to the optical depth's linear dependence on N_{atom} and also their positions within the mode, collective effects of the ensemble are suggested to also play a role.[88, 89, 230] And, venturing into very high optical depths brings in the question of atom-atom interactions inside the fiber.

3.3   Hollow Beam Tunnel for Atoms

With loading efficiencies in the above mentioned scenarios being in the $\sim$1% regime, there appears to be quite some room to better integrate atoms into hollow fibers. Following experiments suggested in Ref.[190], the use of axicon lenses to create blue-detuned hollow beams [182] – which can also create a potential well – to guide atoms into the hollow fiber is considered. Curiously, inverse to the case of light being guided over long-distances by a material hollow optical fiber, in this case, matter is guided by a hollow optical guide! [Fig. 3.14] shows their generation, and how such beams can maintain their intensity profile over long distances.
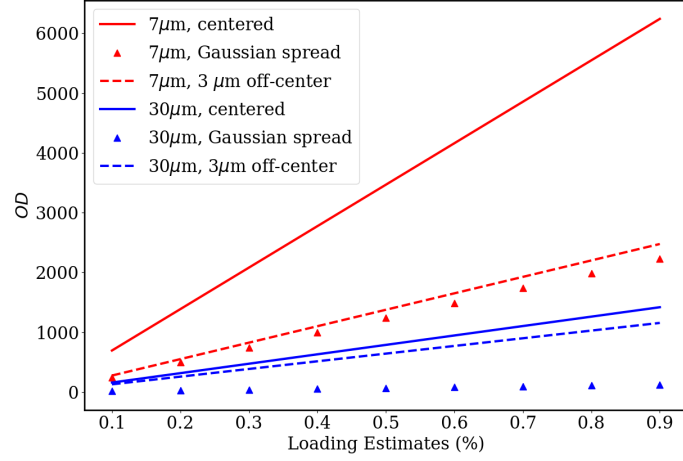
Figure 3.13: For OD_1, two measures of optical depth for centred and off-centred (by 3 μm) Cs atoms in 7μm and 30μm are plotted, where off-centring is incorporated by considering mode area as A_{eff}. Triangular markers denote OD_2 estimates with $w_0 = w_{r,0}$. Starting with 100 million atoms, loading estimates suggests N_{atom}.
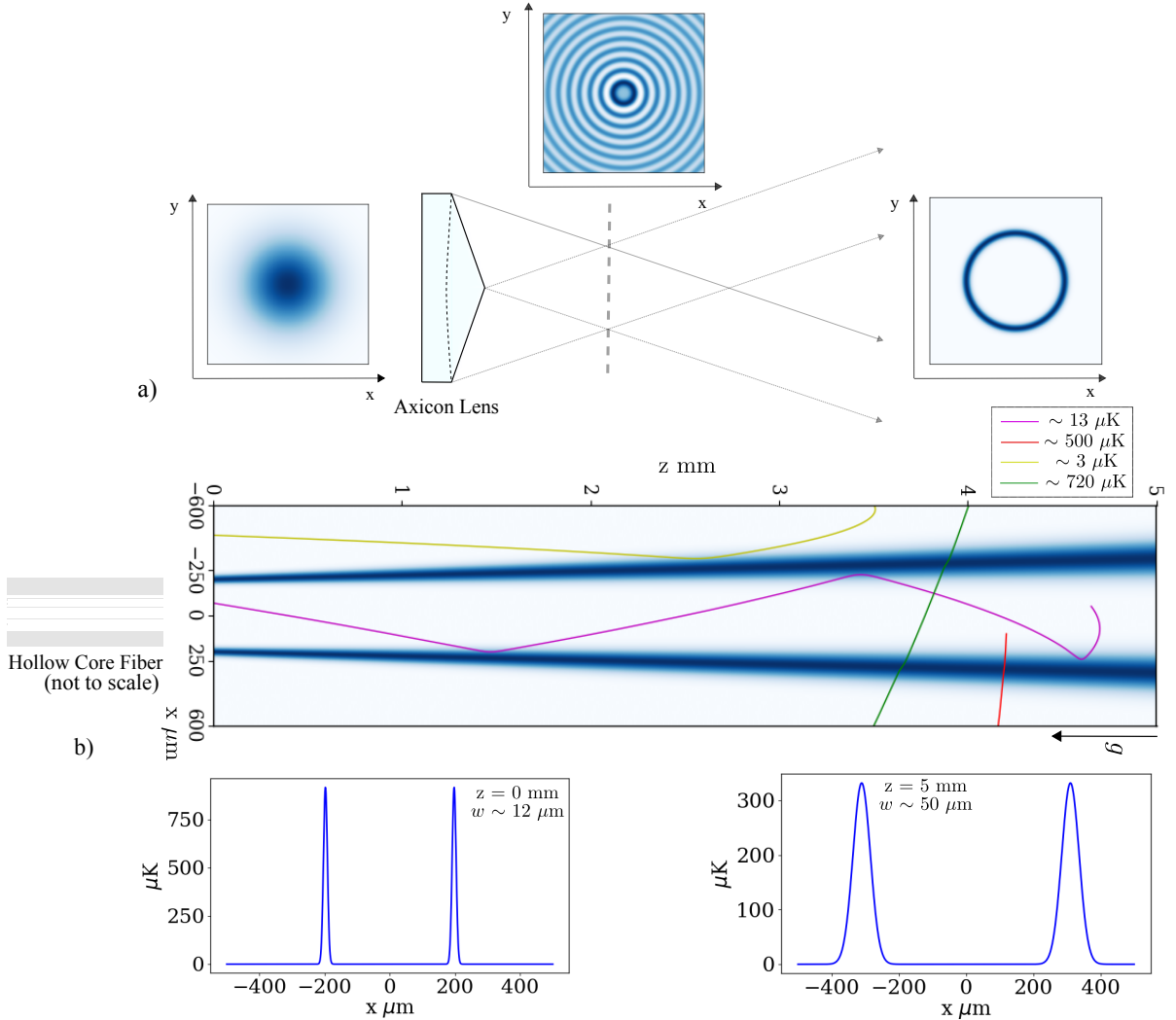
Figure 3.14: a) As depicted in Ref.[183], a conical glass lens (axicon) generates a hollow ring in its far-field and a Bessel-like beam in its near-field. b) This can be used to form a hollow tunnel for the atoms. The hollow beam is approximated using a Gaussian function to correspond to the features mentioned in Ref.[191]. Below, the potential along x formed at the fiber face ($z = 0$ mm) and ($z = 5000$ mm) are shown. Atoms with high velocities (red and green) can escape or enter the tunnel, and atoms with low velocities (purple and yellow) are kept inside or repelled. Coloured legends correspond to the atom's initial transverse kinetic energy. Trajectories are computed with $\Delta t = 0.1$ μs.

The idea to use such beams is to limit [Fig. 3.15] the horizontal spread of atoms [Fig. 3.2] after the MOT is turned off. In the scenario of Ref.[189], [Fig. 3.2], as atoms travel from 5 mm atop the fiber to $z = \sim 500$ μm, a factor of about ~ 50 - 100 are lost; and another factor of ~ 50 are lost while making their way into the fiber. As a starting point, the hollow field [Fig. 3.14] is approximated using Gaussian functions: wherein, the values for the beam waist, potential depth and ring radius are linearly fit to the measurements at two z locations provided in Ref.[190, 191]. The details of which, along with a comparison of the reported and simulated loading efficiencies (for $N_{atom} = 10^6$ and a time-step $\Delta t = 0.01$ μs) are mentioned in the table below [Fig. 3.16 a)]. When appended with a red-detuned Gaussian beam ($P = 100$ mW), [Fig. 3.16 b)] shows results of a preliminary calculation for the Cs atom loading experiment.[189] It suggests a trade-off between the hollow-beam acting as a guide versus blocking atoms which otherwise would have been loaded.
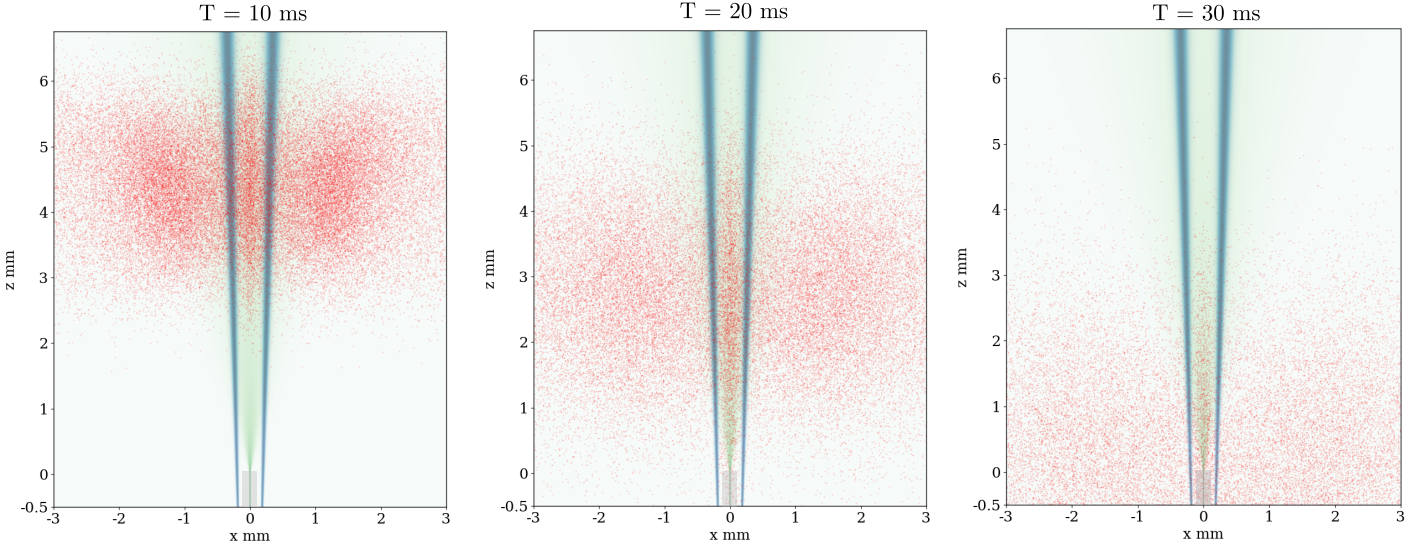
Figure 3.15: An illustration of $\sim$50,000 atoms moving in the presence of the hollow beam tunnel. The conditions of the MOT cloud and the diverging Gaussian trap are the same as in [Fig. 3.2]. $\Delta t = 0.01$ μs are presented.

	Bajcsy et al. [Exp.] [190]
Atomic Species	^{87}Rb
Axicon Power	60 mW
Axicon Wavelength	780.22 nm
Axicon Trap Height at MOT	180 μK
Axicon Trap Height at 1 mm	800 μK
Axicon Ring Waist at MOT	70 μm
Axicon Ring Waist at 1mm	20 μm
Axicon Ring Radius at Fiber Face	$\sim$200 μm
Reported Loading Efficiency	$\sim 30 \times 10^{-4}$
Simulated Loading Efficiency	55×10^{-4}
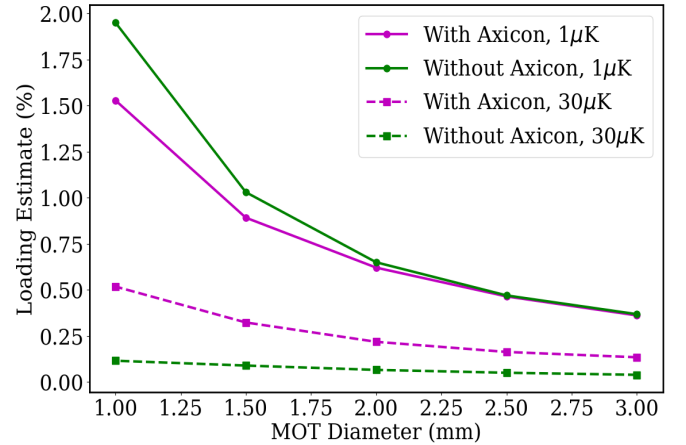
Figure 3.16: Left: Table comparing the simulation with the experiment [190, 191] implementing a hollow blue-detuned tunnel beam to load atoms. Right: For $N_{atom} = 10^6$ and Δt=0.01s, loading estimates when the blue-detuned tunnel beam and a red-detuned Gaussian with laser power P =100 mW are present.

In summary, small clouds prepared at low temperatures (1 μK) along with stronger optical potentials can increase atom numbers by a factor of $\sim$10 for the case of red-detuned Gaussian beams. Appending a axicon-generated hollow blue-detuned beam can, in some cases, increase the efficiency by a factor of $\sim$5. With regards to the discrepancies in comparison and in cases where fields vary quickly, energy conservation and accuracy of the computations needs to be checked for more carefully.

By considering different starting points of the MOT cloud and incorporating other kinds of optical forces, such a study can be extended to test alternative loading procedures. Of interest, is to be able to realize a direct

'pouring' of atoms into the fibers – which can serve us a handle to bring different numbers of atoms into the hollow fiber. Also, the role of higher-order modes of the hollow-core fiber in the loading dynamics and atomic motion inside the hollow-core fiber can be studied.

Chapter 4

Single Photon Wavelength Conversion
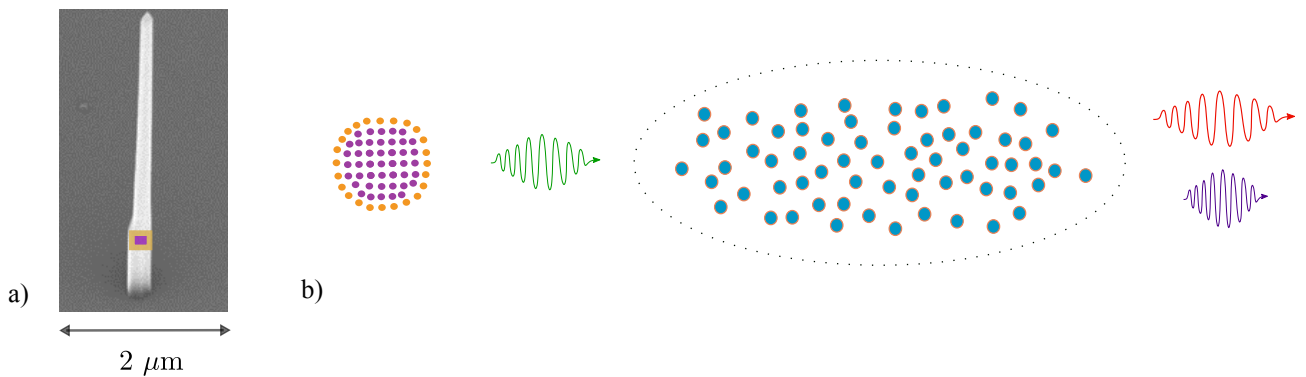
Figure 4.1: a) An SEM (scanning electron microscope) image of an InAsP Quantum Dot (QD) (represented as a coloured rectangle [not to scale]) in a tapered InP nanowire.[277] b) A schematic of interfacing light emitted from a QD with Cs atomic ensembles. If wavelength conversion in atomic ensembles can be efficient at low-light levels, an optical photon can be up or down converted for telecom or satellite-based communication.

As an example of a quantum optics process enhanced by the use of a hollow-core fiber, this chapter explores the conversion of single photons emitted by quantum dots at ∼895 nm to wavelengths that are either suitable for free-space QKD (∼794 nm) (Quantum Key Distribution) or for low-loss propagation in a commercial telecom fiber (∼1469 nm).[Fig. 4.1]

Chapter Overview: Nonlinearities of ◊-level Cs atomic ensembles might allow for such quantum frequency conversion. Following a semi-classical description, a 1D system is described using a coupled quantised equation model put forth in literature.[230] This can aid in setting up experiments by suggesting the required field strengths, detunings and optical depth. This preliminary model for plane-wave fields suggests that conversion efficiencies ∼90 % is conceivable.

Frequency conversion can be a useful tool to integrate networking and information processing elements which run on different spectral bands, and also realize frequency domain quantum information processing.[215] Ideally, apart from their frequency, one'd want all the properties of input and output photons to stay the same in order to maintain the quantum state represented by light. Such a process can also help engender networks that can distribute entanglement over many nodes.[60] For instance, stationary atomic ensembles can serve as quantum memories which can be entangled with travelling photons. Frequency conversion allows for their long-distance travel via telecom optical fibers or free-space satellite channels. Following which, at a remote node, these photons can non-locally connect the atomic clouds.

The nonlinear response of solid-state materials have been used to cross these frequency bridges. Crystals composed of $LiBNO_3$ in PPLN (periodically-poled Lithium Niobate) waveguides [60]; Si_xN_y [206] and GaAs [207] in nanophotonic structures have been used for photon-level frequency conversion. Such phenomena, as suggested by *ab-initio* electronic energy studies, tie to how electrons move upon applied fields. From a quantum mechanical perspective: atoms, in the presence of light, are cast into electronic superposition states. These coherences grant them a variety of unusual optical properties – studied under the broad umbrella of nonlinear optics. This provides one a versatile space to use the same atom for varied purposes via arranging for different kinds of optical responses. Since the 1990s, atomic media have been used to convert frequencies of light.[201]

Nonlinear Wave-Mixing and Energy-Momentum Conservation

Upon increasing the power on a two-level atom, its initially linear response saturates. Density matrix terms exhibit this nonlinearity [Fig. 2.8], and the linear response of a damped harmonic oscillator can be generalized to incorporate higher-order terms. In addition to intensity-related nonlinear effects, a combination of waves – $\vec{E} = \vec{E}_1 + \vec{E}_2 + \vec{E}_3 + \vec{E}_4$ – can be 'mixed' upon interaction.[Fig. 4.2] Classically, this might be thought of via the coupling of different oscillators.
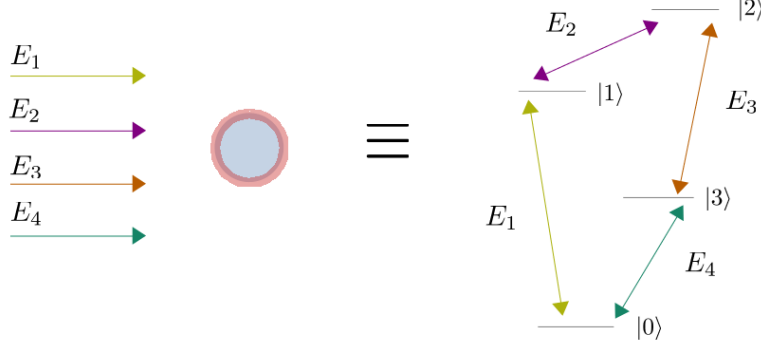
Figure 4.2: An illustration of the mixing of four light fields in the presence of atoms. Here, the discussion considers the case phase-matched co-propagating (also referred to via forward) fields.

Governed by energy-momentum conservation principles, this nonlinear response can give rise to newer frequencies by combining existing frequencies: such as – sum, difference and harmonic generation. That is, the medium can oscillate at a new frequency by accepting particular combinations of other frequencies. Phenomenologically, depending on the number of interacting fields, optical response of matter is categorized into different orders:

$$\vec{P} = \epsilon_0(\chi^{(1)} \cdot \vec{E} + \chi^{(2)} \cdot \vec{E}\vec{E} + \chi^{(3)} \cdot \vec{E}\vec{E}\vec{E} + ...) \rightarrow P_i = \epsilon_0(\chi_{ij}^{(1)} E_j + \chi_{ijk}^{(2)} E_j E_k + \chi_{ijkl}^{(3)} E_j E_k E_l + ...)$$

In effect, χ (susceptibility) engenders an interaction between photons. These multi-photon 'scattering' processes can be viewed diagrammatically [204, 205] and their propagation can be analyzed in terms of coupled wave equations.[238] As many-level systems correspond to multi-mode photon states, nonlinear processes can be used to source correlated lights.[202] And also, the mixing of photon fields within an atomic medium can lead to squeezed and entangled radiation. In fact, the first demonstration of squeezed light was made using a four-wave-mixing process.[213]

Four-wave mixing (FWM) is a third-order $\chi^{(3)}$ nonlinear process which can: $a)$ output two new fields in the presence of two fields such that: $\omega_1 + \omega_2 = \omega_3 + \omega_4$; $b)$ create an additional frequency given three fields $\omega_4 = \omega_1 + \omega_2 \pm \omega_3$; or $c)$ transform one field into three $\omega_1 + \omega_2 \pm \omega_3 = \omega_4$. For the process to be 'on resonance', incoming and outgoing beams also ought to respect momentum $[\Delta\hbar\vec{k} = 0]$ conservation which specifies their allowed directions. In addition, it is suggested that the relative phases $[\phi]$ of the applied fields 'critically determines' the atomic response.[227, 228, 229] This aspect of light transport isn't considered here.

In Rb vapours, frequency conversion via FWM has been demonstrated in $\diamond$-type [222, 223, 224] and double-Λ configurations.[220, 226, 230, 231] $\diamond$-type and double-Λ, though both four level systems, showcase differences when population decay terms are taken into consideration. Here, an attempt to port the discussion of wavelength conversion using a diamond-scheme to the case of Cs atomic ensembles is presented. The enhanced fields that the ensembles see inside a hollow-core fiber might help realizing an efficient conversion. Relatedly, the use of single Cs atom for frequency conversion interfaced to a nanophotonic waveguide has also been recently commented upon in Ref.[236].

Cs atom energies that are relevant for $\diamond$-level up and down conversion are shown in [Fig. 4.3]. One might hypothesize for the optical to telecom conversion to take place in the 30 μm fiber, and the optical to satellite wavelength conversion to take place in the 7 μm fiber [Fig 1.7]. Two telecom band transitions are being considered: an O-band wavelength – $\sim$1360 nm: $6P_{1/2} \leftrightarrow 7S_{1/2}$ and an S-band wavelength – $\sim$1470 nm: $6P_{3/2} \leftrightarrow 7S_{1/2}$. To make the atom oscillate at the S-band telecom transition, given an optical transition – say, $6P_{1/2} \leftrightarrow 6S_{1/2}$ – the sum-difference frequency generation loop: $6S_{1/2} \leftrightarrow 6P_{3/2} \leftrightarrow 7S_{1/2} \leftrightarrow 6P_{1/2} \leftrightarrow 6S_{1/2}$ can be completed. When the $6P_{1/2} \leftrightarrow 6S_{1/2}$ transition is tuned to a quantum dot transition [Fig. 4.1], the conversion of pulsed Fock states can be experimentally explored. Likewise, the sum-difference-frequency generation loop of $6S_{1/2} \leftrightarrow 6P_{3/2} \leftrightarrow 8S_{1/2} \leftrightarrow 6P_{1/2} \leftrightarrow 6S_{1/2}$ can be used to morph $\sim$894 nm photons into $\sim$794 nm photons..

In addition, an analysis of FWM processes might prove to be helpful to understand other quantum optical protocols such as: optical parametric amplification, quantum memories, phase conjugation, and nonlinear switching.

Cs ◊ Energy Levels for Frequency Conversion
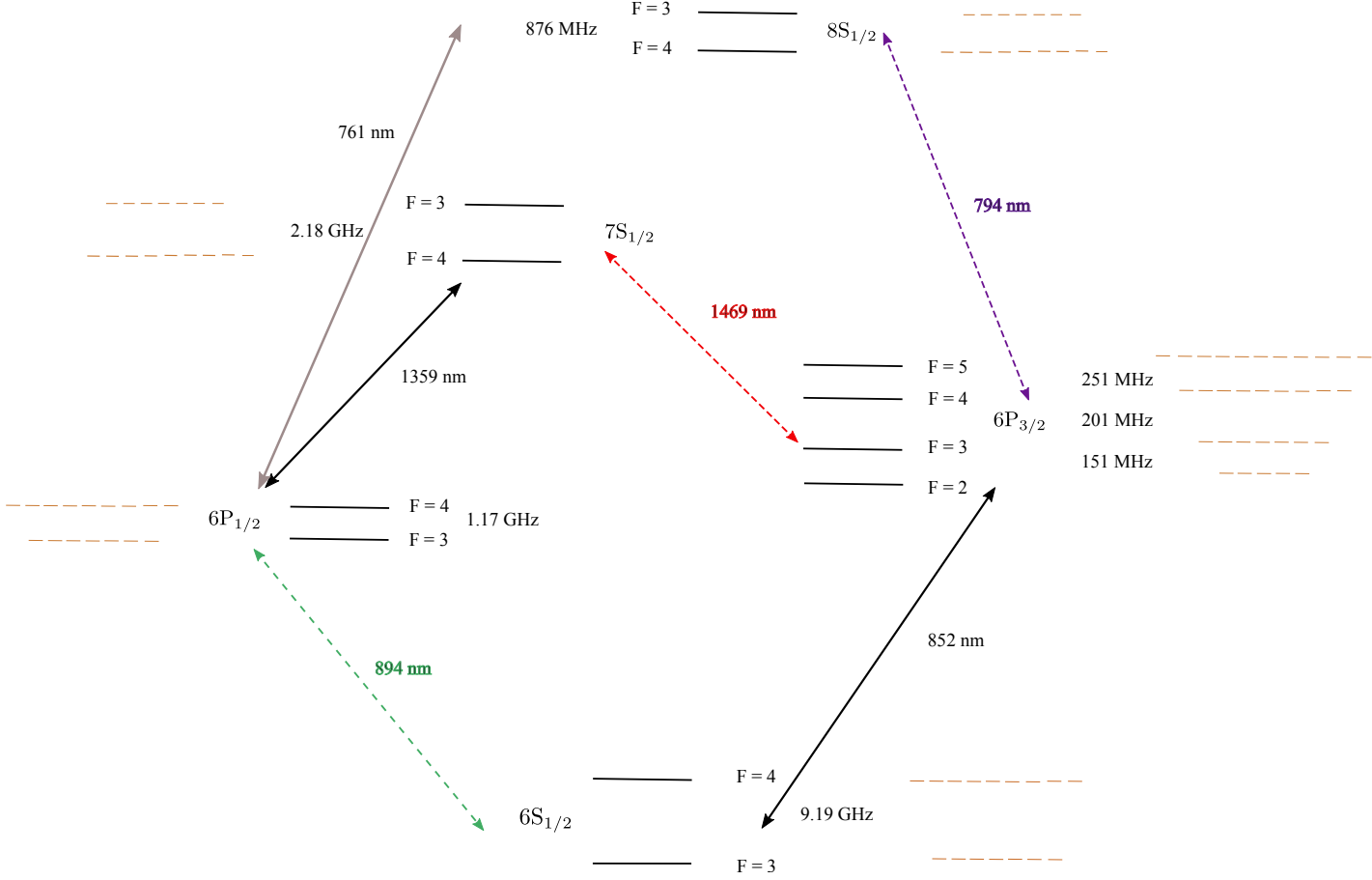
Figure 4.3: Cs fine structure energy levels $6S_{1/2}$, $6P_{3/2}$, $7S_{1/2}$, $8S_{1/2}$, $6P_{1/2}$, with its hyperfine structure and its Zeeman manifold. A more complete analysis of how atom-light interactions move through this space ought to consider all allowed decay channels and polarization-dependent couplings.[194]

[Fig. 4.3] shows Cs atom energy levels, out of which, two ◊ schemes can be used for up and down conversion. For the following discussion, details of its hyperfine levels are not considered. And, the following energy levels and emission pathways are assumed: [194, 195]

Cs Transitions	Wavelengths	Transition Dipole Matrix (μ_{ij})		$\Gamma_{free-space}$
$6S_{1/2} \leftrightarrow 6P_{3/2}$	852.35 nm	6.298 q_e a$_0$	$7S_{1/2} \to 6P_{3/2}$	$2\pi\times$ 1.99 MHz
$6P_{3/2} \leftrightarrow 7S_{1/2}$	1469.89 nm	6.489 q_e a$_0$	$7S_{1/2} \to 6P_{1/2}$	$2\pi\times$ 1.30 MHz
$6P_{1/2} \leftrightarrow 7S_{1/2}$	1359.20 nm	4.249 q_e a$_0$	$8S_{1/2} \to 6P_{3/2}$	$2\pi\times$ 0.56 MHz
$6S_{1/2} \leftrightarrow 6P_{1/2}$	894.59 nm	4.478 q_e a$_0$	$8S_{1/2} \to 6P_{1/2}$	$2\pi\times$ 0.32 MHz
$6P_{3/2} \leftrightarrow 8S_{1/2}$	794.61 nm	1.461 q_e a$_0$	$6P_{1/2} \to 6S_{1/2}$	$2\pi\times$ 4.51 MHz
$6P_{1/2} \leftrightarrow 8S_{1/2}$	761.10 nm	1.026 q_e a$_0$	$6P_{3/2} \to 6S_{1/2}$	$2\pi\times$ 5.23 MHz

4.1   Semi-classical Solution of Four-Level Atom

[Fig. 4.4] shows the two ◊ energy levels which couple two weak (photon) fields with two strong classical laser fields. From an experimental point of view, one'd want to know for a given length of the atomic cloud inside the fiber, what conditions of the applied laser fields – such as their detunings and strengths – lend us appreciable conversion of the input field (E_i) into the frequency-converted signal field (E_s).

First, to get an idea as to how multi-level atoms can couple fields of different frequencies, a basic sketch is presented.[220, 221] Atomic state evolution is penned by Schrodinger's equation, which enters light's propagation equation, specified by Maxwell's equations, via the polarization term: $\vec{P}$. Termed as 'Maxwell-Bloch' or 'Maxwell-Schrodinger' equations, they help describe a range of phenomena such as: absorption, dispersion, lasing, self-induced transparency and formation of solitons.[38] In a steady-state approach, atomic evolution equations can be solved independently; which can then be incorporated into field evolution.

Material Properties from Quantum Theory
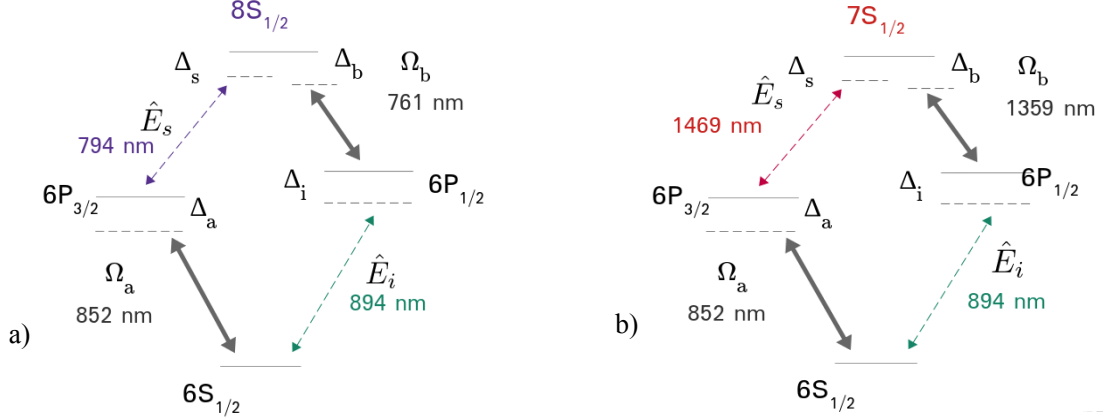
Figure 4.4: Applied laser fields along with input and output coupled fields for the ◇-level schemes outlined in [Fig. 4.3]. The dotted lines represent: $\Omega_i/\hat{E}_i$ (corresponding to the input wave) and $\Omega_s/\hat{E}_s$ (corresponding to the output signal wave). These are much lower in strength than the control fields Ω_a and Ω_b, denoted by bolder arrows. The levels are represented as (in the clock-wise direction): $(|0\rangle, |1\rangle, |2\rangle, |3\rangle \leftrightarrow 6S_{1/2}, 6P_{3/2}, 7S_{1/2}/8S_{1/2}, 6P_{1/2})$.

For a single atom (at some position $\vec{r}_0$), the energies and couplings shown in [Fig. 4.4] are mentioned in the Schrodinger equation. The coupling between the levels due to classical fields is parameterized by Ω_{ij} terms. Here, $\hbar\Omega_{ij} = \mu_{ij}E_{ij}e^{i\Phi_{ij}}$ ($i < j$, E_{ij} is the amplitude of the electric field and $\mu_{ij} = \langle i|\hat{d}|j\rangle$ is the transition dipole matrix element) invokes the dipole approximation, and the rotating wave approximation is assumed. Φ_{ij} takes into account the phase of the electric field: (- $\vec{k}_{ij} \cdot \vec{r}_0 + \omega'_{ij}t + \phi_{ij}$). The applied fields and atomic frequencies relate by:

$$\omega_x = (\omega'_x + \Delta_x)$$

The primed variables are the laser frequencies, Δ_x are detunings, and ω_x corresponds to the actual transitions. (a, b) refer to the two classical laser fields, and (i, s) to the input and signal lights. Given an arrangement of incident lights, a steady-state solution for the electronic wavefunction: $\rho = |\psi\rangle\langle\psi|$ can be sought. For $\vec{r}_0 = 0$, by making the following transformation and assuming that the applied frequencies satisfy the condition: $\omega'_b + \omega'_i = \omega'_s + \omega'_a$, the Hamiltonian can be made time-independent by a transformation:

$$\hat{R} = \begin{pmatrix} 1 & 0 & 0 & 0 \\ 0 & e^{i\omega'_a t} & 0 & 0 \\ 0 & 0 & e^{i(\omega'_s + \omega'_a)t} & 0 \\ 0 & 0 & 0 & e^{i\omega'_i t} \end{pmatrix}$$

$$|\psi\rangle \rightarrow |\tilde{\psi}\rangle = \hat{R}|\psi\rangle \qquad\qquad \hat{H} \rightarrow \tilde{\hat{H}}$$

With this, the time evolution equation: $i\hbar\frac{d|\tilde{\psi}\rangle}{dt} = \tilde{\hat{H}}|\tilde{\psi}\rangle$ can be written as:

$$[2i]\begin{pmatrix} \dot{\tilde{c}}_0 \\ \dot{\tilde{c}}_1 \\ \dot{\tilde{c}}_2 \\ \dot{\tilde{c}}_3 \end{pmatrix} = \begin{pmatrix} 0 & \Omega_a & 0 & \Omega_i \\ \Omega_a^* & 2\Delta_a & \Omega_s & 0 \\ 0 & \Omega_s^* & 2\Delta_{s,a} & \Omega_b^* \\ \Omega_i^* & 0 & \Omega_b & 2\Delta_i \end{pmatrix}\begin{pmatrix} \tilde{c}_0 \\ \tilde{c}_1 \\ \tilde{c}_2 \\ \tilde{c}_3 \end{pmatrix}$$

$(-\Omega \rightarrow \Omega)$ is assumed by setting μ_{ij}'s phase, and $\Phi_{ij} \rightarrow \phi_{ij}$. And, $\Delta_{s,a} = \Delta_{i,b} = \Delta_s + \Delta_a = \Delta_i + \Delta_b$. Steady-states [Fig. 2.3], $\dot{\tilde{c}} \rightarrow 0$, refer to the 'settled' quantum states – which can be expressed in terms of field

strengths, phases and detuning. By approximating the population to be in the ground state (which can be justified when the fields are weak), coefficients $\tilde{c}_1$, $\tilde{c}_2$, $\tilde{c}_3$ are written as: (using [219])

$$\tilde{c}_0 \to 1$$

$$\tilde{c}_1 \to \frac{(-4\Delta_i\Delta_{s,a} + |\Omega_b|^2)\Omega_a^* - \Omega_s\Omega_i^*\Omega_b^*}{8\Delta_a\Delta_i\Delta_{s,a} - 2\Delta_a|\Omega_b|^2 - 2\Delta_i|\Omega_s|^2}$$

$$\tilde{c}_2 \to \frac{\Delta_a\Omega_i^*\Omega_b^* + \Delta_i\Omega_a^*\Omega_s^*}{4\Delta_a\Delta_i\Delta_{s,a} - \Delta_a|\Omega_b|^2 - \Delta_i|\Omega_s|^2}$$

$$\tilde{c}_3 \to \frac{(-4\Delta_a\Delta_{s,a} + |\Omega_s|^2)\Omega_i^* - \Omega_b\Omega_a^*\Omega_s^*}{8\Delta_a\Delta_i\Delta_{s,a} - 2\Delta_a|\Omega_b|^2 - 2\Delta_i|\Omega_s|^2}$$

From such an electronic state, the expectation value of polarization [of a medium with number density (number of atoms per unit volume) $\mathcal{N}$] can be inferred by the averaged value of the position of the electron (dipole moment):

$$P(z,t) = \mathcal{N}\langle\hat{d}\rangle = \mathcal{N}\mathrm{Tr}[\hat{d}\rho] \to \mathcal{N}\mathrm{Tr}[\tilde{\hat{d}}\tilde{\rho}]$$

In the rotated frame, the density matrix elements can be written via $-\tilde{\rho}_{ij} = \tilde{c}_i\tilde{c}_j^*$:

$$\begin{pmatrix} \tilde{\rho}_{00} & \tilde{\rho}_{01} & \tilde{\rho}_{02} & \tilde{\rho}_{03} \\ \tilde{\rho}_{10} & \tilde{\rho}_{11} & \tilde{\rho}_{12} & \tilde{\rho}_{13} \\ \tilde{\rho}_{20} & \tilde{\rho}_{21} & \tilde{\rho}_{22} & \tilde{\rho}_{23} \\ \tilde{\rho}_{30} & \tilde{\rho}_{31} & \tilde{\rho}_{32} & \tilde{\rho}_{33} \end{pmatrix}$$

Also, in the rotated frame, the dipole matrix operator elements would look like:

$$\begin{pmatrix} 0 & \mu_a & 0 & \mu_i \\ \mu_a^* & 0 & \mu_s & 0 \\ 0 & \mu_s^* & 0 & \mu_b^* \\ \mu_i^* & \mu_b & 0 & 0 \end{pmatrix} \to \begin{pmatrix} 1 & 0 & 0 & 0 \\ 0 & e^{i\omega_a't} & 0 & 0 \\ 0 & 0 & e^{i(\omega_s'+\omega_a')t} & 0 \\ 0 & 0 & 0 & e^{i\omega_i't} \end{pmatrix} \begin{pmatrix} 0 & \mu_a & 0 & \mu_i \\ \mu_a^* & 0 & \mu_s & 0 \\ 0 & \mu_s^* & 0 & \mu_b^* \\ \mu_i^* & \mu_b & 0 & 0 \end{pmatrix} \begin{pmatrix} 1 & 0 & 0 & 0 \\ 0 & e^{-i\omega_a't} & 0 & 0 \\ 0 & 0 & e^{-i(\omega_s'+\omega_a')t} & 0 \\ 0 & 0 & 0 & e^{-i\omega_i't} \end{pmatrix}$$

$$\to \begin{pmatrix} 0 & \mu_a e^{-i\omega_a't} & 0 & \mu_i e^{-i\omega_i't} \\ \mu_a^* e^{i\omega_a't} & 0 & \mu_s e^{-i\omega_s't} & 0 \\ 0 & \mu_s^* e^{i\omega_s't} & 0 & \mu_b^* e^{i\omega_b't} \\ \mu_i^* e^{i\omega_i't} & \mu_b e^{-i\omega_b't} & 0 & 0 \end{pmatrix}$$

The input and signal terms in $\mathrm{Tr}[\tilde{\hat{d}}\tilde{\rho}]$ are:

$$(\tilde{\rho}_{12}\mu_s^* e^{i\omega_s't} + \tilde{\rho}_{03}\mu_i^* e^{i\omega_i't}) + (\tilde{\rho}_{12}^*\mu_s e^{-i\omega_s't} + \tilde{\rho}_{03}^*\mu_i e^{-i\omega_i't})$$
$$= (\tilde{\rho}_{12}\mu_s^* e^{i\omega_s't} + \tilde{\rho}_{12}^*\mu_s e^{-i\omega_s't}) + (\tilde{\rho}_{03}\mu_i^* e^{i\omega_i't} + \tilde{\rho}_{03}^*\mu_i e^{-i\omega_i't})$$

In relation to which, input and signal components of atomic polarization can be written as:

$$(P_s(z)\exp i(\omega_s't + \kappa_1) + c.c) + (P_i(z)\exp i(\omega_i't + \kappa_2) + c.c)$$

Including the spatial phase component of the fields $[e^{i\vec{k}\cdot\vec{r}}]$ (assumed to be co-propagating in the z-direction) in Ω_{ij}, $\vec{P}$ (in the steady-state) are written in terms of the electric fields by substituting the coefficients ($\tilde{c}$) into the density matrix terms: (with $E_{ij} \to E_{ij}e^{\phi_{ij}}$)

$$P_i(z) = \chi_i^{(1)}E_i\exp[-i(k_iz)] + \chi_{iabs}^{(3)}E_aE_b^*E_s\exp[-i(k_a + k_s - k_b)\cdot z]$$
$$P_s(z) = \chi_s^{(1)}E_s\exp[-i(k_sz)] + \chi_{sabi}^{(3)}E_a^*E_bE_i\exp[-i(k_b + k_i - k_a)\cdot z]$$
$$+ \chi_{ssaib}^{(4)}E_s^2E_aE_i^*E_b^*\exp[i(2k_s + k_a - k_i - k_b)\cdot z]$$

From here, nonlinear susceptibility terms and momentum conservation (phase-matching) criteria can be inferred. Propagation of fields can be estimated in the slowly-varying envelope approximation (SVEA) regime.[18, 35, 38] ($\mathcal{E}$ and $\mathcal{P}$ are the envelopes of E and P, where $E(z,t) = \mathcal{E}(z,t)\exp i(kz - \omega't) + c.c$ and $P(z,t) = \mathcal{P}(z,t)\exp i(kz - \omega't) + c.c.$) Assuming: $\Delta k = k_s + k_a - k_i - k_b = 0$, and when the input and signal fields are very weak, only their first-order terms are kept, field propagation equations take the form:

$$\frac{\partial\mathcal{E}_i(z)}{\partial z} = \mathcal{N}\frac{i\omega_i'}{2c\epsilon_0}\mathcal{P}_i(z) = \mathcal{N}\frac{i\omega_i'}{2c\epsilon_0}\tilde{\rho}_{21}\mu_i e^{-ik_iz} \to \frac{\partial\mathcal{E}_i}{\partial z} = \alpha_i\mathcal{E}_i + \kappa_{is}\mathcal{E}_s$$

$$\frac{\partial\mathcal{E}_s(z)}{\partial z} = \mathcal{N}\frac{i\omega_s'}{2c\epsilon_0}\mathcal{P}_s(z) = \mathcal{N}\frac{i\omega_s'}{2c\epsilon_0}\tilde{\rho}_{30}\mu_s e^{-ik_sz} \to \frac{\partial\mathcal{E}_s}{\partial z} = \alpha_s\mathcal{E}_s + \kappa_{si}\mathcal{E}_i$$

These coupled equations describe the interplay between the two (input and signal) modes of light. While α_i, α_s are self-coupling coefficients (the field effects its own propagation – such as absorption and dispersion), κ_{is}, κ_{si} talk about the effect of one field on another.

Semi-classical Density Matrix Solution

Two assumptions made in the calculation above can be addressed. First, given that the applied laser field (Ω_a) isn't necessarily weak, steady-state population needn't be in the ground state. Second, an open quantum systems perspective suggests the atomic coupling to the environmental modes can be included in system dynamics via a Lindblad master equation. ($\tilde{\rho}$ are re-written as ρ.)
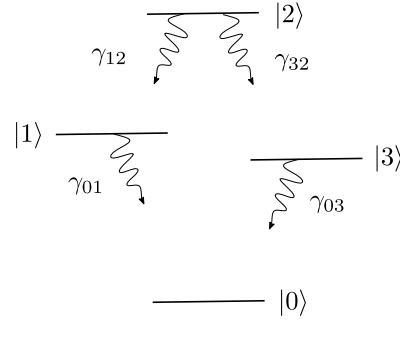
$$\frac{\partial \rho}{\partial t} = \frac{-i}{\hbar}[\hat{H}, \rho] - \hat{D}$$

The decay terms are considered as mentioned in Ref.[218]:

$$\hat{D}_{ij} = -\sum \frac{1}{2}[2\hat{A}_{ij}\rho(t)\hat{A}_{ij}^\dagger - \rho(t)\hat{A}_{ij}^\dagger\hat{A}_{ij} - \hat{A}_{ij}^\dagger\hat{A}_{ij}\rho(t)] \to \hat{D}_{ij} = -\sum[\gamma_{ij}\rho_{jj}|i\rangle\langle i| - \frac{\gamma_{ij}}{2}(\rho|j\rangle\langle j| - |j\rangle\langle j|\rho)]$$

As briefly mentioned earlier, only the following emission processes are considered which maintain the electronic population among the four levels. Extensions to this approach can be considered via adding loss channels through a non-Hermitian Hamiltonian.[236]

$$\hat{D} = \begin{bmatrix} (\gamma_{01}\rho_{11} + \gamma_{03}\rho_{33}) & -\rho_{01}\Gamma_{01} & -\rho_{02}\Gamma_{02} & -\rho_{03}\Gamma_{03} \\ -\rho_{10}\Gamma_{10} & (-\rho_{11}\gamma_{01} + \rho_{22}\gamma_{12}) & -\rho_{12}\Gamma_{12} & -\rho_{13}\Gamma_{13} \\ -\rho_{02}\Gamma_{02} & -\rho_{21}\Gamma_{12} & (-\rho_{22}\gamma_{12} - \rho_{22}\gamma_{32}) & -\rho_{23}\Gamma_{23} \\ \rho_{30}\Gamma_{03} & -\rho_{31}\Gamma_{13} & -\rho_{32}\Gamma_{23} & (-\rho_{33}\gamma_{03} + \rho_{22}\gamma_{23}) \end{bmatrix}$$

$$\Gamma_{01} = \frac{\gamma_{01}}{2}$$
$$\Gamma_{02} = \frac{\gamma_{12} + \gamma_{32}}{2}$$
$$\Gamma_{03} = \frac{\gamma_{03}}{2}$$
$$\Gamma_{12} = \frac{\gamma_{12} + \gamma_{32} + \gamma_{01}}{2}$$
$$\Gamma_{13} = \frac{\gamma_{01} + \gamma_{03}}{2}$$
$$\Gamma_{23} = \frac{\gamma_{03} + \gamma_{12} + \gamma_{32}}{2}$$

Plugging in the terms into the matrix time-evolution equation:

$$\dot{\rho_{00}} = \frac{-i}{2}(\Omega_a\rho_{10} - \Omega_a^*\rho_{01} + \Omega_i\rho_{30} - \Omega_i^*\rho_{03}) + (\gamma_{01}\rho_{11} - \gamma_{03}\rho_{33})$$

$$\dot{\rho_{11}} = \frac{-i}{2}(\Omega_a^*\rho_{01} - \Omega_a\rho_{10} + \Omega_s\rho_{21} - \Omega_s^*\rho_{12}) + (\gamma_{12}\rho_{22} - \gamma_{01}\rho_{11})$$

$$\dot{\rho_{22}} = \frac{-i}{2}(\Omega_s^*\rho_{12} - \Omega_s\rho_{21} + \Omega_b^*\rho_{32} - \Omega_b\rho_{23}) - (\gamma_{12}\rho_{22} + \gamma_{32}\rho_{22})$$

$$\dot{\rho_{33}} = \frac{-i}{2}(\Omega_i^*\rho_{03} - \Omega_i\rho_{30} + \Omega_b\rho_{23} - \Omega_b^*\rho_{32}) + (\gamma_{32}\rho_{22} - \gamma_{03}\rho_{33})$$

$$\dot{\rho_{01}} = \frac{-i}{2}(\Omega_a\rho_{11} - \Omega_a\rho_{00} + \Omega_i\rho_{31} - 2\Delta_a\rho_{01} - \Omega_s^*\rho_{02}) - \Gamma_{01}\rho_{01}$$

$$\dot{\rho_{02}} = \frac{-i}{2}(\Omega_a\rho_{12} + \Omega_i\rho_{32} - \Omega_s\rho_{01} - 2\Delta_{s,a}\rho_{02} - \Omega_b\rho_{03}) - \Gamma_{02}\rho_{02}$$

$$\dot{\rho_{03}} = \frac{-i}{2}(\Omega_a\rho_{13} + \Omega_i\rho_{33} - \Omega_i\rho_{00} - 2\Delta_i\rho_{03} - \Omega_b^*\rho_{02}) - \Gamma_{03}\rho_{03}$$

$$\dot{\rho_{12}} = \frac{-i}{2}(\Omega_a^*\rho_{02} + 2\Delta_a\rho_{12} + \Omega_s\rho_{22} - \Omega_s\rho_{11} - 2\Delta_{s,a}\rho_{12} - \Omega_b\rho_{13}) - \Gamma_{12}\rho_{12}$$

$$\dot{\rho_{23}} = \frac{-i}{2}(\Omega_s^*\rho_{13} + 2\Delta_{s,a}\rho_{23} + \Omega_b^*\rho_{33} - \Omega_i\rho_{20} - \Omega_b^*\rho_{22} - 2\Delta_i\rho_{23}) - \Gamma_{23}\rho_{23}$$

$$\dot{\rho_{13}} = \frac{-i}{2}(\Omega_a^*\rho_{03} + 2\Delta_a\rho_{13} - \Omega_i\rho_{10} - \Omega_b^*\rho_{12} - 2\Delta_i\rho_{13} + \Omega_s\rho_{23}) - \Gamma_{13}\rho_{13}$$

Approximations and Steady-State ρ Elements

Compared to the classical fields Ω_a and Ω_b, one can view input (Ω_i) and signal (Ω_s) fields as weak perturbations on the atom. This suggests that higher-order terms corresponding to their intensities can be neglected.

$$\hat{H} = \hat{H}_{atom} + \hat{H}_{classical} + \hat{H}_{weak} = \hat{H}_{atom-classical} + \hat{H}_{weak}$$

ρ can be expressed as a combination of different orders of responses:

$$\rho(t) = \rho^{(0)} + \rho^{(1)} + \rho^{(2)} + ... + \rho^{(n)} + ...$$

In the absence of decays, assuming the ith order correction to be written as: [216]

$$i\hbar\frac{d\rho^{(i)}}{dt} = [\hat{H}_{atom-classical}, \rho^{(i)}] + [\hat{H}_{weak}, \rho^{(i-1)}]$$

In the zeroth-order, i.e, in the absence of input and signal fields, only the control field couples $|0\rangle$ and $|1\rangle$. So, only $\rho_{00}^{(0)}$, $\rho_{01}^{(0)}$, $\rho_{11}^{(0)}$ remain non-zero, which are of the same form as discussed for the two-level case in Chapter 2. The first-order correction provides the following time-evolution of the density matrix terms are written as:

$$[2i]\dot{\rho}_{03}^{(1)} = \Omega_a\rho_{13}^{(1)} - \Omega_b^*\rho_{02}^{(1)} - 2\Delta_i\rho_{03}^{(1)} - \rho_{00}^{(0)}\Omega_i$$

$$[2i]\dot{\rho}_{12}^{(1)} = \Omega_a^*\rho_{02}^{(1)} + 2\Delta_a\rho_{12}^{(1)} - 2\Delta_{s,a}\rho_{12}^{(1)} - \Omega_b\rho_{13}^{(1)} - \Omega_s\rho_{11}^{(0)}$$

$$[2i]\dot{\rho}_{13}^{(1)} = \Omega_a^*\rho_{03}^{(1)} + 2\Delta_a\rho_{13}^{(1)} - \Omega_b^*\rho_{12}^{(1)} - 2\Delta_i\rho_{13}^{(1)} + \Omega_i\rho_{10}^{(0)}$$

$$[2i]\dot{\rho}_{02}^{(1)} = \Omega_a\rho_{12}^{(1)} - 2\Delta_{s,a}\rho_{02}^{(1)} - \Omega_b\rho_{03}^{(1)} - \Omega_s\rho_{01}^{(0)}$$

Here, the relevant terms are $\rho_{03}^{(1)}$ and $\rho_{12}^{(1)}$. Appending the Γ terms, [216] in the steady state $(\dot{\rho}^{(1)} \to 0)$, these four-equation-four-variables along with the solution of two-level atoms provide us the coefficients α_i, α_s, κ_{is} κ_{si}. This also assumes that the classical fields maintain their intensities along the propagation. [Fig. 4.5] shows ρ_{03} terms as a function of Δ_i in relation to atom-light dressed states for the given Ω and Δ of the applied fields. Onwards, Ω is assumed to be a real number.
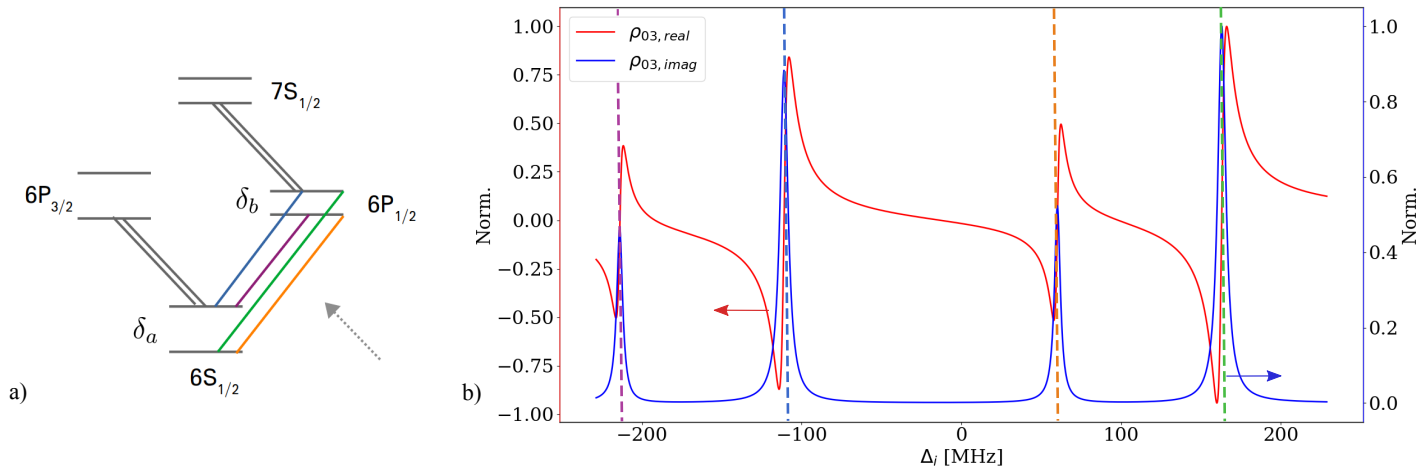
Figure 4.5: a) Energies in [Fig. 4.4] in terms of dressed states.[230, 211] Input Ω_i light can see four resonances. b) Normalized real and imaginary part of ρ_{03} density matrix terms w.r.t its detuning, which can be related to four two-level-like resonances shown in: [Fig. 2.8]. For the 894 nm $\leftrightarrow$ 794 nm conversion protocol, the classical field parameters are: $(\Omega_a, \Omega_b, \Delta_a, \Delta_b) \sim (274, 92, -5, 46)$ MHz. And the weak fields: $\Omega_i \sim 0.05$ MHz, $\Omega_s = 0$ MHz. Solutions obtained using [217].

If the incoming light is on-resonant to one of these dressed energies, it can be lost in the absorption-emission process. It is suggested that by placing the input light in an appropriate parametrically-coupled window, it is possible to morph it into the signal.[230] Relatedly, Refs.[231, 232] suggest the role of achieving entanglement-preserving and noiseless conversion by creating EIT (Electromagnetically Induced Transperancy) windows suitable for the wavelength conversion process.

4.2 Coupling to Quantized Fields

While a full derivation is yet to be carried out, here, an outline of the methods as gathered from Refs.[226, 230, 202, 233, 234, 93] is briefly attempted. And, for the subsequent plots, the results reported in Ref.[230] are adapted to the case of Cs atoms. A travelling photon pulse interacting with a one-dimensional nonlinear medium also ought to benefit from a reflection upon theoretical viewpoints that have been put forth in Refs.[51, 52, 53, 54, 55, 56, 57, 58].

$$\hat{a}_{in} \longrightarrow \qquad\qquad \dashrightarrow \hat{a}_{out}$$

Figure 4.6: 1D propagation through a medium can be expressed via input and output field operators.[226, 233]

In such a description, the input and signal fields are expressed in terms of quantised slowly varying operators, $\hat{a}(z,t)$:

$$\hat{E}_{i,s}(z,t) = \sqrt{\frac{\hbar\omega_{i,s}}{2\epsilon_0 AL}}\hat{a}_{i,s}(z,t)\exp i(k_{i,s}z - \omega_{i,s}t) + c.c.$$

And, polarization of the medium relates with the slowly varying collective atomic operators: [202, 233, 226] $\mathcal{P}_{ge}(z,t) \leftrightarrow \mathcal{N}\hat{\sigma}_{ge}(z,t)$. At each z, atomic operators are averaged over a small volume: (k_{ge} and ω_{ge} are the wave-vector and angular frequencies of the applied fields corresponding to the transitions [g, e are lower and upper energy levels], and N_z is the number density along z direction) [230]

$$\hat{\sigma}_{ge}(z,t) = \frac{1}{N_z}\sum_n^{N_z}|g_n\rangle\langle e_n| \qquad \tilde{\sigma}_{ge}(z,t) = \frac{1}{N_z}\sum_n^{N_z}|g_n\rangle\langle e_n|\exp\left[-i(k_{ge}z - \omega_{ge}t)\right]$$

Field and atomic operators $\hat{a}$ and $\hat{\sigma}$ obey commuting relations: [233]

$$[\hat{a}_i(z),\hat{a}_j^\dagger(z')] = L\delta_{ij}\delta(z-z') \qquad [\hat{\sigma}_{ij}(z),\hat{\sigma}_{kl}^\dagger(z')] = (L/N)\delta(z-z')[\delta_{jk}\hat{\sigma}_{il}(z) - \delta_{il}\hat{\sigma}_{kj}(z)]$$

As each photon couples to the entire ensemble, the energy involves an integral over the medium's length: (in the dipole and RWA approximations, and phase of the previously mentioned Ω are accounted for in $\tilde{\sigma}$) [233, 202]

$$\hat{H} = \frac{\hbar N}{2L}\int dz(2\Delta_a\tilde{\sigma}_{11} + 2\Delta_{s,a}\tilde{\sigma}_{22} + 2\Delta_i\tilde{\sigma}_{33} + g_i\hat{a}_i^\dagger\tilde{\sigma}_{03} + g_s\hat{a}_s^\dagger\tilde{\sigma}_{12} + \Omega_a\tilde{\sigma}_{01} + \Omega_b\tilde{\sigma}_{32}) + c.c \quad g_k = \mu_k\sqrt{\frac{\omega_k}{2\hbar\epsilon_0 AL}}$$

Time evolution of the atomic operators are expressed via Heisenberg-Langevin equations, as stated in Ref.[234]: (Role of quantum noise and transverse field profiles of the modes are not considered; and phase matching is assumed.)

$$\frac{\partial\tilde{\sigma}_{ij}(z,t)}{\partial t} = \frac{i}{\hbar}[\hat{H},\tilde{\sigma}_{ij}] - \gamma_{ij}^{dephasing}\tilde{\sigma}_{ij} + \delta_{ij}\sum_k \gamma_{ki}^{spontaneous}\tilde{\sigma}_{kk} + \hat{\mathcal{F}}_{ij}$$

The propagation of the fields in the steady-state are written as: [230, 202]

$$\frac{d\hat{a}_i(z)}{dz} = A_i\tilde{\sigma}_{03}(z) = \alpha_i'\hat{a}_i(z) + \kappa_{is}'\hat{a}_s(z) \qquad\qquad \frac{d\hat{a}_s(z)}{dz} = A_s\tilde{\sigma}_{12}(z) = \alpha_s'\hat{a}_s(z) + \kappa_{si}'\hat{a}_i(z)$$

It is of interest to see how these two models (semi-classical and quantised) of field propagation compare.[212] It appears that by a "substitution": $\Omega_{i,s} \to g_{i,s}\hat{a}_{i,s}^\dagger$ along with $\rho \to \sigma$ in the set of atomic operator equations as expressed in Ref.[230], one re-obtains expressions for the density matrix terms noted above. However, coupled equations obtained from a quantised field approach seem to house a different constant that relates field propagation $\partial_z\mathcal{E}_i$ to its polarization $\mathcal{P}_i$.[220, 225] Although, as suggested in the analysis of a double-Λ system,[226] conversion efficiency estimates: η, (defined below) are similar for semi-classical and quantised approaches. Also worth noting, Ref.[230] refers to Ref.[88] in order to account for cooperative phenomena in the ensemble.
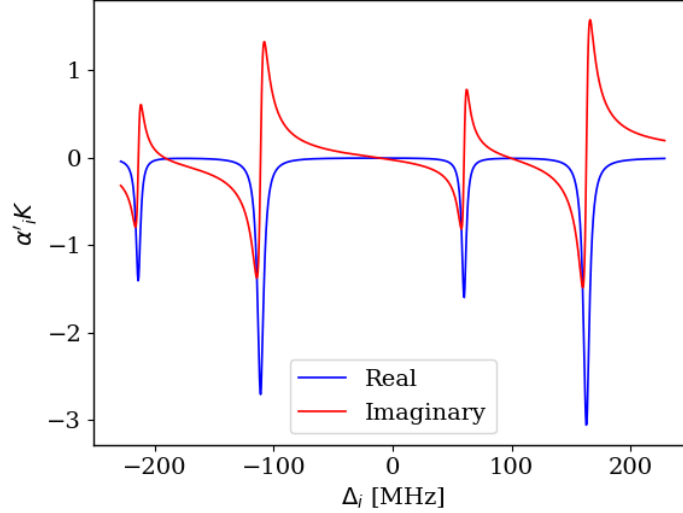
Figure 4.7: Analytically obtained [230] self-coupling coefficient α'_i versus input detuning for the 894 nm $\leftrightarrow$ 794 nm conversion protocol – $(\Omega_a, \Omega_b, \Delta_a, \Delta_b) \sim (274, 92, -5, 46)$ MHz. Such a trend can be contrasted with the Master equation based solution shown in [Fig. 4.5]. As a check, the blue peaks in [Fig. 4.5] correspond to absorption, which appear as negative, real terms in the propagation equation. (Also blue in this picture.) $K = 0.001$.

Finding optimal experimental parameters for conversion

With the coupled equation coefficients ([Fig. 4.7] shows the plot of α'_i v/s Δ_i), the propagation equations lend us the efficiency (η) of conversion. With the boundary condition of the signal field amplitude (at $z = 0$) $\to 0$, the field amplitudes after propagation can be calculated. In general, η is a function of the parameters: $(\Omega_a, \Omega_b, \Delta_a, \Delta_b, \Delta_i, OD, L)$. OD is defined as $\rho\sigma_{cross}L$ – where ρ is the atomic density, σ_{cross} is the absorption cross-section shown in [Fig. 1.5] and L is length of the sample.

$$\eta(\Omega_a, \Omega_b, \Delta_a, \Delta_b, \Delta_i, OD, L) = \frac{\langle \hat{a}_s^\dagger \hat{a}_s \rangle}{\langle \hat{a}_i^\dagger \hat{a}_i \rangle}$$

By fixing any number of the above parameters, we can optimize this function. An illustration of this seemingly non-trivial space of exploration is given in [Fig. 4.8]. Fixing $L = 6$ mm, (as also explored in Ref.[230]) the parameters: $(\Omega_a, \Omega_b, \Delta_a, \Delta_b, \Delta_i)$ are searched through in a range of 300 MHz for each OD value. The optimization attempted is a 'dual annealing' algorithm, which is a standard library routine in the Python numerical package, SciPy. It appears that increasing the number of atoms helps us park ourselves towards higher efficiencies.[Fig. 4.9 a)]. And, by fixing N_{atom}, one can re-write OD in terms of (effective) mode area (if the definition mentioned in Pg. 30 is used [Fig. 4.9 b)]).

Also, at a given OD, for each set of optimal values that is generated: $(\Omega_a, \Omega_b, \Delta_a, \Delta_b)$, Δ_i is varied to check for the 'bandwidth' (the frequency window allowing for plane-wave conversion) of the conversion.[Fig. 4.10] It appears that both, high optical depths and high powers are required for a broadband conversion – a trend also suggested for EIT-based coherent broadband memories in a Λ-level system.[208] However, Ref.[232] briefly mentions that lower optical depths might also aid in realizing efficient conversion.

Required Field Strengths for Hollow Fibers

To check for the power requirements suggested in [Fig. 4.10], [Fig. 4.11] translates Ω for confined Gaussian modes in the $\sim$7 μm and $\sim$30 μm hollow-core fibers. $\Omega \to 1$ GHz field amplitude requirements are attainable with the hollow fibers when mW range powers are used.
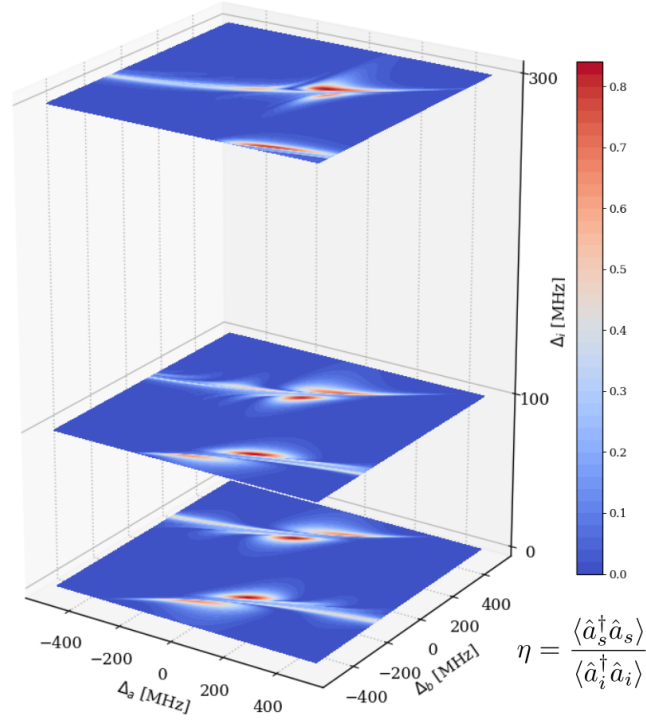
Figure 4.8: Cross-sections of η (for the 894 nm $\leftrightarrow$ 794 nm conversion protocol) v/s (Δ_a and Δ_b) for varying Δ_i; $\Omega_a = 300$ MHz and $\Omega_b = 50$ MHz, OD = 1000, $L = 6$ mm, showing the parametric landscape formed by the fields.
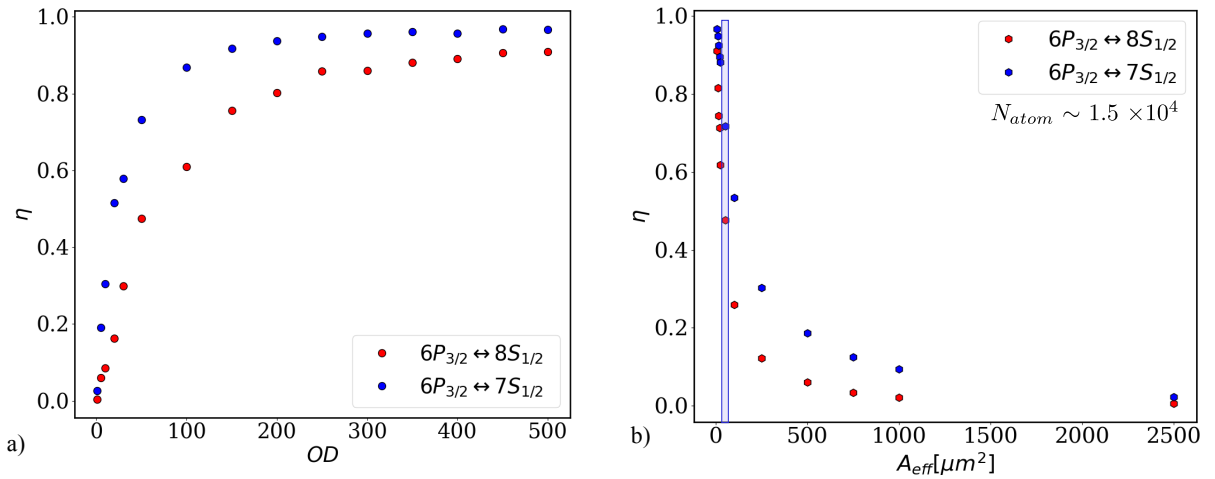
Figure 4.9: a) Estimates of conversion efficiency versus optical depth for a 6 mm atomic cloud. b) Mode area plays the role of providing an effective optical depth. Given a number of atoms, either all centred with the mode or radially separated, we can estimate the range of η possible. For the 894 nm $\leftrightarrow$ 794 nm conversion protocol, and for ~17,000 atoms [189] within a ~7 μm fiber – which can have an A_{eff} effective mode area [Fig. 3.12] ranging from ~25 to 60 μm^2, (OD ~ 40 - 100) – the light blue box roughly suggests an η of ~50 to 80.
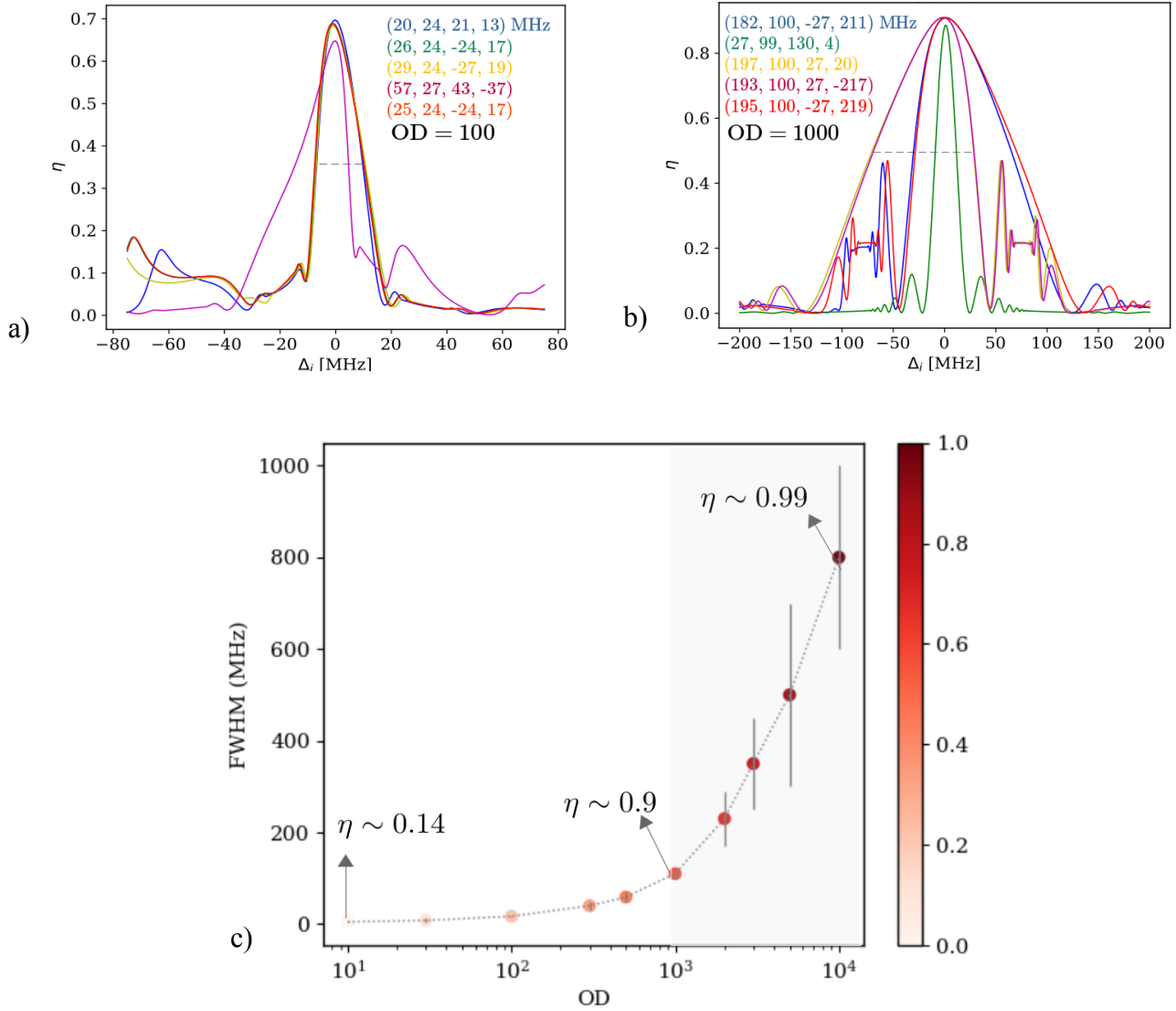
Figure 4.10: For the mentioned parameters of $(\Omega_a, \Omega_b, \Delta_a, \Delta_b)$, η v/s Δ_i plots are obtained. a) Shows some possible results with an OD = 10, and b) OD = 1000. It appears that, in some cases, increasing the optical depth can also increase the frequency range where reasonable conversion efficiencies can be obtained. c) For each OD, estimates of a range of FWHM (full-width half maximum) are plotted. The vertical bars are to denote possible variations in these widths (as can also be gathered from a) and b)). The light gray shaded region indicates where the applied field strengths (Ω) are in the $\sim$ GHz range. These results correspond to the 894 nm $\leftrightarrow$ 794 nm conversion protocol.
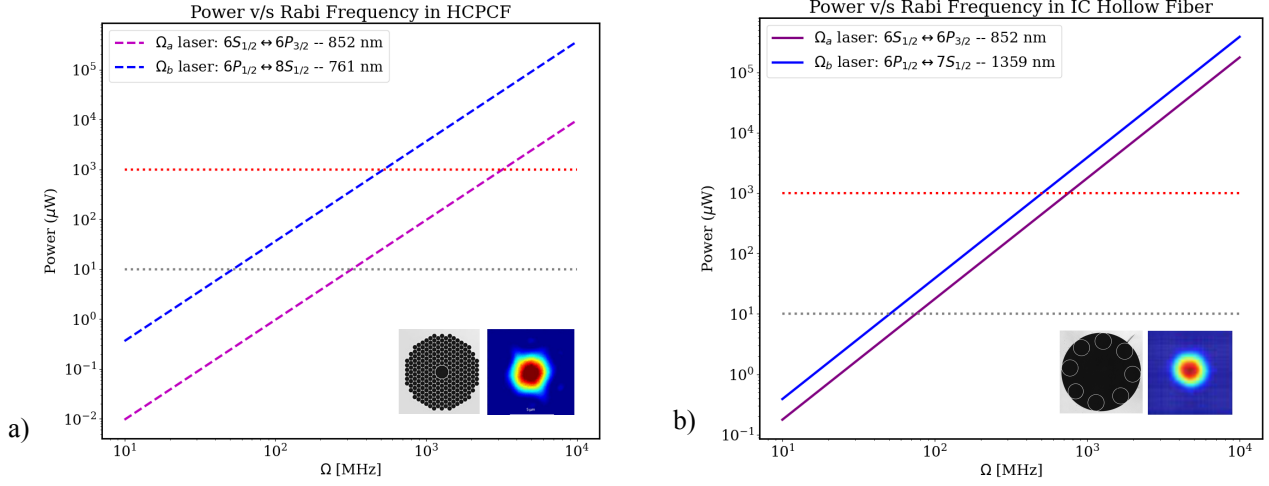
Figure 4.11: Power requirements, according to the relation: $\Omega = \frac{|\mu \vec{E}|}{\hbar}$ for the ~ 7 μm photonic bandgap fiber (optical - infra-red conversion protocol), and the ~ 30 μm IC fiber (optical - telecom conversion protocol) mentioned in [Fig. 1.7]. $|\vec{E}|$ refers to the amplitude of the Gaussian mode. The dotted gray and red lines denote the 10 μW and 1 mW limit, respectively.

4.3 Outlook: How to consider light from Quantum Dots?

Both field and atomic evolution have to be changed to incorporate pulsed input fields. SVEA equations for the field ought to involve a $\partial_t E(z, t)$ term. And the transient behaviour of the density matrix elements limits the steady-state approximation. In relevance to experiment, one has to consider how an ensemble responds to light from a quantum dot whose pulses can be of the order ~ 1 ns. It is possible to convert the four temporal equations mentioned in Pg. 39 (which also apply to atomic operators) into a linear set by moving into the frequency domain, as mentioned in.[203, 208, 210, 233] After following through their propagation, pulses can be put back together via an inverse Fourier transform. Under the assumption that SVEA is valid for short pulses, [Fig. 4.12] presents a preliminary calculation.
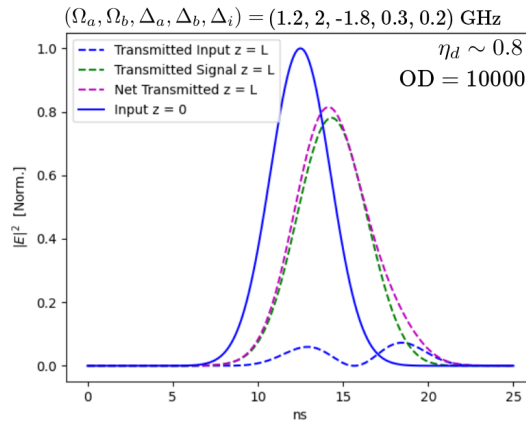
Figure 4.12: A preliminary calculation to consider pulse propagation. Here, for the mentioned field conditions and optical depth, a 5 ns Gaussian pulse is followed as it passes through an ensemble of atoms with $L = 6$ mm.

As an outlook, derivations involving quantum light propagation need to be properly considered, and also, further detail concerning the quantum nature of light needs to be filled in: such as fidelity, quadrature, correlations and the role of quantum noise.[226] And, to form a more complete picture of photon wavelength conversion in the hollow fiber, one also has to incorporate the role of mode-confinement, motion and geometry of the atomic ensemble, the role of phase-matching, hyperfine levels [237] and spatially varying control pulses.[209]

Chapter 5

Electromagnetic Properties of a 2D Photonic Crystal Membrane

The interactions between photons and atoms inside the hollow-core fibre can potentially be further enhanced by integrating an optical resonator (cavity) into the fiber. However, realizing the cavity while making the fiber accessible for atom loading presents a challenge. Recently, [71] reported creating a cavity inside a hollow-core fiber by capping a short section of the fiber with perforated dielectric slabs that act as photonic crystal mirrors. While loading room temperature atoms into such cavities should be straightforward, guiding cold atoms through a photonic crystal slab comes with potential pitfalls and has not been studied yet.

Chapter Overview: In this small chapter, modal and scattered fields of a photonic crystal membrane using computational electromagnetism software are briefly presented. These can help one understand how atoms move in the space around the membrane, and whether they can make their way through the perforations of the membrane.

Micro-to-nano-scale structuring lends natural material their colors, textures [10, 252] and mechanical properties [254]. This also provides us a general top-down design space to tune photonic baths. This, because the length scale of patterning governs the way in which light interacts with the structure. A wavelength-scaled periodic patterning of dielectrics forms a photonic crystal. A thin PC membrane with circular square lattice holes is depicted in [Fig. 5.1].

$$T$$

$a \sim 0.80~\mu\mathrm{m}$

$2r \sim 1.40~\mu\mathrm{m}$

$t \sim 0.50~\mu\mathrm{m}$

$$R$$

$$n_{\mathrm{SiN}} = 2.11$$
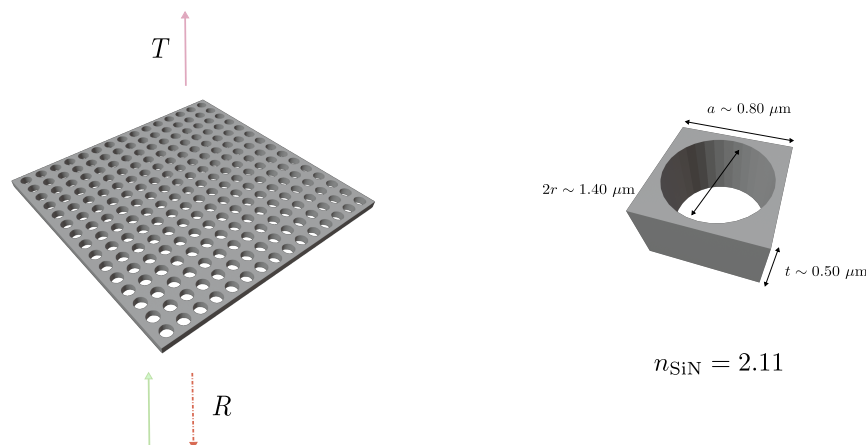
Figure 5.1: Left: A PC membrane with circular holes and a square lattice can have interesting transmission and reflection properties. Right: Basis cell that generates the PC slab upon repetition. This particular geometry, reported in Ref.[72], shows a large reflectivity for wavelengths around ~850 nm.

Interestingly, when designed appropriately, they can serve as near-ideal reflectors.[240, 245, 243] While exploring the design space of such a membrane (lattice parameter a, radius r and thickness t) might be non-trivial, a brute-force optimization can provide for desired values of wavelength-dependent transmission.[72] Placing these upon either side of the hollow fiber forms a Fabry-Perot cavity.[Fig. 5.2] Such micro-scale devices, pointing towards on-chip integration, benefit from the versatile role atoms can play to fashion classical and quantum optical technologies. One might imagine using such a light-matter interface for all-optical switching, superradiant

lasing and quantum information processing nodes.[71] In addition to an exploration of cavity QED in confined spaces, the design space of 2D nanophotonic membranes allows for the creation of birefringent cavities by tuning the polarization selectivity of the mirrors. This adds to the possible quantum optics protocols that can be tested.[73]
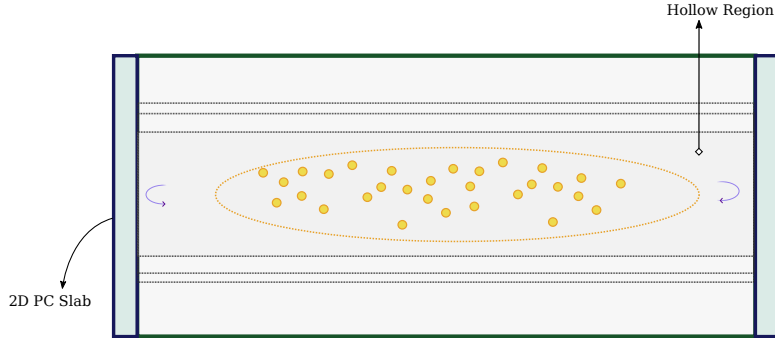
Figure 5.2: A representative cross-section of a hollow fiber capped with a PC slab with an atomic ensemble. If the PC membranes act as a mirror, and also allow for atoms to pass through, they can serve as interesting meso-scale quantum optical cavities.

5.1 Resonances of a Photonic Crystal Membrane

Let's consider a very thin dielectric glass slab of thickness $t = 0.5$ μm. The transmission (T, defined as the ratio of output and input intensities) of normally incident plane-waves through the slab can be imagined via partial reflections and transmissions at each interface, leading to a geometric series. In this case, light passes from n_1 = 1 (air) to $n_2 = 2.11$ (SiN), and back to $n_1 = 1$. T can be written as:[257]

$$T = \left| \frac{4n_1 n_2 e^{-ik_2 t}}{(n_1 + n_2)^2 + (n_2 - n_2)^2 e^{-i2k_2 t}} \right|^2$$

Now, adding periodic holes [Fig. 5.1] to this slab changes the way one readily thinks of T. [Fig. 5.3] shows features of T for a PC membrane (computed using an open-source RCWA (rigorous coupled-wave analysis) solver: S^4) compared to a uniform slab with refractive indices n_2 and $n_{2,avg}$. $n_{2,avg}$ is calculated by taking the weighted average (by area) of the dielectric constant across a PC unit cell.
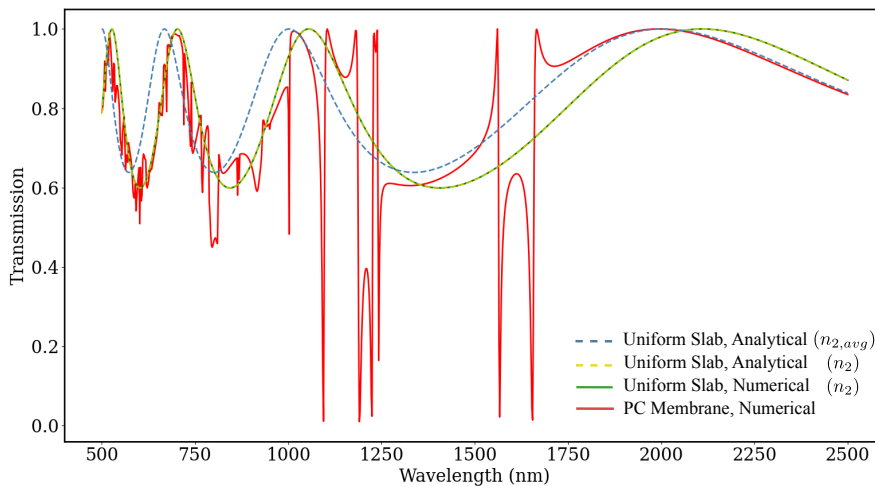
Figure 5.3: Transmission of linearly polarized plane-wave light through a PC membrane and a uniform dielectric slab. Parameters of the PC membrane are: $a = 1$ μm, $r = 0.2$ μm, $t = 0.5$ μm and $n = n_2$. Calculation (with number of Fourier coefficients = 100) is performed adapting an example script provided with S^4.[261] Transmission through a uniform with refractive index: n_2 is calculated analytically and using [261], and for a refractive index: $n_{2,avg}$ is calculated analytically.

These relatively sharp features atop the uniform slab's spectra are suggested to relate with the resonances that photonic crystals house.[240, 241, 243, 72] In Ref.[240], a frequency dependent dielectric constant is used for such a fit. And in [Fig. 5.3], $n_{2,avg}$ and n_2 match the PC membrane transmission for long and short wavelengths, respectively. Much like crystals in condensed matter theory which display electronic resonances, PCs also make light dance in definite rhythms according to its geometry. Maxwell's equations, in terms of the magnetization vector $\vec{H}$, can be expressed as an eigenvalue equation, which provides a geometry-dependent band-structure to photonic crystals.[239]

$$\left[\nabla \times \frac{1}{\epsilon(\vec{r})}\nabla \times\right]\vec{H} = \left(\frac{\omega}{c}\right)^2 \vec{H} \qquad \vec{H}(\vec{r},t) = \exp i(\vec{k}\cdot\vec{r} - \omega t)\vec{H}_{\vec{k}}(\vec{r})$$

Here, $(\vec{k}, \omega)$ refer to the wave-vector and angular frequency of light, $\epsilon(\vec{r})$ refers to the spatially varying dielectric medium and $\vec{H}_{\vec{k}}$ refers to the Bloch wave in the medium. Similarities between the descriptions of electrons in solid-state materials and light in photonic crystals, as adapted from Ref.[239], are summarized in the table below:

	Quantum Mechanics	Electromagnetism
Field	$\Psi(\vec{r},t) = \Psi(\vec{r})e^{-iEt/\hbar}$	$\vec{H}(\vec{r},t) = \vec{H}(\vec{r})e^{-i\omega t}$
Eigen-equation	$\hat{H}\Psi = E\Psi$	$\hat{\mathcal{M}}\vec{H} = \frac{\omega^2}{c^2}\vec{H}$
Hermitian Operator	$\hat{H} = -\frac{\hbar^2}{2m}\nabla^2 + V(\vec{r})$	$\hat{\mathcal{M}}\vec{H} = \nabla \times \frac{1}{\epsilon(\vec{r})}\times$

Modes for the reflective PC membrane geometry [Fig. 5.1], using an open-source eigensolver – MPB, are represented in a band-diagram [Fig.5.4]. As noted in, Ref.[241] the modes of such a square lattice slab can be single or doubly degenerate. From a mathematical point of view, symmetries of the patterning help to categorize different kinds of oscillations which can have intriguing properties, such as resonances with long life-times.[245, 244, 246]

Incident light with a transverse Gaussian pattern (which has a spread $\vec{k}_{||} = 0$) can talk to modes around the Γ-point. One might imagine the dielectric being imbued with currents in order to generate their corresponding modal fields. These excited modes (also referred to as guided resonances [240]), in some cases, can couple to the free-flowing modes (usually within the blue-shaded region in [Fig. 5.4]) in either direction ($\omega = c|\vec{k}|$), whose interference can be mapped to transmission features [Fig. 5.3] of a PC membrane (T). Vaguely, features due to such a process are termed Fano resonances.[240, 241, 243]

As a preliminary check for the role of these resonances in the transmission features of the slab, [Fig. 5.5] plots transmission curves for the reflective geometry shown in [Fig. 5.1]. The plot is overlayed with the modes plotted in [Fig. 5.4]. Also, more generally, by considering electric and magnetic resonances of such membranes, it has been possible to demonstrate a selective interaction with circularly polarized radiation.[255]
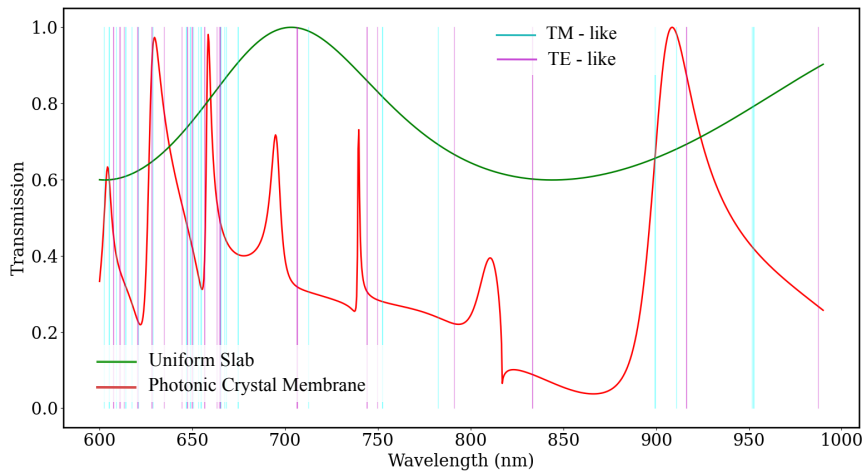
Figure 5.5: Transmission of polarized plane-wave light through a PC Membrane using [261] with the parameters mentioned in [Fig. 5.4], and a uniform slab with $n = n_2$. Vertical lines according to the modes obtained in [Fig. 5.4] are overlayed.
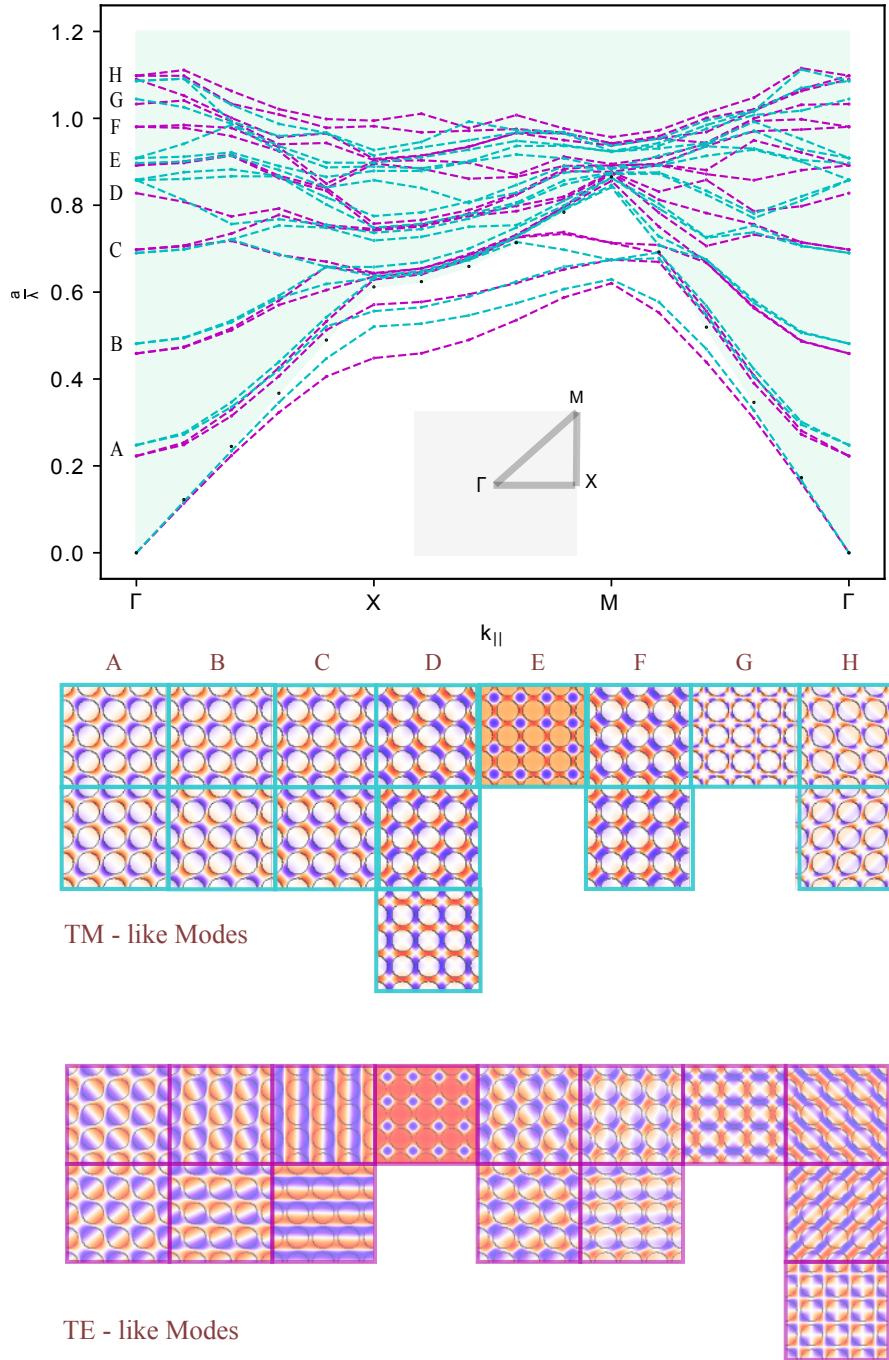
Figure 5.4: The band diagram of the photonic crystal [239] for the geometry of the slab: $a = 0.817$ μm, $r = 0.347$ μm, $t = 0.5$ μm and $n = n_2$. $\left(\frac{a}{\lambda}\right)$ refers to the normalized frequency, $\vec{k}_{||}$ is the wave-vector of the field along the plane of the membrane. The horizontal axis denotes the $\vec{k}$-space as shown in the inset – which corresponds to the Brilloin zone.[239] xy field profiles, as labelled by the alphabet with close energies along the Γ point are presented (covering 3×3 unit cells). Some of the degenerate modes appear as rotations or reflections. TE- and TM-like modes refer to transverse electric $(\vec{D})$ and magnetic $(\vec{H})$ fields. The dotted black line denotes the light line. Calculation is performed adapting an example script provided with Ref.[260].

5.2   A Holey Mirror!

Such resonances have been used to realize narrowband filters and broadband reflectors.[240] For instance, transmission of the PC membrane in the window ~820 - 870 nm [Fig. 5.5] suggests high reflectivity (R). This allows to for a cavity at about 852 nm.[72] Another feature that is of interest is to be relatively transparent at 935 nm, which acts as a magic-wavelength dipole trapping beam to guide atoms.

In addition to the RCWA approach [Fig. 5.3], T and R can be numerically calculated via a time-domain FDTD (finite-difference time-domain) method.[256] In the FDTD case, one can excite the PC membrane with a pulsed plane-wave packet. Fourier-transforming the time-evolved state can, in one computation, determine its spectral response – a feature that is implemented in the open-source MEEP software.[258] Alternatively, one can allow a continuous plane-wave source to find its steady-state at each wavelength. This data generated using Lumerical FDTD software [276], along with the other mentioned methods are plotted in [Fig. 5.6].
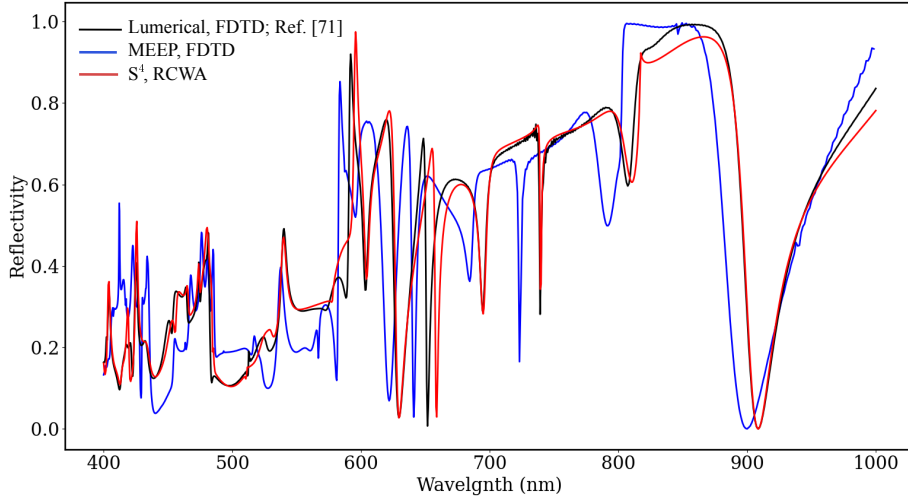
Figure 5.6: Reflectivity for the PC membrane with geometry and refractive specified in: [Fig. 5.4]. Black squares correspond to the simulated reflectivity values and the dashed lines connect them. Spatial resolution of the MEEP computation is $\Delta x = \Delta y = \Delta z = 0.05$ μm, with the pulse `decay-by` factor $= 10^{-7}$. Number of Fourier coefficients in S^4 computation is set to 100. Lumerical dataset corresponds to Fig. 2a in [71].

It would be worth checking how to account for the variations among these approaches. In relation to which, a further study of the role of the modes shown in [Fig. 5.5] would be helpful.

5.3   EM Fields around the PC Membrane
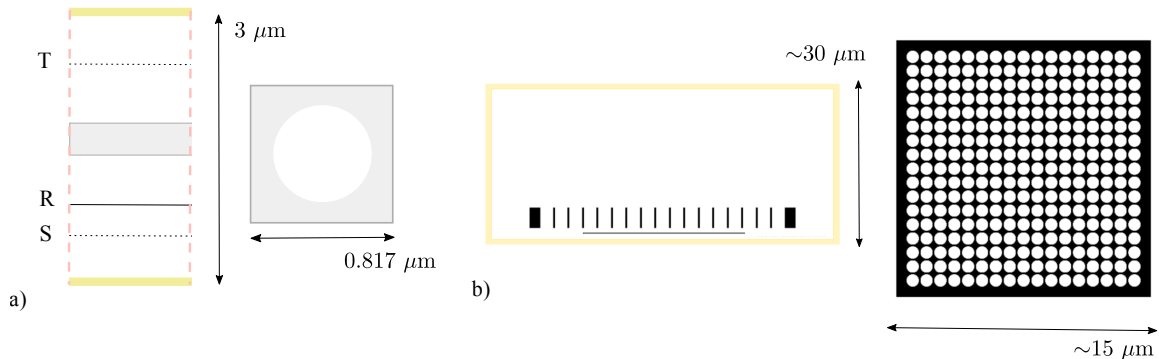
Figure 5.7: a) A lattice of holes is formed with periodic boundary conditions (along the dotted red lines). S, R and T planes refer to the source, reflection monitor and transmission monitor. b) Sideways and top-down simulation region for a Gaussian mode transmission calculation.

To estimate the feasibility of loading atoms using optical forces, the incident field is modelled as a plane-wave [Fig. 5.8] and a Gaussian wave [Fig. 5.7, Fig. 5.10] incident upon the membrane to obtain its EM field

environment, such as its the 3D intensity profiles and polarization of the field.[Fig. 5.8] While the former can be calculated by treating the PC membrane as a unit cell, large region FDTD simulations lend us the fields when a Gaussian beam is incident.[Fig. 5.7)] For these computations, λ is set to 935 nm and the software package MEEP is used to obtain the results.[258]
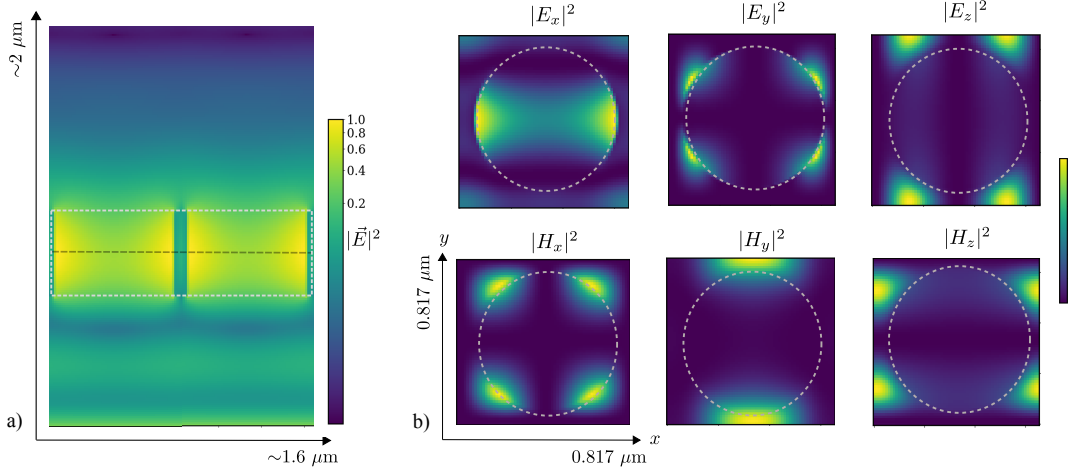
Figure 5.8: a) Normalized field intensity cross-section for (continuous-wave) incident linearly (x) polarized plane-wave fields upon the PC membrane. The unit-cell is duplicated for plotting. The simulation region is sketched in [Fig. 5.7 a)]. b) Normalized profiles of the fields within the slab long different (along the dotted black line shown in a)) directions: $\vec{E} = E_x\hat{i} + E_y\hat{j} + E_k\hat{k}$ and $\vec{H} = H_x\hat{i} + H_y\hat{j} + H_k\hat{k}$. The computation was performed with [258, 259].

The width of the Gaussian beam is set to $w = 2.75$ μm in order to test the effect of a ~7 μm hollow fiber's mode scattering outwards. As a starting point, instead of the larger region [Fig. 1.4, [72]] spanned by the periodic structure, a limited-sized the PC slab of size ~15 μm [Fig. 5.7] is considered. [Fig. 5.10] and [Fig. 5.9] show field and amplitude variations when a linearly polarized Gaussian mode is scattered by a PC membrane. Alternatively, Gaussian incident fields have also been computed using an RCWA approach.[261]
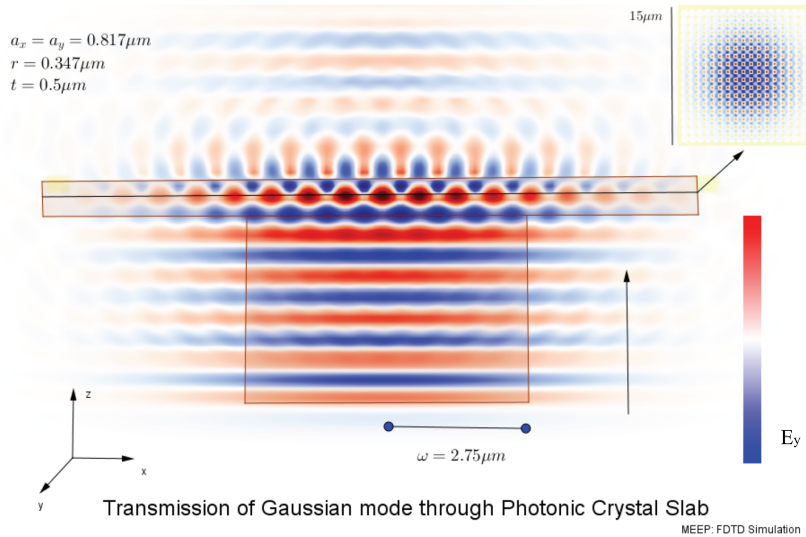
Figure 5.9: Snapshot of an FDTD simulation when a Gaussian (linearly polarized) mode, representing the HCPCF mode, is assumed to strike the PC membrane. The color represents the phase of the EM field. Software used for this simulation: [258].

5.4   Outlook: How might atoms move around photonic crystals?

As suggested in [Fig. 5.11], one can calculate atomic motion in this field with intensity gradient fields. A fuller consideration ought to involve the role of field variations, Δr_{atom}, [Fig. 2.9] and momentum diffusion terms.[122]
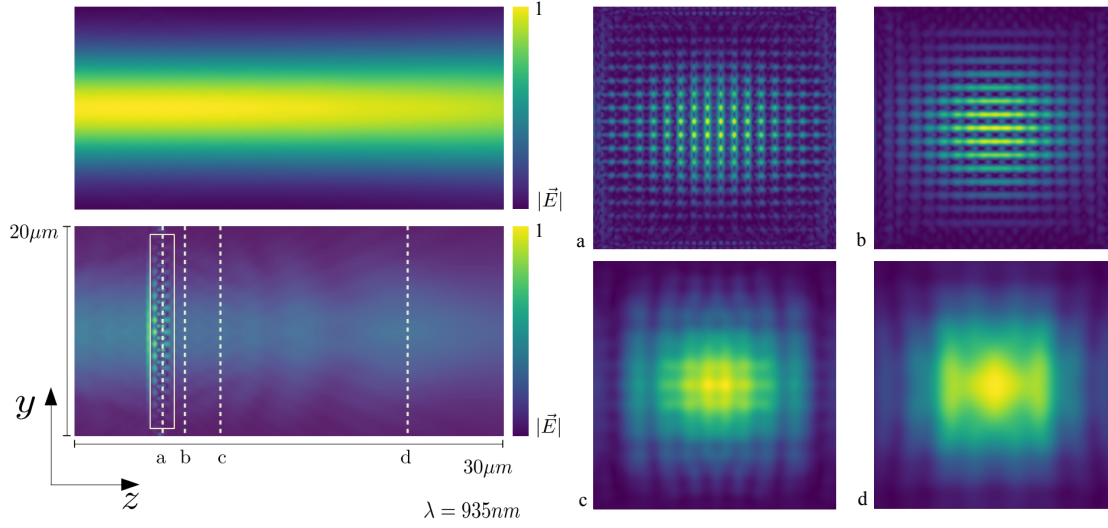
Figure 5.10: a) Normalized intensities of the scattered field with and without the PC membrane. Extending the simulation region, one can follow the near to far field evolution of the field. b) To the right are: xy profiles at each location (represented by dashed lines). This allows one to quantify intensity gradient optical potentials until the field dons its eventual Gaussian profile. In contrast, free-space evolution shows the slight dispersion of the Gaussian field. Simulation software: [258]. With a resolution of $\Delta x = \Delta y = \Delta z = 0.05\ \mu$m, the computation was performed using: [259].

In addition, field polarization and near-field effects of the material have to be accounted for.[125] Also, when close to the surface (within a $\sim$100 nm range), surface potentials can play a role in determining atomic motion. Related efforts trying to integrate atoms with nanostructures: Refs.[149, 150, 152, 153, 154, 155, 156] comment about atom trajectories near dielectric surfaces and photonic crystals, which can serve as helpful starting points.
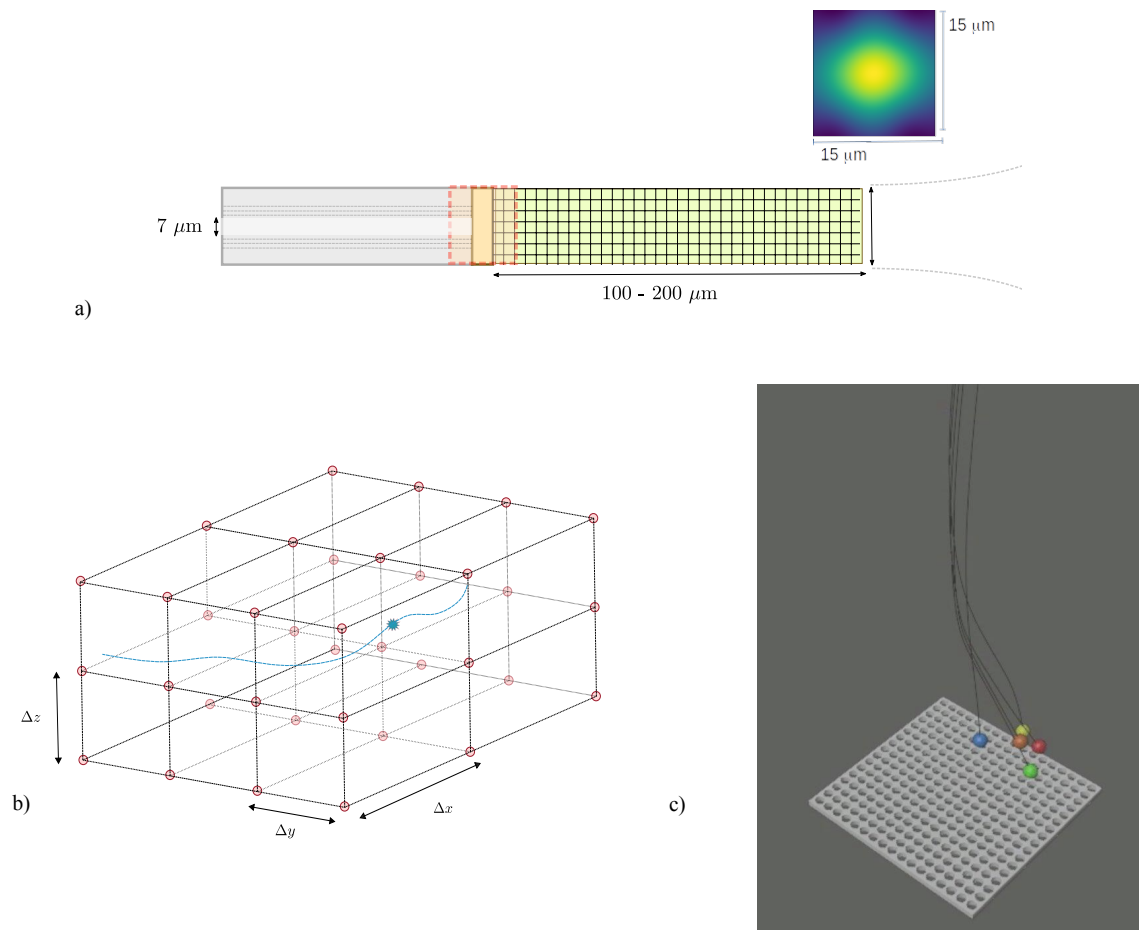
Figure 5.11: a) About 100 - 200 μm from the fiber surface, the field can be followed by its analytical expression in the intermediate region, as suggested in [Fig. 5.10] b) 3D data fields can be used to calculate atomic trajectories by interpolating the function. c) Illustrating atomic trajectories when only dipole potentials from the data-set [Fig. 5.10] are used. Here, accuracy of the numerical methods for integrating atomic motion needs to be checked.

Chapter 6

Summary and Outlook

$\rightarrow$ Describing nature seems to require a new language. Realizing micro-scale platforms where we can reliably transact energy with atoms can not only help clarify such an understanding, but can also further sustainable technological progress. This thesis attempts at discussing two ongoing projects of the NPQO lab.

• One aims to follow atomic motion into hollow-optical fibers with and without photonic crystal membranes. Without the PC membrane, parallel simulations of gravity-assisted atomic motion around hollow fibers allows us to recreate the dropping of cold atomic clouds in different configurations. This helps to study their loading. Atoms can be guided via red-detuned far-off resonant funnel beams diffracting from the hollow-fibers. Inside the fibers, the ensemble geometry can also be visualized. While small atom-clouds and low temperatures ($\sim$1 μK) seem to help us shuttle more atoms into the fiber, it appears that the initial arrangement of atoms limits the fraction to about $\sim$1 %. Alternatively, blue-detuned hollow-tunnel beams can also be used. In some cases, this can increase loading by a factor of $\sim$5. Alternative starting conditions of a MOT cloud might help one better fountain atoms into hollow-optical fibers.

• Photonic crystal membranes can enhance light-matter interaction by forming mesoscale cavities around the hollow-optical fiber: thanks to their mirror-like properties. With enhanced nonlinearities, these ensembles can be used for photon-level optical switching and superradiant lasing. A very short study of its electromagnetic fields, obtained by piggybacking on open-source electromagnetism software is presented. Appropriately stitching this information into parallel algorithms might allow one to visualize atomic motion in relatively generalized environments. A helpful and fun side-goal – especially as an on-chip integration of atoms into nanophotonic cavities and waveguides can be very enabling for both: our own familiarization of the atomic landscape, and technologically – would be to leverage the rendering capabilities of graphics processors to make this software interactive.

$\rightarrow$ The second aims to employ atomic ensembles inside hollow optical fibers as quantum networking nodes. Depending on how we talk to them, atoms can serve a versatile role – such as generating, modifying or storing quantum states of light. A preliminary approach to use Cs atomic ensembles for quantum frequency conversion is provided. Rb atoms have been pursued both theoretically and experimentally in this regard. Here, this discussion is ported to the case of $\diamond$-level Cs atom schemes. On an introductory level, one can note how nonlinearities 'appear' when atom-light interactions are semi-classically considered. Next, following an existing theoretical model, the coupled propagation of two fields is discussed: an optical input field at (894 nm) which can be tuned to a quantum dot transition, and an output field – suitable either for telecom fiber integration (1470 nm) or coupling to satellites via free-space channels (790 nm). Such a model illustrates the dependence of conversion efficiency on parameters of light fields such as the strength and detuning of the applied laser fields along with the optical depth of the ensemble.

• It would be helpful to understand photon pulse propagation through ensembles in hollow optical fibers, and what factors limit an efficient and noiseless conversion. Progress in these aspects can also help one study other atomic ensemble-light interaction based phenomena in hollow fibers: such as quantum memories, super-radiance and pair-production.

$\rightarrow$ Relevant codes are made available here.

Letters of copyright permission

RE: Query regarding the use of images in MSc thesis

pubscopyright <copyright@osa.org>

Fri 4/23/2021 12:51 PM

To: Sai Sreesh Venuturumilli <ssvenuturumilli@uwaterloo.ca>; pubscopyright <copyright@osa.org>

Dear Sreesh,

Thank you for contacting The Optical Society.

For the use of figures 5 and 6 from B. Debord, A. Amsanpally, M. Chafer, A. Baz, M. Maurel, J. M. Blondy, E. Hugonnot, F. Scol, L. Vincetti, F. Gérôme, and F. Benabid, "Ultralow transmission loss in inhibited-coupling guiding hollow fibers," Optica 4, 209-217 (2017):

> OSA considers your requested use of its copyrighted material to be Fair Use under United States Copyright Law. It is requested that a complete citation of the original material be included in any publication.

While your publisher should be able to provide additional guidance, OSA prefers the below citation formats:

> For citations in figure captions:
>
> [Reprinted/Adapted] with permission from [ref #] © The Optical Society. (Please include the full citation in your reference list)
>
> For images without captions:
>
> Journal Vol. #, first page (year published) An example: Biomed. Opt. Express 6, 793 (2015)

Please let me know if you have any questions.

Kind Regards,
Hannah Greenwood

Hannah Greenwood
April 23, 2021
Authorized Agent, The Optical Society

The Optical Society (OSA)
2010 Massachusetts Ave., NW
Washington, DC 20036 USA
www.osa.org

Reflecting a Century of Innovation

Sai Sreesh Venuturumilli <ssvenuturumilli@uwaterloo.ca>

Wed 4/21/2021 5:15 PM

To: copyright@osa.org <copyright@osa.org>

Hello,

I am a graduate student the University of Waterloo, and I am preparing my thesis for deposit in UWSpace, the university's institutional repository.
I understand that you are the copyright holder for the following article:
B. Debord et al. Ultralow transmission loss in inhibited-coupling guiding hollow fibers, Optica Vol. 4, Issue 2, pp. 209-217 (2017)

I would like permission to include Figure 5) [b), d)] and an inset of Figure 6 a) in my thesis which will be made openly available as part of my thesis, tentatively titled, 'Laser-cooled atomic ensembles in hollow optical fibers'. Proper citation will be included with the reproduction of this figure.

Please let me know what your process is for providing permission, and if you need any further information from me.
If you do not hold the copyright for this material, or the right to grant this type of permission, I would greatly appreciate any information you can provide to me regarding the rights holder(s), including any contact information.

Thank you for considering this request,
Sreesh

RE: Query regarding the use of images in MSc thesis

Karen Scammell <karen.scammell@nktphotonics.com>
Wed 4/28/2021 7:08 AM

To: Sai Sreesh Venuturumilli <ssvenuturumilli@uwaterloo.ca>
Cc: Chris Meyers <Christopher.Meyers@nktphotonics.com>

Dear Sreesh,
You have permission to use the images of NKT Photonics Inc., as long as you give credit to NKT Photonics.

Best wishes for success with your research!

Kind regards,
Karen L. Scammell, VP OEM Sales

NKT Photonics Inc.

23 Drydock Ave • Boston, MA 02210 • USA
Tel: +1 978 761 7528

Sai Sreesh Venuturumilli <ssvenuturumilli@uwaterloo.ca>
Mon 4/26/2021 4:36 PM

To: kasc@nktphotonics.com <kasc@nktphotonics.com>

Hello Ma'am,

I am a graduate student the University of Waterloo, and I am preparing my thesis for deposit in UWSpace, the university's institutional repository. I understand that NKT Photonics INC is the copyright holder for the graphs and pictures of the (HC-800-02) hollow-core fiber in the link:
https://www.nktphotonics.com/wp-content/uploads/sites/3/2015/01/hc-800-1.pdf?1539002002

I would like permission to include the pictures of the: fiber cross-section, attenuation v/s wavelength plot and the near-field profile (shown in the spec-sheet) for my thesis (tentatively titled, "Laser-cooled atomic ensembles in hollow optical fibers"), which will be made openly available. Proper citation will be included
with the reproduction of this figure.

Please let me know what your process is for providing permission, and if you need any further information from me.

Thanks a lot for your time,
Sreesh

References

General:

[1] i) E. Schrodinger, Are There Quantum Jumps?
   ii) S. Haroche: Controlling photons in a box and exploring the quantum to classical boundary.

[2] i) E. Schrodinger, What is life – with 'Mind and Matter' and Autobiographical Sketches, CUP, 1944
   ii) Wikipedia: Quantum Zeno Effect

[3] Text: R. Puri, Mathematical Methods of Quantum Optics, Springer, 2001

[4] Text: D. A. Steck, Quantum and Atom Optics, 2007

[5] L. Allen et al. Optical Resonance and Two-Level Atoms, Dover, 1987

[6] Y-H Deng et al. Quantum interference between light sources separated by 150 million kilometers, PRL, 2019

[7] Talk: T. Shafer, Three Pictures in Quantum Mechanics

[8] P. W. Milloni et al. Chaos in the Semiclassical N-Atom Jaynes-Cummings Model: Failure of the Rotating-Wave Approximation, PRL, 1983

[9] T. E. Li et al. Comparison of Different Classical, Semiclassical, and Quantum Treatments of Light Matter Interactions: Understanding Energy Conservation, JCTC, 2019

[10] C. Verstraete et al. Linear and nonlinear optical effects in biophotonic structures using classical and non-classical light, J. Biophotonics, 2018

[11] K. Y Bliokh, Spin–orbit interactions of light, Nature Photonics, 2015

[12] G. Y. Slepyan et al. Quantum Antenna, Advanced Quantum Technologies, 2020

[13] A. Mikhalychev et al. Synthesis of Quantum Antennas for Shaping Field Correlations, PRA, 2018

[14] R. Mitsch et al. Quantum state-controlled directional spontaneous emission of photons into a nanophotonic waveguide, Nature Communications, 2014

[15] S. Scheel et al. Directional spontaneous emission and lateral Casimir-Polder force on an atom close to a nanofiber, PRA, 2015

[16] J-W. Pan et al. Multiphoton entanglement and interferometry, Rev. Mod. Phys. 2012

[17] A. Zavatta et al. A high-fidelity noiseless amplifier for quantum light states, Nature Photonics, 2010

[18] Lecture: D. Mittleman, Slowly Varying Envelope Approximation, Brown University

[19] M. Schneider et al. Green's-function formalism for waveguide QED applications, PRA, 2016

[20] D. Roy et al. Colloquium: Strongly interacting photons in one-dimensional continuum, Rev. Mod. Phys. 2017

[21] K. Fischer et al. Scattering into one-dimensional waveguides from a coherently-driven quantum-optical system, Quantum, 2018

[22] A. Asenjo-Garcia et al. Atom-light interactions in quasi-1D nanostructures: a Green's function perspective, arXiv, 2017

[23] a) R. Mitsch et al. Quantum state-controlled directional spontaneous emission of photons into a nanophotonic waveguide, Nat. Comm. 2014
b) F. L. Kien et al. Spontaneous emission of a cesium atom near a nanofiber: Efficient coupling of lightto guided modes, PRA, 2005

[24] M. Arcari et al. Near-Unity Coupling Efficiency of a Quantum Emitter to a Photonic Crystal Waveguide, PRL, 2014

[25] S. Mahmoodian et al. Engineering chiral light–matter interaction inphotonic crystal waveguides with slow light, OSA, 2016

[26] D. Gottesman et al. Encoding a qubit in an oscillator, PRA, 2000

[27] I. Carusotto et al. Quantum fluids of light, Rev. Mod. Phys, 2013

[28] News: H. Johnston, Three photons bind together to make a 'molecule' of light, Physics World, 2018

[29] S. Takeda et al. Perspective: Toward large-scale fault-tolerant universal photonic quantum computing, arXiv, 2019

[30] D. Bohm, Wholeness and Implicate Order, Routledge, 1980

[31] P. Ferrera et al. Generation of single photons with highly tunable wave shape from a cold atomic ensemble, Nature Communications, 2016

[32] News: D. Castelvecchi, Quantum network is step towards ultrasecure internet, Nature, 2021

[33] M. Striebel et al. Absorption and Extinction Cross Sections and Photon Streamlines in the Optical Near-field, Scientific Reports, 2017

[34] Group Website: Nanophotonic and Quantum Optics Laboratory, University of Waterloo

[35] Course Notes: M. Lukin, Modern Atomic and Optical Physics II, Harvard Univ., 2005

[36] Course Notes: R. Cleve, Introduction to Quantum Information Processing, Univ. Waterloo, 2011

[37] Talk: E. Martinez, (Some) Relativistic aspects of the Light-Matter interaction, Univ. Waterloo

[38] Lecture: P. Jessen, Maxwell-Bloch Equations, Univ. Arizona

On Quantization and Quantized Light Propagation:

[39] C. G. Torre, What is a photon?, Notes: Foundations of Quantum Field Theory

[40] Text: A. Furusawa, Quantum States of Light, Springer, 2015

[41] W. Louisell et al. Quantum Statistical Properties of Radiation, Wiley, 1990

[42] M. G. Raymer et al. The Maxwell wave function of the photon, SPIE Conference, 2005

[43] R. Bennett et al. A physically motivated quantization of the electromagnetic field, Eur. J. of Physics, 2015

[44] I. Birula, Photon Wave Function, Progress in Optics, 1996

[45] P. J. Mohr, Solutions of the Maxwell equations and photon wave functions, Annals of Physics, 2010

[46] Art Hobson, There are no particles, there are only fields, American Journal of Physics, 2012

[47] Text: P. W. Miloni, The Quantum Vacuum: An Introduction to Quantum Electrodynamics, Elsevier, 1994

[48] P. W. Milonni, Why Spontaneous Emission?, American Journal of Physics, 1984

[49] P. A. M. Dirac, The quantum theory of the emission and absorption of radiation, Proc. RSA, 1927

[50] P. A. M. Dirac, Quantised singularities in the electromagnetic field, Proc. RSA, 1931.

[51] K. Blow, et al. Continuum fields in quantum optics, PRA, 2990

[52] I. Deutsch et al. Paraxial quantum propagation, PRA, 1991

[53] A. Silberfarb et al. Continuous measurement with traveling wave probes, PRA, 2003

[54] PhD Thesis: B. Q. Baragiola, Open systems dynamics for propagating quantum fields, Univ. New Mexico, 2014

[55] P. Domokos, et al. Quantum description of light pulse scattering on a single atom in waveguides, PRA, 2002

[56] M. Manzoni et al. Simulating quantum light propagation through atomic ensembles using matrix product states, Nat. Comm., 2017

[57] A. A. Svidzinsky et al. Quantum versus semiclassical description of light interaction with atomic ensembles: Revision of the Maxwell-Bloch equations and single-photon superradiance, PRA, 2015

[58] B. Baragiola et al. N-photon wave packets interacting with an arbitrary quantum system, PRA, 2012

[59] M. McIrvin, Some Frequently Asked Questions About Virtual Particles, UCR, 1994

Quantum Information with Atomic Ensembles:

[60] Y, Yu et al. Entanglement of two quantum memories via fibres over dozens of kilometres, Nature, 2020

[61] K. Hammerer et al. Quantum interface between light and atomic ensembles, Rev. Mod. Phys. 2010

[62] N. Sangouard et al. Quantum repeaters based on atomic ensembles and linear optics, Rev. Mod. Phys. 2011

[63] PhD Thesis: L. Veisser et al. Quantum memory protocols in large cold atomic ensembles, UPMC, 2013

[64] A. Gorshkov et al. Universal Approach to Optimal Photon Storage in Atomic Media, PRL, 2007

[65] Y. Li et al. Non-Abelian geometric quantum memory with an atomic ensemble, PRA, 2004

[66] H. Krauter et al. Deterministic quantum teleportation between distant atomic objects, Nature Physics, 2013

[67] R. McConnell et al. Entanglement with negative Wigner function of almost 3,000 atoms heralded by one photon, Nature, 2015

Hollow Optical Fibers as a Platform for Quantum Optics Experiments:

[68] B. Debord et al. Hollow-Core Fiber Technology: The Rising of Gas Photonics, Fibers, 2019

[69] A. Taranta et al. Exceptional polarization purity in antiresonant hollow-core optical fibres, Nature Photonics, 2020

[70] B. Debord et al. Ultralow transmission loss in inhibited-coupling guiding hollow fibers, OSA, 2017 Gas-phase photonic and microwave materials group, XLIM Research Institute

[71] C. M. Haapamaki et al. Mesoscale cavities in hollow-core waveguides for quantum optics with atomic ensembles, Nanophotonics, 2015

[72] PhD Thesis: J. Flannery, Optical Resonators Integrated into a Hollow Core Photonic Crystal Fiber for Enhanced Light-Matter Interactions, U. Waterloo, 2019

[73] K. Debnath et al. Lasing in the superradiant crossover regime, PRA, 2018

[74] L. Caspani et al. Integrated sources of photon quantum states based on nonlinear optics, Light: Science and Applications

[75] D. E. Chang, et al. Crystallization of strongly interacting photons in a nonlinear optical fiber, Nature Physics, 2008

[76] M. Hafezi et al. Quantum transport of strongly interacting photons in a one-dimensional nonlinear waveguide, PRA, 2012

[77] NKT Photonics: HC-800-02 - Hollow Core Photonic Bandgap Fiber

[78] V. Venkataraman et al. Phase modulation at the few-photon level for weak-nonlinearity-based quantum computing, Nature Photonics, 2013

[79] M. R. Sprague et al. Broadband single-photon-level memory in a hollow-core photonic crystal fibre, Nature Photonics, 2014

[80] S. Okaba et al. Superradiance from lattice-confined atoms inside hollow core fibre, Communication Physics, 2020

[81] S. Okaba et al. Lamb-Dicke spectroscopy of atoms in a hollow-core photonic crystal fibre, Nature Communications, 2014

[82] W. S. Leong et al. Large array of Schrödinger cat states facilitated by an optical waveguide, Nature Communications, 2020

[83] M. Xin et al. Transporting long-lived quantum spin coherence in a photonic crystal fiber, PRL, 2019

[84] M. Xin et al. An atom interferometer inside a hollow-core photonic crystal fiber, Science Advances, 2018

[85] P. Londero et al. Ultralow-Power Four-Wave Mixing with Rb in a Hollow-Core Photonic Band-Gap Fiber, PRL, 2009.

[86] N. Horiuchi, Hollow-core fibre, Nature Photonics, 2013

[87] F. Blatt et al. One-dimensional ultracold medium of extreme optical depth, Optics Letters, 2014

<u>Collective Effects:</u>

[88] F. T. Arecchi et al. Atomic Coherent States in Quantum Optics, PRA, 1972

[89] F. T. Arecchi et al. Cooperative Phenomena in Resonant Electromagnetic Propagation, PRA, 1970

[90] Lecture: A. A. Garcia et al. Collective phenomena in light-matter interfaces

[91] L. Pezze et al. Quantum metrology with nonclassical states of atomic ensembles, Rev. Mod. Phys, 2018

[92] Course Notes: Light-Matter Interactions and Quantum Optics, [Chapter 8]

[93] M. Lukin et al. Dark-State Polaritons in Electromagnetically Induced Transparency, PRL, 2000

[94] M. Lukin et al. Quantum Noise and Correlations in Resonantly Enhanced Wave Mixing Based on Atomic Coherence, PRL, 1999

[95] M. Bajcsy et al. Stationary pulses of light in an atomic medium, Nature, 2003

[96] A. Andre et al. Manipulating Light Pulses via Dynamically Controlled Photonic Bandgap, PRL, 2002

[97] M. Bajcsy et al. Nonlinear Optics with Stationary Pulses of Light, PRL, 2005

[98] M. Lukin et al. Entanglement of Atomic Ensembles by Trapping Correlated Photon States, PRL, 1999

[99] PhD Thesis: A. Andre, Nonclassical states of light and atomic ensembles, Harvard Univ., 2005 (Section 4.3, Appendix C)

[100] PhD Thesis: M. Hafezi, Strongly interacting systems in AMO physics, Harvard Univ., 2009 (Section 3.2)

[101] PhD Thesis: D. Chang, Controlling atom-photon interactions in nano-structured media, Harvard Univ., 2008 (Chapter 5, Appendix F)

[102] PhD Thesis: K. S. Choi, Coherent Control of Entanglement with Atomic Ensembles, CalTech, 2011 [Chapter 2]

[103] J. Kumlin et al. Non-exponential decay of a collective excitation in an atomic ensemble coupled to a one-dimensional waveguide, arXiv, 2020

[104] P. Solano et al. Super-radiance reveals infinite-range dipole interactions through a nanofiber, Nature Communications, 2017

[105] A. S. Prasad et al. Correlating photons using the collective nonlinear response of atoms weakly coupled to an optical mode, Nature Photonics, 2020

On Entanglement

[106] A. Einstein et al. Can QM Description of Physical Reality be Considered Complete? Physical Review, 1935

Atomic Motion in Optical Environments:

Introduction:

[107] Nobel Prize in Physics, 2001: Bose-Einstein Condensation in Alkali Gases

[108] YouTube Video: Single Atoms Pong, Ultrafast Quantum Optics Lab, KAIST, 2020

[109] H. Bernie et al. Probing many-body dynamics on a 51-atom quantum simulator, Nature, 2017

[110] D. Ohl de Mello et al. Defect-Free Assembly of 2D Clusters of More Than 100 Single-Atom Quantum Systems, PRL, 2019

[111] D. Barredo et al. Synthetic three-dimensional atomic structures assembled atom by atom, Nature, 2018

[112] Or in sub-wavelength lattices: Y. Wang et al. Dark State Optical Lattice with a Subwavelength Spatial Structure, PRL, 2018

[113] M. Babiker et al. Atoms in complex twisted light, J. Optics, 2019

[114] B. Houchmandzadeh, The Hamilton–Jacobi equation: An alternative approach, Am. J. Phys, 2020

[115] Wikipedia: Schrodinger equation, Matrix mechanics

[116] Wikipedia: Born-Oppenheimer Approximation

[117] E. Sanchez-Burrilo et al. Theory of Waveguide QED with Moving Emitters, PRA, 2020

[118] D. M. Meekhof et al. Generation of Nonclassical Motional States of a Trapped Atom, PRL, 1995

[119] Lecture: Two-level model for atoms, PY4117, UCC

Pedagogical References:

[120] Review: R. Grimme et al. Optical Dipole Traps For Neutral Atoms, arXiv, 1999

[121] Text: H. Metcalf and P. van der Straten, Laser Cooling and Trapping, Springer, 1999 (Chapters 2 and 3)

[122] Course: C. Tannoudji, Atomic motion in laser light, 1992

[123] Text: P. Meystre, M. Sargent, Elements of Quantum Optics, Springer, 4th Edition, 2007 (Chapter 6)

[124] Text: J. Weiner, P.-T. Ho, Light-Matter Interactions, Vol. 1: Fund. and Appl., Wiley, 2003 (Chapter 6)

[125] Course: Nano-Optics, Forces in Confined Fields, ETHZ

[126] Text: B.L Moiseiwitsch, Variational Principles, Dover Publications, 1966

[127] Text: A.P Kazantsev, G. I. Surdutovich, P.V Iakovlev, Mechanical Effects of Light on Atoms, World Scientific, 1990

Optics and Mechanics

[128] J. Masoliver. From Classical to Quantum Mechanics through Optics. European Journal of Physics, 2009.

[129] J. Butterfield. On Hamilton-Jacobi Theory as a Classical Root of Quantum Theory. 2003.

[130] Text: R. Dugas. A History of Mechanics, Routledge, 1955

Light Affecting Atomic Motion

[131] W. D Phillips. Laser cooling and trapping of neutral atoms. Rev. Mod. Phys., 1998.

[132] J. Dalibard, et al. Atomic motion in laser light: connection between semiclassical and quantum descriptions. J. Phys. B, 1985

[133] O. Nairz et al. Diffraction of Complex Molecules by Structures Made of Light. PRL, 2001.

[134] E. M Rasel et al. Atom Wave Interferometry with Diffraction Gratings of Light. PRL, 1995.

[135] C. N. Cohen-Tannoudji et al. Manipulating atoms with photons, Rev. Mod. Phys. 707, 1998.

[136] V. E. Lembessis et al. Optical dipole trapping beyond the rotating wave approximation: the case of large detuning, J. Optics B, 2005

[137] Y. Roichmann et al. Optical forces arising from phase gradients, PRL, 2008

[138] J. D. Franson, Velocity-dependent optical forces and Maxwell's demon, Scientific Reports, 2019

[139] J. Gordon et al. Motion of atoms in a radiation trap, PRA, 1980

Atom Interferometry

[140] O. Nairz et al. Quantum interference experiments with large molecules. AAPT, 2003.

[141] S. Nowak et al. High-order Talbot fringes for atomic matter waves. Optics Letters, 1997.

[142] A. D Cronin et al. Optics and Interferometry with Atoms and Molecules. Rev. Mod. Phys, 2009.

Atom Trajectories near Photonic Structures

[143] D. E. Chang et al. Colloquium: Quantum matter built from nanoscopic lattices of atoms and photons. Rev. Mod. Phys, 2018

[144] M. E. Kim et al. Trapping single atoms on a nanophotonic circuit with configurable tweezer lattices. Nature Communications, 2019

[145] E. Da Ros et al. Cold atoms in micromachined waveguides: a new platform for atom-photon interactions. Phys. Rev. Research, 2020.

[146] X. Luan et al. The Integration of Photonic Crystal Waveguides with Atom Arrays in Optical Tweezers, Wiley: Advanced Quantum Technologies, 2020.

[147] C. A Mejia et al. Light-assisted templated self assembly using photonic crystal slabs. OSA, 2011

[148] PhD Thesis: J. D. Thompson. A quantum interface between single atoms and nanophotonic structures. Harvard, 2014.

[149] PhD Thesis: X. Luan. Towards atom assembly on nanophotonic structures with optical tweezers. CalTech, 2018.

[150] S-P Yu et al. Two-dimensional photonic crystals for engineering atom–light interactions. PNAS, 2014

[151] A. Goban et al. Atom–light interactions in photonic crystals. Nature, 2014.

[152] A. P. Burgers et al. Clocked Atom Delivery to a Photonic Crystal Waveguide. PNAS, 2018.

[153] C. L. Hung et al. Trapped atoms in one-dimensional photonic crystals. NJP, 2013

[154] N. P. Stern et al. Simulations of atomic trajectories near a dielectric surface. NJP, 2011

[155] A. Gonzalez-Tudela et al. Subwavelength vacuum lattices and atom–atom interactions in two-dimensional photonic crystals, Nature Photonics, 2015

[156] J. Beguin et al. Reduced volume and reflection for bright optical tweezers with radial Laguerre–Gauss beams, PNAS, 2020

Numerical Integration Algorithms and Parallel Programming:

[157] Excerpt: H. Gould et al. Numerical Integration of Newton's Equation of Motion, An Introduction to Computer Simulation Methods, 2007

[158] Course Notes: P. Young, Symplectic Algorithms for Integrating Newton's Laws of Motion

[159] Lecture: M. Teschner: Simulation in Computer Graphics Particle Motion, U. Freiburg

[160] Course Notes: A. Sandvik, Numerical Solutions of Classical Equations of Motion, PY 502, Boston University, 2018

[161] Lecture: K. Haule, ODEs - Basic Numerical Algorithms, Computational Physics, Rutgers Univ., 2015

[162] S. A. Chin, Structure of numerical algorithms and advanced mechanic, arXiv, 2019

[163] Computational Collaboration Project : Democritus – Integration Algorithms

[164] CUDA Toolkit: Documentation

[165] Thesis: J. Anderdahl et al. Particle Systems Using 3D Vector Fields with OpenGL Compute Shaders

[166] Course Material: J. Novak et al. GPU Computing – Particle Simulation, KIT

[167] R. Patro et al. Speeding Up Particle Trajectory Simulations Under Moving Force Fields using Graphic Processing Units, J. Computing and Info. Science, 2012

[168] J. Phillips et al. Scalable molecular dynamics on CPU and GPU architectures with NAMD, J. Chem, 2020

[169] J. Stone et al. Accelerating molecular modeling applications with graphics processors, J. Comp. Chem, 2007

[170] Excerpt: K. Niemeyer et al. GPU-Based Parallel Integration of Large Numbers of Independent ODE Systems, Numerical Computations with GPUs, Springer, 2014

[171] H. Homann et al. SoAx: A generic C++Structure of Arrays for handling particles in HPC codes, Comp. Phys. Comm., 2017

[172] Excerpt: K. Ahnert, Solving Ordinary Differential Equations on GPUs, Numerical Computations with GPUs, 2014

[173] CUDA Samples: N-body gravity simulation

Cooling and Loading Cold Atoms into Hollow Fibers:

[174] J. D. Miller et al. Far-off-resonance optical trapping of atoms, PRA, 1993

[175] Student Essay: K. Akkarawong, Dressed atom approach to laser cooling: dipole forces and Sisyphus cooling, Physical Review – 8.06

[176] PhD Thesis: P. Phoonthong, State-Insensitive Traps for Caesium Atoms, UCL, 2012

[177] Masters Thesis: A. Szulc, Simulating Atomic Motion in a MOT, Ben-Gurion Univ. of the Negev, 2016

[178] D. Schrader et al. An optical conveyor belt for single neutral atoms, Appl. Phys. B, 2001

[179] S. Kuhr et al. Coherence Properties and Quantum State Transportation in an Optical Conveyor Belt, PRL, 2005

[180] M. Langbecker et al. Highly controlled optical transport of cold atoms into a hollow-core fiber, NJP, 2018

[181] S. Kuhr et al. Deterministic Delivery of a Single Atom, Science, 2001

[182] PhD Thesis: Y.Song, Hollow Beam Atom Tunnel, Univ. Maryland, 1999

[183] OSA: Optics and Photonics News - Unravelling Bessel Beams, 2013

[184] D. Boiron et al. Laser cooling of cesium atoms in gray optical molasses down to 1.1 μK, PRA, 1996

Numerical References of Loading into Hollow Fibers

[185] T. Yoon et al. Simulating gravity-assisted loading of laser-cooled atoms into a hollow-core photonic-bandgap fiber, J. Physics B, 2020

[186] Y. Wang et al. Loading Dynamics of Cold Atoms into a Hollow-Core Photonic Crystal Fiber, Fibers, 2020

[187] J. Poulin et al. Optimized coupling of cold atoms into a fiber using a blue-detuned hollow-beam funnel, Physical Review A, 2011

[188] PhD Thesis: J. Poulin, Toward Cold Atom Guidance in a Hollow-Core Photonic Crystal Fibre Using a Blue-Detuned Hollow Laser Beam, Univ. Montreal, 2015

Experimental References of Loading into Hollow Fibers

[189] T. Yoon et al. Laser-cooled cesium atoms confined with a magic-wavelength dipole trap inside a hollow-core photonic-bandgap fiber, PRA, 2019

[190] M. Bajcsy et al. Laser-cooled atoms inside a hollow-core photonic-crystal fiber, PRA, 2011

[191] PhD Thesis: M. Bajcsy, Novel Systems and Techniques for Nonlinear Optics at Low-light Levels, Harvard Univ., 2009

[192] A. P. Hilton et al. High-efficiency cold-atom transport into a waveguide trap, PRA, 2018

[193] C. A. Christensen et al. Trapping of ultracold atoms in a HCPCF, PRA, 2008

Cesium Atom Energies Data

[194] D. Steck, Cs D Line Data, 1998

[195] G. Toh et al. Measurement of the lifetime of the $7s^2S_{1/2}$ state in atomic cesium using asynchronous gated detection, PRA, 2018

Rubidium Atom Energies Data

[196] D. Steck, Rb 85 D Line Data, 2008

[197] D. Steck, Rb 87 D Line Data, 2001

Nonlinear Optics:

[198] D. E. Chang et al. Quantum nonlinear optics - photon by photon, Nature Photonics, 2014

[199] Talk: R. Boyd, Quantum Nonlinear Optics: Nonlinear Optics Meets the Quantum World, 2016

[200] M. Lukin et al. Resonant Nonlinear Optics in Phase-Coherent Media, Adv. in Atomic, Molecular and Optical Physics, 2000

[201] M. Jain et al. Efficient Nonlinear Frequency Conversion with Maximal Atomic Coherence, PRL, 1996

[202] P. Kolchin, Electromagnetically-induced-transparency-based paired photon generation, PRA, 2007

[203] N. B. Phillips et al. Slow light propagation and amplification via electromagnetically induced transparency and four-wave mixing in an optically dense atomic vapor, J. Modern Optics, 2009

[204] A. Yariv, The Application of Time Evolution Operators and Feynman Diagrams to Nonlinear Optics, IEEE, 1977

[205] T. K. Yee et al. Diagrammatic analysis of the density operator for nonlinear optical calculations: Pulsed and CW responses, PRA, 1978

[206] Q. Li et al. Efficient and low-noise single-photon-level frequency conversion interfaces using silicon nanophotonics, Nature Photonics, 2016

[207] M. W. McCutcheon et al. Broadband frequency conversion and shaping of single photons emitted from a nonlinear cavity, Optics Express, 2009

[208] Y-C Wei et al. Broadband coherent optical memory based on electromagnetically induced transparency, PRA, 2020

[209] J. Guo et al. High-performance Raman quantum memory with optimal control in room temperature atoms, Nat. Comm. 2019

[210] N. Filipvic et al. Slow and fast light propagation through ladder-type atomic media with degenerate energy levels, Facta Universitatis, 2019

[211] Text: S. Rand, Lectures on Light: Nonlinear and quantum optics using the density matrix, Oxford Univ. Press, 2016

[212] PhD Thesis: J. Keith, Quantum noise propagation in nonlinear optical media, MIT, 1999

[213] U. L. Anderson et al. 30 years of squeezed light generation, arXiv, 2006

[214] Q. Glorieux et al. Double-lambda microscopic model for entangled light generation by four-wave-mixing, PRA, 2010

[215] C. Joshi et al. Frequency-Domain Quantum Interference with Correlated Photons from an Integrated Microresonator, PRL, 2020

[216] M. Roberts et al. A density matrix approach to problems in time-dependent perturbation theory, J. Phys. A. Math., 1979

Softwares

[217] QuTiP: Quantum Toolbox in Python

[218] QuTiP: Lindblad Master Equation Solver

[219] Mathematica

Four-Level Dynamics and Frequency Conversion:

Experiment

[220] D. A. Braje et al, Frequency Mixing Using EIT in Cold Atoms, PRL, 2001

[221] PhD Thesis: D. A. Braje et al. Low-light-level nonlinear optics using electromagnetically induced transparency, Stanford Univ. 2004

[222] F. E. Beccera et al, Nondegenerate four-wave mixing in rubidium vapor: The diamond configuration, PRA, 2008

[223] R. T. Willis et al. Four-wave mixing in the diamond configuration in an atomic vapor, PRA, 2009

[224] A. Radnaev et al. Quantum Memory with Telecom Transitions, Nature, 2010

[225] Z-Y Liu et al. High-efficiency backward four-wave mixing by quantum interference, Scientific Reports, 2017

Theory

[226] C-Y. Cheng et al. Quantum frequency conversion based on resonant four-wave mixing, PRA, 2021

[227] G. Morigi et al. Phase-dependent interaction in a four-level atomic configuration, PRA, 2002

[228] K-S Sarah et al. Phase-dependent light propagation in atomic vapors, PRA, 2007

[229] E. A. Korunsky et al. Phase-dependent nonlinear optics with double-Lambda atoms, PRA, 1999

[230] H. H Jen, et al. Efficiency of light frequency conversion in an atomic ensemble, PRA, 2010

[231] A. Gogyan, Qubit transfer between photons at telecom and visible wavelengths in a slow-light atomic medium, PRA, 2008

[232] A. Gogyan et al. Entanglement-preserving frequency conversion in cold atoms, PRA, 2008

[233] N. Lauk et al. Fidelity of photon propagation in electromagnetically induced transparency in the presence of four-wave mixing, PRA, 2013

[234] PhD Thesis: N. Lauk, Quantum networks for photons: nonlinear effects in quantum memories, quantum interfaces andsingle-photon filter, TUK, 2016

[235] PhD Thesis: J-C Liu et al. Dynamics of multi-photon processes in nonlinear optics and x-ray spectroscopy, KTH, 2009

[236] S. G. Menon et al. Nanophotonic quantum network node with neutral atoms and an integrated telecom interface, NJP, 2020

[237] M. Parniak et al. Interference and nonlinear properties of four-wave-mixing resonances in thermal vapor: Analytical results and experimental verification, PRA, 2015

[238] C. W. Thiel, Four-Wave Mixing and its Applications, Review Essay

Electromagnetic Properties of Photonic Crystals:

[239] Text: S. Johnson et al. Photonic Crystals: Molding the Flow of Light, Princeton University Press, 2008

[240] S. Fan et al. Analysis of guided resonances in photonic crystal slabs, PRB, 2001

[241] A. E. Miroshnichenko et al. Fano resonances in nanoscale structures, Rev. Mod. Phys. 2010

[242] J. P. Moura et al. Centimeter-scale suspended photonic crystal mirrors, arXiv, 2018

[243] W. Zhou et al. Fano resonance principles in photonic crystal slabs, Semiconductors and Semimetals, 2019

[244] Z. Sadrieva et al. Multipolar origin of bound states in the continuum, PRB, 2019

[245] C. W. Hsu et al. Observation of trapped light within the radiation continuum. Nature, 2013

[246] B. Zhen et al. Topological Nature of Optical Bound States in the Continuum, PRL, 2014

[247] A. C. Overvig et al. Selection Rules for Quasi-Bound States in the Continuum, arXiv, 2020

[248] S. John et al. Spontaneous emission near the edge of a photonic band gap, PRA, 1994

[249] J. Thompson et al. Choose your interaction, Nature Photonics, 2015

[250] M. Bello et al. Unconventional quantum optics in topological waveguide QED, Science Advances, 2019

[251] N. Parappurath et al. Direct observation of topological edge states in silicon photonic crystals: Spin, dispersion, and chiral routing, Science Advances, 2020

[252] C. Verstraete et al. Linear and nonlinear optical effects in biophotonic structures using classical and nonclassical light, J. Biophotonics, 2018

[253] D. G. Angelakis et al. Photonic Crystals and Inhibition of Spontaneous Emission: An Introduction, arXiv, 2008

[254] B. Shouse, How Geckos Stick on der Waals, Science, 2002

[255] B. Semnani et al. Spin-preserving chiral photonic crystal mirror, Light: Science and Applications, 2020

[256] Text: A. Taflove, Computational Electrodynamics. The Finite-Difference Time-Domain Method, ArtTech House, 2005

[257] Text: S. J. Orfanidis, Electromagnetic Waves and Antennas, Rutgers Univ. 2016

Softwares

[258] MEEP: MIT Electromagnetic Equation Propagation

[259] AWS: Simpetus Electromagnetic Simulation Platform

[260] MPB: MIT Photonic Bands

[261] S^4: Stanford Stratified Structure Solver (RCWA)

[262] Lumerical: FDTD and MODE Solutions

[263] Symposium on Open-Source Computational Electromagnetics

Notes:

[264] Colloquially, quantum is defined as 'the smallest amount or unit of something'. Source: Quantum, Cambridge Dictionary

[265] Super-resolution and novel metasurfaces might provide alternative routes towards increasing the interaction probability by surpassing the diffraction-limit.

[266] Usually, alkali atoms are considered in such discussions. It might be of interest to explore multi-electron atoms in relation to their optical properties and applications.

[267] This is an estimate based on the equation specifying the relation between $\Gamma_{wavguide}$, n_g (set to 1 for hollow-core fibers) and A_{eff} mentioned in Ref.[151].

[268] The definition of A_{eff} used in Ref.[151] is different from the one mentioned in Pg.30.

[269] Electronic wavefunctions in atoms, such as s and p orbitals are parity invariant and thus, have no net dipole moment. 'Transitioning' to states with different ($\pm = 1$) parities, a dipole moment can be associated to the electron wavefunction.[4]

[270] "Bohr recognized a nonclassical element in spontaneous emission, for to him spontaneous meant acausal." P. W. Milloni [49]

[271] Some alternative perspectives on field theory include: neoclassical theory, classical electromagnetism and self-field QED.

[272] Laptop serial processor speeds of ∼3 GHz suggest billion arithmetic operations per second. Although, naive code might perform calculations at the MHz level.

[273] Relativistic versions of which, underpinning ideas of spin and quantum electrodynamics [47], were provided by Dirac.

[274] As a tangential aside on computing, a paper on "On the Universality of Potential Well Dynamics" talks about how motion in potential wells can be considered Turing complete. More generally, natural systems which are often described by ODEs and PDEs can also be mapped to universal computation.

[275] 'Analog' routes towards computing?: O. Bournez et al, Computing with Polynomial Ordinary Differential Equations, Journal of Complexity, 2016, D. Graca et al, Robust Simulations of Turing Machines with Analytic Maps and Flows, Conference on Computability in Europe, 2005

[276] Photonic crystal reflectivity data-set using Lumerical FDTD was provided by Dr. Jeremy Flannery [72].

[277] Picture courtesy and sample growth facility: National Research Council, Canada.